

Venus' Free Obliquity

Charles F. Yoder

Jet Propulsion Laboratory, California Institute of Technology
4800 Oak Grove Drive
Pasadena CA 91109
Tel.: 818-354-2444

Email: Charles.F.Yoder@ccmail.JPL.Nasa.gov

Date: April 29, 1995

Tables: 8; Figures: 27; Manuscript: 16

Received:; Accepted:

Abstract

The predicted orientation of Venus' rotation axis relative to its orbit can be uniquely determined given knowledge of its J_2 gravity coefficient and polar moment of inertia C if its *free obliquity is fully damped*. This assumption seems warranted given the dominant damping mechanism: turbulent fluid friction at a core-mantle boundary (CMB). This skin friction results from differential obliquity of mantle and core spin axes, and the associated damping rate could be as short as $1/10^6$ yr. However, the observed pole orientation indicates a free obliquity amplitude $\epsilon \simeq 2.1^\circ$ compared with a nominal forced amplitude of 0.5° . There are two plausible explanations. The most likely is that the observed obliquity is a tidally evolved end state in which core friction, modulated by CMB ellipticity and core obliquity amplitude, counterbalances solid and atmospheric tidal torques. This concept is similar to the explanation for the retrograde spin ω as an end state in which solid and atmospheric thermal tidal torques balance at the present spin rate because of the ω^{-1} dependence of the axial thermal torque. Large core ellipticity $\epsilon_c \equiv (C_c - \frac{1}{2}(A_c + B_c))/C_c$ ($C_c \geq B_c \geq A_c$ are core moments of inertia) can substantially increase fluid friction damping time if ϵ_c is significantly larger than the whole body ellipticity $\epsilon_o = J_2 MR^2/C \simeq 1.3 \times 10^{-5}$ by reducing the relative obliquity of core and mantle spin vectors. Note that the hydrostatic contribution to oblateness $\sim 1.7 \times 10^{-7}$ is presently negligible. Weaker effects such as solid and thermal tides can then compete with core friction and for plausible models, their sum tends to increase free obliquity. The obliquity balance is controlled by

the nonlinear (and nearly quadratic) dependence of the CMB turbulent ‘skin friction’ torque on obliquity. I find that a steady state is achieved for $\epsilon_c \simeq 29\epsilon_0 \simeq 4 \times 10^{-4}$. If the CMB topography is dynamically supported, then the necessary bottom density anomaly is constrained to the bottom $\sim 10\%$ of the mantle.

An alternative model is that the obliquity results from resonant excitation due to small amplitude (≤ 0.0020), prograde oscillations in Venus’ orbit, one of which happens nearly to match Venus’ precession rate σ . This mechanism can account for the obliquity even if the iron core has solidified, but also requires a tectonically quiescent planet ($d|J_2/dt| < 10^{-15} \text{ yr}^{-1}$). This model has been explored numerically for a wide range of initial conditions, tidal parameters, temporal J_2 variations and chaotic wander of the driving frequencies for the orbit. Only four frequencies, in or near the predicted band for σ , have a significant effect and also have a narrow range of effectiveness. I estimate the polar moment to be in range: $(0.0341 \pm 0.0031) MR^2$ and hence the precession rate σ to be in range: $44.1 \leq \sigma \leq 45.8'' \text{ yr}^{-1}$ based on construction of a suite of density profiles in which mantle composition and core size have theoretically limited variations. Comparing resonance widths to the σ uncertainty, I find that the resonance hypothesis has about a 30% chance of being correct.

Core ellipticity also has a profound effect on tidal evolution of Venus obliquity. The ratio of turbulent core and solid tidal friction scales like ω^{-6} , implying that core friction ‘turns on’ only as the spin ω approaches its end state. I also find that the semiannual atmospheric tide can have a dramatic effect on evolution, allowing for inversion of spin orientation from prograde to retrograde if the initial obliquity is sufficiently large ($\geq 45^\circ$).

Potential measurements which have bearing on these models including precession rate, tidal Love number k_2 and semidiurnal variation in atmospheric pressure at Venus’ surface. Perhaps the most useful parameter is k_2 which is detectable from orbit, requires only a modest improvement in the tracking accuracy and spacecraft stability over that provided by Magellan and is an excellent proxy for core fluidity and if fluid, core size and composition.

1. introduction and Background

The discovery of Venus' retrograde rotation prompted Gold and Soter [1969] to propose that this slow rotation is near steady-state. A balance is achieved between solid friction torque which drives Venus toward synchronous rotation and a thermally driven, atmospheric torque which drives it away from synchronous rotation. The spin stabilizes because the tidal phase lag ($\propto Q^{-1}$) is weakly dependent on the semidiurnal frequency while the atmospheric phase lead is expected to be inversely proportional to frequency [Ingersoll and Dobrovolskis, 1978]. Implicit in the above choice of a negative spin is that the obliquity ϵ is near 0° . One could just as easily choose a positive spin and a corresponding obliquity near 180° .

However, other attempts to understand the rotational dynamics of Venus (and initially based on suggestive but inaccurate data) have foundered once more precise determination of spin rate and wobble amplitude (proportional to the C_{21}/S_{21} gravity coefficients) were obtained. The successful explanation of Mercury's rotation rate in terms of a resonant spin-orbit couple with the sun led Gold and Soter [1969] to propose a similar mechanism for Venus [also see Goldreich and Peale, 1970] involving earth instead of the sun as the external body controlling the spin. The predicted Venusian rotation rate ω necessary for this mechanism to maintain this spin-orbit lock is $2\pi/243.16$ d. The latest results from geodetic analysis of overlapping, Magellan SAR images [Davies *et al.*, 1992] find an observed rate ω (see table 1) that is not close enough to the resonant rate to maintain this spin-orbit configuration.

Ward and DeCampi [1979] proposed that turbulent, fluid friction at a fluid core-mantle boundary should drive the spin pole to a fully damped state. The observed rotation pole position happened to be near the normal to the invariable plane and seemed to require a $J_2 \sim 10^{-7}$ or about 100 times smaller than Earth's non-hydrostatic $J_2 = 1.1 \times 10^{-5}$. The hydrostatic contribution of rotation and solar tides to Venusian J_2 is $\sim (\omega^2 + \frac{3}{2}n^2)R/g \approx 2 \times 10^{-7}$, where the orbital mean motion

$n = 2\pi/224.695\text{d}$, radius $r = 6051.8\text{ km}$ and surface gravity $g = 8.870\text{ m s}^{-2}$. Yoder and Ward [1979] proposed that the Venusian J_2 probably is comparable in magnitude to the non-hydrostatic J_2 of Earth, but that the effective J_2 about the spin axis can be significantly reduced by a factor of $\sim(1 - \frac{33}{2} \sin^2 \epsilon_W)$ if the wobble amplitude ϵ_W is near 54° . The wobble damping is entirely controlled by solid friction and that the damping time constant $7 \times 10^5 Q_W \text{ yr}$ is of order 10^7 to 10^8 yr (where $\sim 10 < Q_W \leq 300$ is the dissipation factor associated with flexing at the wobble period $\sim 243\text{d}/(1 + \frac{3}{2}(n/\omega)^2)e_0$). Earth-like excitation amplitudes were scaled to Venus and the results suggested that climatic or tectonic activity might justify a wobble amplitude as large as 10° or more. Solutions for the gravity field using PVO Doppler data [Mottlinger *et al.*, 1985] soon demonstrated that the $J_2 \simeq 4.5 \times 10^{-6}$ (confirming the value obtained from Venera 9 and 10 tracking data [Akim *et al.*, 1978]) and detected a wobble amplitude of $2.6 \pm 0.3^\circ$.

At this point the apparently undamped free obliquity of Venus lacked an explanation, but the significant free wobble seemed to support a dynamically active Venus. However, recent solutions for the Venus C_{21}/S_{21} gravity coefficients [McNamee *et al.*, 1993; Konopliv *et al.*, 1993] which include Magellan Doppler data point to a much reduced wobble amplitude $0.45^\circ \pm 0.04^\circ$. This factor may support the proposition that Venus is significantly less active than Earth, where ‘activity’ is due to climate or tectonics. Crater populations and estimates of the last major (and apparently nearly global) resurfacing event [Schaber *et al.*, 1992] about $0.5 \pm 0.3\text{ Gyr}$ ago tend to support this interpretation. Arkani-Hamed [1993] argues that the lack of evidence of ongoing resurfacing, the apparently small convergence rate $\sim 0.1\text{ cm yr}^{-1}$ for some of the folded terrain, the possible dominance of hot spots for heat flow [Morgan and Phillips, 1983] and the absence of a magnetic field support a “cold” Venus model [Arkani-Hamed and Toksöz, 1984; Arkani-Hamed, 1993], where the mean mantle temperature is $\sim 100^\circ\text{K}$ cooler than earth’s mantle at the same pressure. Numerical convection models constructed by Arkani-Hamed and Toksöz [1984] with active recycling of crust result in a frozen core. However, it is expected that the presence of impurities such as sulphur suppress the Fe eutectic melting point by several hundred degrees [Usselman, 1975], enough to

prevent freezing. For Earth, where the presence of volatiles and a less buoyant crust should speed the convective process, only 570 has frozen out at the bottom of the core, producing Earth's inner core. In fact, the absence of a Venusian magnetic field has been linked to the absence of a solid inner core [Stevenson *et al.*, 1983], partly based on the idea that core freezing provides the energy (through bottom layer buoyancy) necessary to drive fluid convection. In the following material, the fluidity of the core is an essential element in a new model which accounts for Venus' spin pole location. The self-consistency of the model and the predictions concerning the thermal boundary layer at the base of Venus' mantle, in effect, demonstrate the existence of a fluid core given the absence of a compelling alternative.

A second alternative has been found involving resonant excitations. This mechanism works only for a limited range of precession rate σ and requires a tectonically dead planet.

This paper includes a thorough discussion of most aspects of this problem. The first objective is to derive the free obliquity amplitude and show that for a reasonable range of core parameters that obliquity damping should be rapid unless core ellipticity is large (sections 2.-5). First, Venus' forced obliquity is derived in section 2 using a simplified model and compared with the observed pole location. Second, a plausible range of Venusian structure models are constructed to determine a plausible range for moment of inertia and potential Love number k_2 (also see appendix A for more on this material). Third, brief descriptions of the tidal and atmospheric torques [e.g. Dobrovolskis, 1978] are described in section 3 (Also, see Appendix 1) for development of a general model for tidal potential). Fourth, a model is constructed in section 4 for the core-mantle torque caused by fluid friction at the core mantle boundary (CM)), which I show is almost certainly turbulent. This model is compared with the predictions of a laminar friction model and laboratory experiments [Vanyo, 1991] which determine the onset of turbulence. The linearized, dynamical model is described in section 5 and appendix C and the conditions for obliquity to achieve a stationary state are enumerated.

The second objective is to explore the implications of the inferred c_{011} internal structure and

this new CMF model of tidal histories. The geophysical consequences of a large CMB ellipticity are explored in section 6. I attempt to justify the core oblateness as a dynamic balance between CMB deformation and a thermal boundary layer just above it. Section 7 presents the consequences of this model on tidal evolution of spin and obliquity. The most interesting result is that for a certain class of models, the spin axis can flip from prograde to retrograde orientation.

The third objective is to consider the potential effect of resonant excitation (perhaps driven temporal changes in J_2) on the steady state hypothesis (sections 8 and 9 (numerical integrations)). First I show that resonant excitation could temporarily increase the obliquity by as much as a factor of 3 greater than its equilibrium value. However, since the CMF torque is proportional to σ_c^{-3} , the inferred core ellipticity is reduced at most by a factor of 0.7. Finally, an alternative model is developed using chaotic wander of the weak driving frequencies (calculated in appendix B) to excite a free obliquity. This second model requires a quiescent planet and is consistent with core solidification.

2. Determination of the free obliquity

Since it is central to my argument, I shall first derive the predicted pole position based on a simplified model which momentarily omits the effects of core and tides. The solar torque acting on Venus' oblate figure is proportional to the difference $p - P$, where the whole-body, obliquity variable p and orbit normal variable P are defined by

$$p = \sin \epsilon e^{-i\phi} ; P = \sin I e^{-i\Omega}. \quad (1)$$

The complex, Cartesian variable p ($p = p_x - ip_y$) describes variation of the obliquity ϵ and nodal orientation ϕ with respect to the invariable plane. The uppercase P variable is similarly related to the orbit inclination I and orbital nodal angle Ω . The changes in P arise from the orbit-averaged action of the other planets [Laskar, 1988, 1990] and can be expanded in a periodic series $P(t) = \sum_j \sin I_j \tilde{e}^{-i(t)}$. The frequencies $d\Omega_j/dt$ are nearly all negative. The 8 terms corresponding

to the linearized Laplace-Lagrange solution for both eccentricity and inclination are given in table 2 [Laskar, 1990]. The two largest $\sin I_j$ terms have amplitudes of 0.013 and 0.019 and rates -5.62 "yr $^{-1}$ ant] -18.85 "yr $^{-1}$, respectively.

The linearized dynamical equation describing the variation in obliquity is

$$-\ddot{\theta} + \left\{ \left(\frac{1}{\tau} + \frac{1}{\tau'} \right) \right\} (\dot{\theta} + \frac{1}{\tau}) (\dot{\theta} - \frac{1}{\tau'}) = 0, \quad (2)$$

where τ is a decay time scale. The free precession rate σ [e.g. Smart, 1961] is

$$\sigma = -\frac{3}{2} J_2 \frac{n^2}{\omega} \frac{MR^2}{C} (1 - \epsilon^2)^{-3/2} \cos \epsilon, \quad (3)$$

where rotation rate $\omega = -2\pi/243.0185 \pm 0.0003$ d [Davies *et al.*, 1992], orbital mean motion $n = 2\pi/224.6954$ d, mass $M = 48.685 \times 10^{23}$ kg and radius $R = 6051.8$ km are well determined quantities. Venus' present orbital eccentricity $\epsilon = 0.0068$, however its long term average is 0.034 (see table 2), while I shall argue that the present obliquity is 2.1° . These two factors change σ by only 0.1%.

The most recent published solution for J_2 ($J_2 = 4.44 \pm 14 \times 10^{-6}$ [Konopliv and Sjogren, 1994]) has been updated to ($J_2 = 4.424540.0013 \times 10^{-6}$ [M GNP75], Konopliv, priv. comm.) from a solution for a gravity field of degree and order 75. The presence of a fluid core with polar moment C_c and core nutation frequency σ_c reduces σ by a factor $\approx (1 - C_c \sigma / C \sigma_c)$ (see equation [53]) and hence can reduce σ by as much as 1 % although the most plausible reduction is 0.5%. Estimates of the principal moment C are less certain (although a plausible uncertainty is about 3%) and must be derived from structural models with quasi-earth-like profiles [Basaltic Volcanism Study Project, 1981] which only need satisfy the mean density constraint, $\bar{\rho} = 5.204$ g cm $^{-3}$.

A suite of models have been constructed (see appendix A for more details), using a version of the parametric earth model (PEM) [Dziewonski *et al.*, 1975; see Fig. 2 ant] table 5] as a starting point, and for which a polynomial representation dependent on pressure is employed, Mantle composition is varied by changing the molar fraction of Fe relative to Mg ($f_{Fe} = Mg/(Mg + Fe)$)

using the properties of forsterite (Mg_2SiO_4) and fayalite (Fe_2SiO_4) as analogues. The core density is varied from an earth-like model by introducing a constant difference $\delta\rho_c$ (see eq. (1.09)). The results of this study are shown in figures 3-5 and table 6 (in appendix A). Figures 3, 4, and 5 display plots of the k_2 tidal Love number versus whole-body moment of inertia, core moment of inertia and $\delta\rho_c$, respectively. The most curious result is that k_2 is most strongly correlated with $\delta\rho_c$. A plausible range for k_2 is 0.23 to 0.29. The Love number has also been calculated for the case where the core is completely solid and the results indicate a reduction in magnitude to $k_2(\text{solid}) \simeq 0.17$.

Variation of a plausible f_{Fe} is limited to ± 0.05 about an earth-like mean of 0.89. This constraint is supported by *in situ* x-ray fluorescence spectra of surface rocks obtained by Venera landers which indicate an earth-like basaltic composition [Moroz, 1983]. The corresponding fractional change in mantle density is 3.0.03. Core density is limited to changes of less than $\pm 0.5 \text{ g cm}^{-3}$ based partly on the idea that Earth's inner core density (which supposedly includes the effect of freezing and distillation of iron from its lighter component) is only 0.6 g cm^{-3} more dense than the fluid outer core at the inner core boundary. Parametric models of Venusian convection suggest that Venus thermal profile is hotter and is perhaps offset by $\sim 100\text{K}$ from Earth's thermal profile at the same pressure [Stevenson *et al.*, 1983]. At the opposite extreme, Arkani-Hamed [1993] argues that Venus' thermal profile is $\sim 100\text{K}$ cooler, and this lower mantle temperature is supported by parametric convection models with free upper surface [Turcotte *et al.*, 1979]. The corresponding change in mantle density is $\pm 0.4\%$, based on a nominal thermal expansion coefficient of $4 \times 10^{-5} \text{ K}^{-1}$ and is therefore much less significant than composition in influencing Venusian structural profile. The corresponding constraint on total and core moments are

$$0.331 < \frac{C}{MR^2} < 0.341 \quad (4)$$

$$0.041 \geq \frac{C_c}{MR^2} \geq 0.020$$

Note that core moment size and total moment are anti-correlated.

This leads to the following estimate of σ .

$$44.3''\text{yr}^{-1} \leq \sigma \leq 45.8''\text{yr}^{-1}, \quad (5)$$

if the core is solid. This range is shifted downward to about

$$44.1''\text{yr}^{-1} \leq \sigma \leq 45.6''\text{yr}^{-1}, \quad (6)$$

for a fluid core and mantle which satisfy constraints on σ_c and C_c .

Because Venus' spin is retrograde relative to its orbit, the Venusian figure precesses in a positive sense, contrary to the major terms acting on the orbit plane. The effect of the primary terms have been obtained using Laskar's [1988] numerical theory which includes a FFT estimation of the largest ~ 70 terms affecting Venus down to the 2×10^{-4} level as it is probably the most precise for time scales $\leq 10^6$ yr. However, there are prograde terms which are omitted from published tables because of their small magnitude, which for Venus $\leq 1 \times 10^4$ in amplitude.

I have reconstructed these terms (see appendix B) using Laskar's later [1990] model as a starting point. Represent this sum as

$$P(2\omega) = \sum J_{mnojkl} e^{-i\psi_{mnojkl}} \quad (7)$$

The index $mno11$ corresponds to frequency $9_{\gamma} + g_m - s_o$, while the index $mnoj1l$ indicates the j th sideband of the (eccentricity) g_n primary frequency and the l 'th sideband of the (inclination) SO frequency. Table 3 contains a list of all prograde terms with amplitude $\geq \sim 1 \times 10^{-5}$, terms with amplitude 2×10^{-6} in band $43'' \rightarrow 44'' \text{ yr}^{-1}$ and all terms in the frequency band $44'' \rightarrow 47'' \text{ yr}^{-1}$ with amplitude greater than 3×10^{-7} . The amplitude spectra shown in Fig. 6 indicate the predicted band for Venusian precession rate is near the edge of a gap in the spectra, with one strong peak having frequency $44.223'' \text{ yr}^{-1}$ just inside the predicted band in (6).

The response of Venus' orientation as a function of σ to both the prograde and retrograde terms of P is shown in figure 7 using a nominal $\tau = 1 \times 10^7 \text{ yr}$. The normal to the invariable plane is

al, the origin, and the location of the observed orbit normal and observed pole of rotation are also marked [Davies *et al.*, 1992]. The difference between a point on the curve and spin pole coordinates corresponds to the free obliquity. The size of the circular curves associated with each resonance is inversely proportional to τ .

Only three prograde terms within or near the expected frequency band produce significant perturbations in pole position. Clearly, if τ were reduced by a factor of 3-4, then the loop associated with the driving frequency $44.775'' \text{ yr}^{-1}$ could intersect the pole location. A more plausible scenario is that these small prograde terms may be a potential source of the free obliquity through resonance excitation due to slow changes in J_2 or the driving frequencies, and this idea shall be explored later.

If driving terms in P in the frequency band $\{43.7 \text{ to } 47'' \text{ yr}^{-1}\}$ are excluded, the predicted pole location is insensitive to σ .

$$\begin{aligned}
 p_{x,\text{forced}} &= 0.01877 \text{ rad} \\
 &= 1.0765^\circ \\
 p_{y,\text{forced}} &= 0.02204 + \frac{\sigma - 45}{0.5} 0.0001 \\
 &\simeq 1.263^\circ
 \end{aligned} \tag{8}$$

The observed position is

$$\begin{aligned}
 p_{x,\text{obs}} &= -0.00287 \\
 &= -0.164^\circ \\
 p_{y,\text{obs}} &= -0.00768 \\
 &= -0.440^\circ
 \end{aligned} \tag{9}$$

The difference is the free obliquity

$$\begin{aligned}
p_{x,free} &= -0.02163 \\
&= -1.239^\circ \\
p_{y,free} &= -0.02972 \\
&= -1.703^\circ
\end{aligned}
\tag{10}$$

or an amplitude of 2.10. If one adopts a positive Venusian spin, then the corresponding obliquity is 177.9° . The next step shall be to construct models which account for this last result.

3. Tides

The formal, secular equations due to both solid (K_{ts}, K_{tp}) and atmospheric (K_{as}, K_{ap}) tides for small obliquity are [Dobrovolskis, 1978, 1980; Dobrovolskis and Ingersoll, 1980]

$$\frac{I}{\omega} \frac{d}{dt} \omega = K_{ts} + K_{as}, \tag{11}$$

$$\frac{1}{\sin \epsilon} \frac{d}{dt} \epsilon = K_{tp} + K_{ap}. \tag{12}$$

The solid tidal friction factors K_{ts} and K_{tp} are

$$K_{ts} = \frac{3k_2 n^2 M R^2 H_\odot}{4C\omega} 6t(2n - 2\omega), \tag{13}$$

$$K_{tp} = - \frac{3k_2 n^2 M R^2 H_\odot}{4C\omega} [\delta_t(2n - 2(1) + \delta_t(2n - \omega) - 6, (-LO)]. \tag{14}$$

Solid tides on Venus are set by the parameter H_\odot [Kaula, 1964; appendix D (see Eq. [145])]

$$H_\odot = \frac{M_\odot}{M} \frac{R}{a}^3 = 7.15 \times 10^{-8}. \tag{15}$$

The semidiurnal surface tidal displacement at the equator is $3h_2 H_\odot R \sim 60\text{cm}$, where h_2 is the tidal Love number for vertical displacement. The tidal gravitation field due to deformation is proportional to the Love number k_2 . The tidal phases lags $\delta_t(s)$ have the same sign as the flexing frequency, s . It is generally accepted that their magnitude changes slowly with frequency. Presently

$\omega = -0.9246n$, where n is the orbital mean motion. Therefore, solid tidal friction tends to drive spin toward synchronous rotation where $\omega = n$. The maximum change in the spin is a factor of 80 over 4.6×10^9 yr. given a constant semidiurnal S_2 phase $\delta(2n - 2\omega) = 1/Q = 1/50$ and a small obliquity over the interval

The atmospheric torque is more complex, and an accurate estimate requires detailed modeling of thermal, wind and density profiles. Dobrovolskis [1978, 1980] (also see Ingersoll and Dobrovolskis, [1978] and Dobrovolskis and Ingersoll, [1980]) derived a simple model which contains the important physics. The atmospheric contributions K_{as} and K_{ap} to eqs. (11, 12) are

$$K_{as} = -\frac{8\pi R^3 H_\odot (1 - k'_2)}{5C\omega} \delta P(2n - 2\omega), \quad (16)$$

$$K_{ap} = \frac{8\pi R^3 H_\odot (1 + k'_2)}{10C\omega} [\delta P(2n - 2\omega) + \delta P(2n - \omega) - J] \quad (17)$$

The factor $(1 - k'_2)/(1 - k_2 - h_2) \simeq 0.75$ compensates for elastic mantle loading by the atmosphere. The surface pressure oscillation $\delta P(s)$ arises primarily from heat absorbed near the ground, $P_0 \simeq 100 \text{ W m}^{-2}$ at surface temperature $T_0 \simeq 730^\circ \text{K}$ and atmospheric specific heat $c_p \simeq 1000 \text{ J kg}^{-1} \text{K}^{-1}$. The factor $\delta P(s)$ depends on the ratio of heat absorbed during time $1/s$ to the thermal energy per unit mass, $c_p T_0$.

$$\delta P(s) = \frac{15}{64} \frac{g P_0}{s c_p T_0}. \quad (18)$$

Table 4 contains estimates for $\delta P(s)$ for four important constituents. They are derived from more sophisticated atmospheric models which take into account winds and vertical structure and include strong bottom heating [Dobrovolskis, 1978, 1980; Peckmann and Ingersoll, 1984; Shen and Zhang, 1989, 1990].

Atmospheric tides drive the spin away from synchronous rotation and may also tend to increase obliquity. The spin rate achieves a stationary, stable state when $(K_{ts} - K_{as})$ vanishes. However, the factor controlling obliquity evolution $(K_{tp} + K_{ap}) \simeq -1.4 K_{ts} > 0$ unless one either chooses the

tidal phase and pressure factors to have the same frequency dependence (in which case the spin balance is neutrally stable) or adopt a tuned atmosphere model which happens to introduce just the right counterbalance. Finally, the four models of Dobrovolskis listed in table 4 indicate that $(K_{tp} + K_{ap})$ ranges from $-0.4K_{ts}$ to $-1.8K_{ts}$ if the solid phase lags are independent of frequency.

4. Core Mantle Fluid Friction

The magnitude of the Reynolds number Re , defined as

$$Re = ud/\nu, \quad (19)$$

determines the onset of fluid turbulence, Here ν is kinematic viscosity, $u \sim |\omega| R_c \sin \Delta\epsilon$ is the shear velocity and $d \sim u/|\omega|$ is the lateral displacement of the fluid at the CMB caused by the differential motion. The angle $\Delta\epsilon$ subtends the core and mantle spin vectors. A typical Re for precessional flow is

$$Re = R_c^2 |\omega| \sin^2 \Delta\epsilon / \nu \sim 3 \times 10^{10} \sin^2 \Delta\epsilon (\text{cm}^2 \text{s}^{-1} / \nu) \quad (20)$$

for a Venusian core (core radius $R_c \simeq \frac{1}{2}R$). Turbulence usually sets in for $Re \sim 10^5$ to 10^6 . The core Re number is so large that turbulence at the CMB is almost certain unless $\Delta\epsilon$ is exceptionally small.

An estimate of the turbulent stress can be obtained using mixing length theory [Goldstein, 1965] in which the laminar, viscous boundary layer is replaced with two layers: an interior, laminar viscous sublayer with thickness δ which is matched with an exterior turbulent boundary layer. Within each layer, the stress is assumed constant. The velocity profile in the laminar sublayer increases linearly with the distance ξ from the wall ($\mathbf{u} = \mathbf{u}_\delta \xi / \delta$) up to a layer thickness δ and velocity u_δ . The viscous stress is

$$\tau_v = \rho \nu \mathbf{u}_\delta / \delta. \quad (21)$$

The laminar stress is matched with the turbulent stress at $\xi = \delta$ to determine δ in terms of the other parameters. The turbulent local stress τ_t is governed by

$$\tau_t \simeq \rho \kappa^2 \xi^2 \left| \frac{d}{d\xi} U \right| \frac{d}{d\xi} \mathbf{u} \quad (22)$$

where $\kappa \simeq 0.40$ is the *Kármán constant*. The expected logarithmic velocity profile within the outer turbulent layer can be approximated by

$$\tau_t \simeq \frac{\rho \kappa^2 |\mathbf{u}(\xi)| \mathbf{u}(\xi)}{\ln^2 |\xi/\delta + e - 1|} = \rho \kappa^2 |\mathbf{u}_\delta| \mathbf{u}_\delta, \quad (23)$$

which exhibits the appropriate behavior as $\xi \rightarrow \delta_+$.

Matching the two stresses at the boundary $\xi = \delta$ determines δ : $\delta = \nu / \kappa^2 u_\delta$. The outer boundary at $\xi \sim d$ where the velocity reaches its limiting value u_o leads to the following expression for the local stress.

$$\tau_t \simeq \rho \kappa^2 \left(\frac{u_\delta}{u_o} \right)^2 |\mathbf{u}_o| \mathbf{u}_o, \quad (24)$$

$$\frac{u_\delta}{u_o} \simeq \frac{1}{\ln \frac{u_\delta}{u_o} \kappa^2 Re}. \quad (25)$$

Analysis of the Navier-Stokes dynamical equation in which the velocity \mathbf{u}_o is not held fixed leads to a similar relation.

Now the velocity $\mathbf{u}_o = (\vec{\omega}_c - \vec{\omega}) \times \mathbf{R}_c$ and the local torque exerted by the local stress is $\mathbf{n} = \mathbf{R}_c \times \vec{\tau}$. Except near the polar circle with colatitude $\theta = \Delta\epsilon$, the shear velocity relative to the boundary location at θ and longitude β is periodic and has amplitude

$$u_o \simeq |\omega| R_c \sin \Delta\epsilon \sin \theta \sin(\omega t - \beta - \Delta\phi), \quad (26)$$

where $\Delta\phi$ is the relative nodal intersection line. The CMB torque is obtained by integrating $\mathbf{R}_c \times \vec{\tau}$

over the sphere. Before performing this operation, replace $|\mathbf{u}_o|$ in (24) with its time averaged value $\omega R_c \sin \Delta \epsilon \sin \theta / \sqrt{2}$.

The resulting global torque is \mathbf{N}_t ,

$$\mathbf{N}_t = C_c K_c(\text{turb.})(\vec{\omega}_c - \vec{\omega}) \quad (27)$$

The core moment $C_c \simeq \frac{2}{5} M_c R_c^2$ and the turbulent coupling parameter is

$$K_c(\text{turb.}) \simeq \frac{45\pi}{32\sqrt{2}} \kappa^2 \left(\frac{u_\delta}{u_o} \right)^2 \sin \Delta \epsilon |\omega|. \quad (28)$$

In this calculation, u_δ/u_o was held fixed and is obtained from [25] using the nominal value for the Reynold's number. The value $\frac{u_\delta}{u_o} \leq \frac{1}{10}$ for the expected core parameters.

The equivalent expression for laminar boundary layer friction [Roberts and Stewartson, 1965; Busse, 1968] is

$$K_c(\text{lam}) = 2.6 \sqrt{\nu |\omega|} / R^2 = 2.6 \sin \Delta \epsilon |\omega| R c^{-1/2}. \quad (29)$$

$K_c(\text{lam})$ is smaller than $K_c(\text{turb})$ if $Rc \geq 27 (\ln \frac{u_\delta}{u_o} \kappa^2 Rc)^4$ or if $\nu \leq 0.4 \text{ cm}^2 \text{ s}^{-1}$. The laminar boundary layer thickness is $\sim R \sqrt{\frac{\nu}{\omega R_c^2}}$.

For large core viscosity such that $\frac{\nu}{\omega R_c^2} \gg 1$, the Stokes limit applies. The core velocity \mathbf{u}_c relative to the mantle is given by (see eq.3.1 in Roberts and Stewartson [1965])

$$\mathbf{u}_c \simeq \frac{1}{10} \frac{\omega R_c^2}{\nu} r \left(1 - \frac{r^2}{R_c^2} \right) \hat{\mathbf{z}} \times \vec{\omega} \times \hat{\mathbf{r}}. \quad (30)$$

where $\hat{\mathbf{z}}$ is the spacial axis about which the mantle precesses. The dissipation is obtained from the volumetric integral of $\rho_c \mathbf{u}_c \cdot \hat{\mathbf{z}} \times \vec{\omega} \times \mathbf{r}$. This result is then equated with the work $\mathbf{N}_t \cdot (\vec{\omega}_c - \vec{\omega})$. In the strong coupling limit, $\vec{\omega}_c - \vec{\omega} = \hat{\mathbf{z}} \times \vec{\omega} \times \hat{\mathbf{r}} \frac{\omega}{K_c}$. The coupling parameter obtained from this exercise is [Vanyo, 1991]

$$K_c(\text{Stokes}) = 35 \frac{\nu}{\omega R_c^2} \omega, \quad (31)$$

and $K_c(\text{Stokes})$ is always greater than σ_c or σ_o . The dissipation caused by toroidal shear in this limit is ~~a~~ not physically interesting.

Vanyo's experiments on precessing, liquid-filled spheres near the onset of fully developed turbulence [Vanyo, 1973; Vanyo and Paltridge, 1981; Vanyo, 1991], predict $K_c(\text{turb}) \simeq 0.0035(\pm 50\%)|\omega| \sin \Delta\epsilon$, where I have inferred the uncertainty from the graphed experimental scatter. The two expressions for $K(\text{turb})$ are equivalent if $\frac{u_\delta}{u_o} \simeq \frac{1}{12}$ and $Re \sim 1 \times 10^7$. Unfortunately, the range of Reynolds number explored by Vanyo is too restricted to see the predicted logarithmic dependence on Re . Surface roughness is an additional complication which can increase the turbulent torque, but shall not be considered further given the many other factors which affect our results.

Poirier [1988] argues that at core pressures core viscosity $\eta = \rho\nu$ is close to the STP value for liquid iron near its melting point (0.06 P), although this is uncertain by at least an order of magnitude. Pinning the inner core boundary at the melting point, he estimates that $\eta = 0.03$ P at the CMB. Gans' [1972] estimate for η based on Andrade's theory of liquids is similarly low ($0.04\text{P} \leq \eta \leq 0.21\text{P}$). In these calculations, I shall adopt $\nu = \eta/\rho = 0.01 \text{ cm}^2\text{s}^{-1}$, although changing this number by a factor of 10 changes the major results by only 10%.

Turbulent CMF has already been applied to the moon [Yoder, 1981; Dickey *et al.*, 1994] to account for an apparent 0.26'' offset of the spin axis relative to its expected mean planar alignment with the plane formed by lunar and earth orbit normals. The lunar core $Re \sim 3 \times 10^8$, $\frac{u_\delta}{u_o} \simeq \frac{1}{15}$, and turbulent friction must be the dominant mechanism controlling the CMF torque. This model predicts a liquid lunar core radius $\simeq 350\text{km}$ that roughly agrees with a controversial Apollo magnetometer estimate [Russell *et al.*, 1981].

5. Dynamical Equations

The dynamical equations describing the coupling of a fluid core, contained in an ellipsoidal cavity, to the forced, short period nutational motion of the mantle are well developed for studying Earth's nutations. However, the general approach approximates the precessional motion as a zero frequency

tilt-over mode in calculating the core nutations and its effect on the mantle. A more complete set of equations has been derived by comparing the linearized, rigid body development [Borderies and Yoder, 1990] and the core mantle equations derived by Sasao *et al.* [1977, 1980]. See Appendix C for more details. One must take into account that the rigid body equations refer mantle nutations to an inertial, space-fixed reference frame while core response is usually referred to a body fixed frame in which the nutations have nearly diurnal frequency.

There are distinct advantages in expressing the core polar motion m_c in the space-fixed reference frame instead of the body-fixed frame as is usually the case. First, precessional motion is a slow process instead of nearly diurnal and second it is easier to estimate the correction caused by the core on the forced and free precession of the mantle.

The off-axis spin components $\tilde{m} = \omega_x - i\omega_y$ are related to the p variable ($\equiv \sin \epsilon e^{-i\phi}$) by

$$\tilde{m} = \left(\cos \epsilon \frac{d}{dt} \epsilon - i \sin \epsilon \frac{d}{dt} \phi \right) e^{i(\omega t - \phi)} \quad (32)$$

or

$$Dp = \tilde{m} e^{-i\omega t}. \quad (33)$$

Here D is the time operator d/dt . Sasao *et al.* [1980] derived the following core equation relating changes in \tilde{m} and \tilde{m}_c in the *body-fixed frame*.

$$(D - i\omega(1 + c_c) - 1/K_c) \tilde{m}_c = -D\tilde{m} - D\tilde{c}_{21}^c, \quad (34)$$

where $c_c = (C_c - A_c)/C_c$. The core \tilde{m}_c is the *difference* in angular velocities of core and mantle ($\tilde{m}_c = \omega_x^c - i\omega_y^c - \tilde{m}$). The function \tilde{c}_{21}^c , which shall momentarily be ignored, is an elastic deformation correction.

Define the equivalent representation of core spin \tilde{m}_c in the inertial frame, m_c .

$$m_c = \tilde{m}_c e^{-i\omega t} \quad (35)$$

The core equation in the inertial frame is therefore

$$(D + i\sigma_c + K_c)m_c = -(D + i\omega)Dp, \quad (36)$$

and $\sigma_c = -e_c\omega$ is the unperturbed, free core nutation (FCN) frequency. The above form explicitly shows that for a slow precession (with frequency s) of the whole-body pole, the core response is of order s/σ_c smaller. Also, a nearly diurnal wobble with frequency $(-\omega + s)$ results in a core response which is s/ω smaller.

The relative obliquity of core and mantle spin vectors is obtained from (155) and is

$$\sin \Delta\epsilon = \left| \frac{m_c}{\omega} \right|. \quad (37)$$

Sasao *et al.* [1980] also derived the following equation for the whole body, here transformed to the inertial frame.

$$(D + i\omega + ie_o\omega)Dp - D(\alpha m_c + \tilde{e}_{21}\epsilon^{-i\omega t}) = ie_o\omega\tilde{\phi}\epsilon^{-i\omega t} \quad (38)$$

with $e_o = (2C - A - B)/2C$. Coupling of the mantle to the core is proportional to the ratio of the moments of inertia, $\alpha = C_c/C$. Now, $\tilde{\phi}$ is an external forcing function proportional to $P - p$. This function can be identified by comparing with Borderies and Yoder's [1990] result for a rigid body. One finds

$$ie_o\tilde{\phi}\epsilon^{-i\omega t} = 3/2(n/\omega)^2 \{e_o(p - P) + e_{22}\epsilon^{-i2\omega t}(q - Q)\} \quad (39)$$

with q and Q the complex conjugates of p and P , respectively and

$$e_{22} = \frac{B - A}{-Z}, \quad (40)$$

Through this process, a more accurate, whole-body dynamical equation is recovered.

$$\begin{aligned} & ((1 - e_o)D^2 - i\omega(D - iK_{ta}))p - \\ & e_{22}(3n^2q\epsilon^{-i2\omega t} - D[e^{-i2\omega t}Dq]) \\ & = -\alpha Dm_c - \omega\sigma_o(P - \frac{e_{22}}{e_c}Q\epsilon^{-i2\omega t}) \end{aligned} \quad (41)$$

Here,

$$K_{ta} = K_{tp} + A'_{ap} \quad (42)$$

and

$$\sigma_o = -\frac{3}{2} \frac{n^2}{\omega} c_o. \quad (43)$$

Examination of Eq.(41) for its free solutions in the limit $\alpha \rightarrow 0$ reveals two modes: a nearly diurnal mode with frequency

$$\omega \left(1 + \frac{3}{2} \left(\frac{n}{\omega} \right)^2 \right) \sqrt{(c_o + c_{22})(c_o - c_{22})}, \quad (44)$$

and a slow mode with frequency σ_o . The former mode is the equivalent Venusian Chandler wobble and the latter mode (sometimes called the ‘tilt-over mode’) is the unperturbed (by the core) free mantle nutation or precession (FMN).

This second mode (FMN) qualifies as a so-c. alled free mode even though its frequency and precession axis depends on Sun’s gravitational torque. Like other free modes, FMN has arbitrary initial conditions and can damp in response to internal friction. Besides, the solar torque increases the wobble mode frequency in the body-fixed frame by $(1 + \frac{3}{2}(\frac{n}{\omega})^2)$, and this additional boost does not change our sense that the wobble is still a ‘free’ mode. The semidiurnal term proportional to c_{22} is unimportant for nutational motion and shall be hereafter dropped.

Elastic corrections are related to \tilde{m} , $\tilde{\phi}$ and \tilde{m}_c by

$$\begin{aligned} \tilde{c}_{21} &= m_v(\tilde{\kappa}(\tilde{m} - \tilde{\phi}) + \alpha\tilde{\gamma}\tilde{m}_c), \\ \tilde{c}_{21}^c &= m_v(\tilde{\gamma}(\tilde{m} - \tilde{\phi}) + \tilde{\beta}\tilde{m}_c). \end{aligned} \quad (45)$$

Sasao *et al.* [1980] define factors similar to $\tilde{\kappa}$, $\tilde{\gamma}$ and $\tilde{\beta}$, and these factors are solutions to elastic potential deformation due to either tidal distortion or CMB distention due to fluid core nutation. All have about the same magnitude as the Love number k_2 (in fact, $\tilde{\kappa} \approx k_2$), and for an earth-size core $\tilde{\gamma} \approx 2k_2$ and $\tilde{\beta} \approx 0.6k_2$. The parameter $m_v = \frac{\omega^2 R M R^2}{3g C} \approx 6 \times 10^{-8}$ (surface gravity $g = 887$ cm S⁻²), and therefore \tilde{c}_{21} and \tilde{c}_{21}^c are negligible compared to the observed ellipticities for Venus at the present time.

The eigenfunction equation for an unforced motion proportional to $\exp(-i\gamma t)$ is

$$(\gamma \sigma_c + iK_c)(-\gamma^2(1-\alpha) + \omega(\gamma - \sigma_o - iK_{ta})) = \alpha\gamma^2(\omega - \gamma). \quad (46)$$

The solutions for the nutation-like modes are (neglecting the higher order $\gamma^2(1-\alpha)$ and $\alpha\gamma^3$ terms in the above equation)

$$\gamma_{\pm} = \gamma_{R\pm} + i\gamma_{I\pm}. \quad (47)$$

The real and imaginary components are

$$\gamma_{R\pm} = \frac{\sigma_c + \sigma_o \pm \sqrt{\frac{a + \sqrt{a^2 + b^2}}{2\sqrt{a^2 + b^2}}}}{2(1 - \alpha)}, \quad (48)$$

$$\gamma_{I\pm} = \frac{\left(K \frac{\sigma_c - \sigma_o(1 - 2\alpha)}{\sqrt{\frac{1}{2}(a + \sqrt{a^2 + b^2})}} + K_{ta} \frac{\sigma_c(1 - 2\alpha) - \sigma_o}{\sqrt{\frac{1}{2}(a + \sqrt{a^2 + b^2})}} \right)}{2(1 - \alpha)}. \quad (49)$$

with

$$\begin{aligned} a &= (\sigma_c - \sigma_o)^2 - (K_c + K_{ta})^2 + 4\alpha(\sigma_c\sigma_o + K_cK_{ta}), \\ b &= -2K_c(\sigma_c - \sigma_o(1 - 2\alpha)) - 2K_{ta}(\sigma_c(1 - 2\alpha) - \sigma_o). \end{aligned} \quad (50)$$

First, consider the case where $K_{ta} = K_c = 0$. The two solutions are

$$\gamma_{\pm} = \frac{(\sigma_c + \sigma_o) \pm \sqrt{(\sigma_c - \sigma_o)^2 + 4\alpha\sigma_c\sigma_o}}{2(1 - \alpha)} \quad (51)$$

If $\sigma_c > \sigma_o > 0$, then the + and - signs correspond to the FCN and FMN modes, respectively. The most intriguing result is that the FMN and FCN frequencies are precluded from being identical.

If $CC \gg \epsilon_o$ and the K_c and K_{ta} factors are nonzero, then the two frequencies are

$$\gamma_+ \simeq \sigma_c(1 + \alpha)(1 - i(K_c - \alpha K_{ta})) \quad (52)$$

$$\gamma_- \simeq \sigma_o \left(1 - \alpha \frac{\sigma_o}{\sigma_c} \right) + i \left(K_{ta} - \alpha \left(\frac{\sigma_o^2}{(\sigma_c - \sigma_o)^2 + K_c^2} \right) K_c \right) \quad (53)$$

For $K_c \ll \sigma_c$, the FMN mode has a real frequency (neither damps or grows) if $K_{ta} - \alpha \left(\frac{\sigma_o}{\sigma_c}\right)^2 K_c = 0$. Now KC is itself proportional to $\sin \Delta \epsilon$ and from (36,3-),

$$\sin \Delta \epsilon \simeq \frac{\sigma_o}{\sqrt{(\sigma_c - \sigma_o)^2 + K_c^2}} \quad (54)$$

A stationary end state is achieved when the ratio σ_o/σ_c satisfies

$$\alpha \left(\frac{\sigma_o}{\sigma_c}\right)^3 \left(\frac{u_\delta}{u_o}\right)^2 \simeq -\frac{K_{to}}{K_{ts}} \left(\frac{3k_2}{2Q} \frac{n^2 M R^2 M_\odot}{\omega^2 C} \frac{1}{M} \left(\frac{R}{a}\right)^3 \right) \times \quad (55)$$

$$\frac{32\sqrt{2}}{45\pi \kappa^2} \frac{1}{\sin \epsilon}$$

The core friction parameter $\frac{u_o}{u_\delta} \equiv \text{in } \frac{u_\delta}{u_o} \kappa^2 Re$ was derived earlier in (25). The Reynolds number Re from Eq. (20) is

$$Re \simeq \frac{\omega R^2}{\nu} \left(\frac{\sigma_o}{\sigma_c}\right)^2 \sin^2 \epsilon. \quad (56)$$

The left hand side of (55) is reasonably well determined and independent of parameters on the right side. Plausible values for the input parameters are $C/MR^2 = 0.336$, $k_2 = 0.25$, $Q = 50$, $\sin \epsilon = 0.036$ and $K_{ta} \simeq -1.4 K_{ts}$. The resulting value for the right side factor in (55) is $\alpha \left(\frac{\sigma_o}{\sigma_c}\right)^3 \left(\frac{u_\delta}{u_o}\right)^2 \simeq 1.5 \times 10^{-7}$.

The constraints imposed on Venus' structure suggest that $0.070 \leq \sigma \leq 0.12$ as compared with $\alpha_\oplus \simeq 0.114$. Adopting $R_c = 3100 \text{ km}$ and $\alpha = 0.084$ and $\nu = 0.01 \text{ cm}^2 \text{ s}^{-1}$, we obtain $Re = 2 \times 10^7$, $u_o/u_\delta \simeq 11$, $\sigma_c/\sigma_o \simeq 17$ and

$$e_c \simeq 29e_o = 3.9 \times 10^{-4}. \quad (57)$$

Since $e_c = (a_c^2 - c_c^2)/(a_c^2 + c_c^2) \simeq (a_c - c_c)/a_c$, the difference in core equatorial and polar axes is 1.3 km. This is to be compared with earth's non-hydrostatic core ellipticity, $\Delta e_c = 1.2 \times 10^{-4}$ [Herring *et al.*, 1986], whole body $\Delta e_o = 3.15 \times 10^{-5}$ [Yoder, 1995] and ratio $\Delta e_c/\Delta e_o = 3.8$. Clearly, a firm determination of ϵ from observation can be combined with a modestly firm estimate of the tidal and core parameters to provide a useful estimate for the unknown e_c , since it depends on the cube root of these controlling factors.

The above analysis conveniently ignored the nonlinear aspects of the turbulent coupling, and omitted the contribution the forced obliquity has on the average $|\sin \Delta \epsilon|$. For large σ_c , the time average core obliquity due to the retrograde frequency orbit terms is $|\sin \Delta \epsilon_{\text{forced}}| \sim 0.0006(\sigma_o/\sigma_c)$ and is 1/6 smaller than the free component. Clearly $|\sin \Delta \epsilon|$ should depend on the RMS sum of both forced and free contributions, and the turbulent coupling parameter has a minimum value set by $|\sin \Delta \epsilon_{\text{forced}}|$. This complication will be largely ignored in the remainder of the paper, and $|\sin \Delta \epsilon|$ is replaced with its free component. However, the following example is a case where the forced obliquity dominates.

So far, I have assumed that Venus' core is oblate, but it is obvious that a slightly prolate core would have negative FCN frequency. Therefore, one should ask whether adjustment of core parameters could entirely account for obliquity as a near resonant response. First consider the core and mantle response [Sasao et al., 1977] to a unit forcing with frequency s (i.e. $P = e^{-ist}$). From eqs. (36, 41), the solutions for core and mantle are

$$m_c = \frac{is\omega}{\sigma_c - s - iK_c} p \quad (58)$$

$$p = \frac{\sigma_o}{\sigma_o - s + iK_{ta} - \frac{\alpha s^2}{\sigma_c - s - iK_c}} \quad (59)$$

The maximum value for the imaginary part of p is achieved when $\sigma_c = s(1 - \alpha s/(\sigma_o - s))$, and if we ignore K_{ta} , then

$$p \approx \frac{\sigma_o}{\sigma_o - s} \cdot \frac{(i + \widehat{K}_c)}{\widehat{K}_c} \quad (60)$$

with $\widehat{K}_c = K_c(\sigma_o - s)/(\alpha s^2) > 0$. The core response at the peak is $m_c = -i\sigma_o/(\alpha \widehat{K}_c)$. Clearly \widehat{K}_c must ≤ 1 for a strong core effect on the mantle. Figure 8 displays the response curves for p ($p = p_r - ip_i$) as a function of σ_c/s for several values of \widehat{K}_c with fixed $\sigma_o \approx 45.5'' \text{ yr}^{-1}$, $s = -18.85'' \text{ yr}^{-1}$ and $\alpha = 0.15$.

Figure 9 plots the predicted pole location for σ_c in the range: $-6.5'' > \sigma_c > -19'' \text{ yr}^{-1}$ due to both prograde and the retrograde terms and with $K_c = 6 \times 10^{-7} \text{ yr}^{-1}$. This fixed value of K_c

(again ignoring the potential dependence of K_c on the core nutation amplitude) was chosen such that the curve passes near the observed pole position at $\sigma_c = -18.5'' \text{ yr}^{-1}$. However, the required core friction parameter $K_c \simeq 6 \times 10^{-7}$ is a factor of $\sim 10^3$ smaller than $K_c(\text{turb})$ (see Eq. (28)) given that for this case the differential core-mantle obliquity is $\sim 1/\alpha$ larger than the forced mantle obliquity. Although this possibility presents an interesting physical limit, it can be safely discarded as irrelevant to Venus.

Finally consider the predicted range of obliquity damping rate (7.) for both Venus (figure 10) and Earth (figure 11) restricted to the contribution from a fluid core of arbitrary viscosity. The contributions to damping from toroidal shear driven by nutation include 1) turbulent friction (the dashed lines are based on Vanyo's experimental results), 2) thin laminar boundary layer friction and 3) whole body, Stokes shear. The peak in damping rate occurs when $K_c \simeq \sigma_c$. The difference in peak position and amplitude for Earth and Venus are due to the large difference in the frequency ratio σ_o/σ_c , the difference in rotation rate and core FCN frequency.

The obliquity growth or damping rate due to a solid tide in a viscous core is estimated using

$$-\frac{3n^2 M R^2 H_\odot}{4C\omega} \alpha \tilde{\gamma} \sum_{j=1}^3 \left(\frac{\frac{19}{2} \frac{\nu s_j}{\rho_c R_c g_c}}{1 + \left(\frac{19}{2} \frac{\nu s_j}{\rho_c R_c g_c} \right)^2} \right) \quad (61)$$

where the angular flexing rates s_j are $2n - 2\omega$, $2n - \omega$ and ω , respectively. The form inside the sum is appropriate to that of a uniform body and is proportional to Q^{-1} while $\tilde{\gamma}$ is the equivalent inviscid core love number (see eq. (45) and table 6 caption). Tidal shear of a viscous core can either cause damping or growth for Venus, depending on whether the viscosity favors either the semidiurnal s_2 tide ($s_j = 2n - 2\omega$) or diurnal K_1 tide ($s_j = \omega$), and because these three frequencies are well separated. The damping band is absent for Earth because the P_1 ($s_j = 2n - \omega$) and K_1 tide frequency are quite close and they almost cancel independent of core viscosity. However, Venusian obliquity damping requires a narrowly tuned core viscosity near $\sim 2 \times 10^{18} \text{ cm}^2 \text{ s}^{-1}$, while significant obliquity growth rates occurs over a much wider range of core viscosity and can achieve much higher peak magnitude. Also note that there is a wide range of core viscosity between the

two peaks where the core is effectively locked to mantle precession (and as far as this measurement is concerned, Venus' core appears solid) while at the same time has little effect on tidal flexing amplitude (and hence the Love number k_2) and thus appears liquid in response to tidal flexing.

6. Geophysical Consequences

The observed second harmonic gravity coefficient $J_2 = 4.46 \times 10^{-6}$ arises from three factors: 1) the CMB ellipticity $e_c = 3.9 \times 10^{-4}$, 2) surface topography with coefficient $r_{20} = -5.6 \pm 0.4 \times 10^{-5}$ [McNarnet et al., 1993], (and which may be partially compensated by a factor f ($0 < f < 1$)) and 3) an internal density anomaly $\rho_{20}(r)$ averaged over the mantle.

$$J_2 = -\frac{3}{5\bar{\rho}} \left(\rho_s(1 - f + fH)r_{20} + \int_{R_c}^R \rho_{20}r^4 dr \right) + \alpha \frac{\Delta\rho_c}{\bar{\rho}} \frac{C}{MR^2} e_c \quad (62)$$

The isostatic factor $H = 4d/R$ (for Airy or "iceberg" style compensation) depends on the depth of compensation d , which for Venus is ≤ 200 km. The correlation of topography and gravity is high except for the second harmonic coefficient. This seems to suggest that the factor f is close to 1 for degree n greater than 2, but small for degree 2. However, the explanation for the gravity-topography correlation ($n > 2$) which best fits the variation of admittance with harmonic degree is that of dynamic support [Kiefer et al., 1986] and which allows for an undetermined increase in viscosity with depth [Bills et al., 1987]

Despite the low spectral power in the gravity at degree 2, there is some tectonic evidence for hemispheric symmetry [Morgan and Morgan, 1991] or asymmetry [Suppe and Connors, 1992] in the large scale tectonic and non-crustal geoid patterns [Erickson and Phillips, 1992] which is nearly aligned with the rotation axis and may be due to an underlying second harmonic convection pattern.

Dynamic support implies a causal relationship between the boundary mass displacements and the counterbalancing density anomaly. To clarify this, replace the above expression with $J_2 = J_{2a} + J_{2\rho} + J_{2c}$, where the identification with each component is obvious. The relative ratio $\{J_2 : J_{2a} : J_{2\rho} : J_{2c}\}$ which satisfies observations and the above relationship is

$$\{4.5 : 18(1 - f) : -27 + 18f : 13.5\}. \quad (63)$$

Instead of a volumetric anomaly $J_{2\rho}$, consider an internal surface density anomaly at depth R_σ with contribution $J_{2\sigma}$. In a dynamic model in which $J_{2\sigma}(R_\sigma)$ drives convection, one expects that as R_σ approaches either boundary that the deformation of the opposite boundary, and the total J_2 vanishes [Richards and Hager, 1984]. For a simple earth model with uniform mantle density and viscosity and an anomaly $J_{2\sigma}$ near the CMB, the predicted values for the following ratios are (from figure 6a in Richards and Hager, 1984)

$$\frac{J_2}{J_{2a}} \simeq 0.7(1 - z); \quad \frac{J_2}{J_{2c}} \simeq 7z, \quad (64)$$

where $z = (R_\sigma - R_c)/(R - R_c)$. Applying this model to Venus suggests that the crustal compensation factor $f \sim 0.6$ and $z \sim 0.05$. Replacing the surface anomaly with a CMB boundary layer, volumetric anomaly will about double the required z for a boundary layer thickness of ~ 300 km. A thermal boundary layer ~ 200 K hotter the mantle above it and with ~ 100 km variations in its thickness could isostatically compensate for the ~ 1.3 km CMB topography. The inferred crustal factor should not be taken too seriously given the obvious simplifications of the model and the possibility that near surface contributions could dominate. However, the fact that the inferred boundary layer thickness is comparable to earth's D'' layer is very likely significant, and examining properties of earth's D'' obtained from a variety of sources suggests differences.

inversion of tomographic data for both density and boundary deformation initially predicted 2-6 km relief on the Earth's CMB [Hager *et al.*, 1985, Hager and Richards, 1989] implying that the nonhydrostatic $e_c \sim 1 \times 10^{-3}$. However, the observed, excess e_c is much smaller ($\simeq 1.2 \times 10^{-4}$) and is inferred from its effect on the retrograde annual nutation [Herring *et al.*, 1986, Gwinn *et al.*, 1986]. This result has been independently confirmed from analysis of the diurnal signatures in gravimetric data [Neuberg *et al.*, 1987]. A model to account for the decade scale changes in length of day via topographic coupling (fluid velocity induced pressure acting on the CMB topographic

“mountains”) predict length of day changes that are ~ 6 times larger than observed. Therefore, Hide *et al.* [1992] infer that CMB relief must be ~ 6 times milder. The tomographic data is explained by introducing topography and density contrast at the top of D'' . in order to satisfy convection model predictions (in fact, to allow the CMB to partially relax), the viscosity within D'' must be significantly lower [Hager and Richards, 1989] than the lower mantle viscosity. Applying the same train of argument to Venus suggests that Venus’ D'' layer is significantly stiffer than earth’s CMB boundary layer in order to maintain degree 2 bottom topography. This result will have a direct bearing on interpreting differences in convection style and heat flow from the core. For example, the large e_c and e_c/e_o ratio observed for Venus are potential indices of episodic convection [Turcotte, 1993] during the quiescent buildup stage. It may be, that in a geologic time sense, convective overturn is eminent.

7. Tidal Histories

How certain should we be that the obliquity has achieved its fully damped state? This question cannot be unequivocally resolved since both the initial rotation state and tidal models are insufficiently well known to recover a unique tidal history. However, one can investigate a wide range of models and determine a probable history. The most significant difference between this study and previous investigations is that the CMF model is more accurate and displays a rapid increase in strength as Venus approaches its present spin state. In addition, Venus can evolve from prograde to retrograde rotation, and initially large obliquities, for a special suite of initial conditions and atmospheric tidal models. To avoid further confusion, I should again emphasize that I have adopted the convention that the spin is negative and the present obliquity is small. An equally valid convention is to choose spin to be positive and obliquity near 180° .

The total CO is a sum of a quasi-rigid part due to internal strength and convection and a

hydrostatic part due to rotation:

$$e_o = e_o(\text{rigid}) + e_o(\text{hyd.}). \quad (65)$$

The changing hydrostatic contribution $e_o(\text{hyd.})$ as a function of rotation is approximately (assuming $C/MR^2 = 1/3$)

$$\begin{aligned} e_o(\text{hyd.}; T) &= \frac{39}{41} \frac{\omega^2 R}{g} \\ &= 6.7 \times 10^{-8} \left(\frac{\omega(T)}{\omega(\text{now})} \right)^2. \end{aligned} \quad (66)$$

and contributes only 0.5% to the total at the present. The core e_c similarly is made up of these two parts, and has $e_c(\text{hyd.}; T) \simeq 3/4 e_o(\text{hyd.}; T)$ for an earth-like core.

The ratio $\sigma_o/\sigma_c = 1.5(e_o/e_c)(n/\omega)^2$, and the hydrostatic contribution to oblateness due to rotation is small as long as the rotation period is $> 20\text{d}$. Since the contribution from CMF is proportional to $(\sigma_o/\sigma_c)^3 \omega$, the damping due to CMF was dramatically smaller when Venus' rotation period $= 2\pi/|\omega|$ was smaller, although this reduction can be partially counterbalanced by a change in e_o/e_c to more earth-like values $\sim 1/10$ during most of its history,

For large obliquity, the sum of solid tide phase lags in brackets defining the obliquity rate factor K_{tp} in eq.(14) should be replaced by [Dobrovolskis, 1978; appendix D]

$$\begin{aligned} &c_2^6 \delta(2n - 2\omega) + s_2^6 \delta(2n + 2\omega) + c_2^4 (2 - c_1) \delta(2n - \omega) + \\ &s_2^4 (2 + c_1) \delta(2n + \omega) - c_1^3 \delta(-\omega) - \frac{1}{2} s_1^2 c_1 \delta(-2\omega) + \frac{3}{4} s_1^2 \delta(2n) \end{aligned} \quad (67)$$

Here $c_j = \cos(\epsilon/j)$ and $s_j = \sin(\epsilon/j)$. For obliquity near 90° and $|\omega| \gg n$, all the terms either vanish or tend to cancel in pairs, except for the semiannual M_{ssa} term with lag $\delta(2n)$. The above angular dependence of K_{tp} for phases $\delta(s)$ which are constant and equal in magnitude and with $|\omega| \gg 71$ is

$$c_1 \left(1 + \frac{3}{4} s_1^2 \right) \delta(2n - 2\omega) + \frac{3}{4} s_1^2 \delta(2n) \quad (68)$$

The solid tide semiannual constituent ($\propto \delta(2n)$) always tends to drive the obliquity to the prograde state, However, we shall discover that the equivalent atmospheric term may dominate and can cause Venus to tidally evolve from a prograde to retrograde state if the initial obliquity is sufficiently large.

The tidal spin deceleration does not depend on the $\delta(2n)$ phase lag and is much less sensitive to obliquity for $|\omega| \gg n$ as long as the phase lags only weakly depend on frequency. The solid tide lag $\delta(2\omega - 2n)$ in (13) is replaced by

$$\begin{aligned} & c_2^8 \delta(2n - 2\omega) - s_2^8 \delta(2n + 2\omega) + \frac{1}{4} s_1^4 \delta(-2\omega) + \\ & \frac{1}{2} (c_2^4 s_1^2 \delta(2n - \omega) - s_2^4 s_1^2 \delta(2n + \omega) + s_1^2 c_1^2 \delta(-\omega)) \end{aligned} \quad (69)$$

for large obliquity. The above angular dependence of K_{ts} is

$$(5/8 + 3/4 c_1^2 - 3/8 c_1^4) \delta(2n - 2\omega) \quad (70)$$

for constant $\delta(s)$ and $|\omega| \gg n$. The atmospheric tides are modified in a similar manner with $\delta(s)$ replaced by $\delta_1(s)$. Note that $\delta P(s) \propto S^{-1}$.

The tidal equation for spin deceleration due to CMF is obtained from [Goldreich and Peale, 1970]

$$\frac{d}{dt} \omega_{CMF} = \omega \tan \epsilon \frac{d}{dt} \epsilon_{CMF}. \quad (71)$$

and is derived from the condition that the total component of spin momentum normal to the orbit $\cos \epsilon C\omega$ is conserved. This is not entirely obvious since what is really conserved, if no other planet except Venus is considered, is the sum of the orbital and spin momentum, of which the z component is

$$\cos I M n a^2 + \cos \epsilon C \omega. \quad (72)$$

The spin-orbit interaction couples the two parts, but one can show that this results in a variation in I that is, at most, a factor $\frac{C\omega}{Mna^2}$ smaller than that in ϵ , while the semimajor axis a is unaffected. Hence the above approximation [eq. 71] for the secular change in spin is quite accurate. The fact that $\cos \epsilon C\omega$ is nearly conserved once CMF begins to dominate implies that if the initial obliquity is large, the obliquity damping rate is initially proportional to ω^8 compared to a solid tide $\propto \omega^{-1}$.

Two additional modifications of the linearized equations must be included before obtaining tidal histories. First, the FMN frequency must be modified for large obliquity and is $\sigma_0 \cos \epsilon$. Second, I

have attempted to account for both rotationally induced oblateness and a more earth-like value for the ratio e_o/e_c during most of its history. Laminar CMF' begins to dominate over turbulent CMF' for Reynolds no. $\sim 10^{10} \sin^2 \epsilon (\omega_o/\omega(t))^3 < 10^5$, but this occurs in a regime where CMF' is already small compared to tides.

The relative rate of damping of obliquity and spin are shown in Fig. 12 for a suite of initial obliquities and an initial spin 30 times the present rate. A separatrix (dotted lines) delineates the two types of history: 1) Evolution from prograde to either prograde or retrograde orientation and 2) evolution from prograde to retrograde end state. The initial separatrix obliquity is $\sim 45^\circ$. This maximum can be reduced further either by starting the system with faster spin or, more controversial, by resonance excitation as suggested by Laskar and Robutel [1993]. Fig. 13 displays the history of the rate $\sigma_o \cos \epsilon$ for several of the lines which begin with prograde orientation. Note that these lines have a nearly flat history over a considerable range that happens to coincide with the frequency band -4 to $-8'' \text{ yr}^{-1}$. Thus it may be possible to chaotically drive the spin to high obliquity early in its tidal history via these resonance terms and allow the semiannual tide to drive it toward a retrograde state. It may be that temporal, stochastic variations in $e_o(\text{rigid})$ also are essential. Further study shall determine if evolution to a retrograde end state might be almost independent of initial conditions for a body like Venus.

The contribution of the semiannual tide is essential as demonstrated in Fig. 14 for which the semiannual contributions from both solid and thermal tides are omitted. It is not at all certain that this atmospheric component dominates throughout Venus' history or is unaffected by the changing dynamics arising from such factors as rotation.

However, the potential dominance of the atmospheric M_{ssa} tide does open the possibility that Venus may have started with a prograde rotation much like the other terrestrial planets. One can imagine a large impact on Venus which, unlike the proposed impact, creating the Earth-Moon system [e.g. Newsom and Taylor, 1989], dramatically tilted the spin axis to greater than $\sim 45^\circ$ and perhaps slowed the planetary spin to say 5-10d. A slow rotation guarantees that any debris disk

is inside synchronous rotation orbit (for Venus, a 5d synchronous radius $\simeq 20R$) and will tidally evolve any primordial satellite onto Venus [Ward and Reid, 1973].

These histories demonstrate the dramatic onset of turbulent CMF once the spin is sufficiently slow (≤ 3 times its present value). This result is quite different from other studies which fail to consider core ellipticity and find rapid evolution of both spin and obliquity due to CMF early in its history [Dobrovolskis, 1980; Shen and Zhang, 1989]. In any case, one should expect that the obliquity has presently attained near equilibrium if the spin has also achieved near equilibrium.

The last issue is the response time of the obliquity to ongoing changes in e_o/e_c , given that spin and obliquity have achieved near equilibrium. If e_o/e_c were halved, the spin equilibrium is unaffected, but the new equilibrium obliquity is increased by a factor of 8. The evolution of the obliquity is governed by $t = (1/K_{ta}) \ln |7x/8(1-x)|$, where $x = \epsilon(t)/\epsilon(\infty)$. Since $1/K_{ta} \sim 5 \times 10^7 \text{ yr}$ for the parameters chosen here, damping is reasonably rapid on a geologic timescale ($x = 0.9$ when $t = 2/K_{ta}$).

8. Obliquity Resonance

An alternative explanation for Venus' obliquity is that it may have recently passed through or is presently locked in a obliquity resonance arising from some very small orbital variations in inclination driven primarily by a fourth order ($e^2 J^2 \cos 2\omega$) interaction between Earth and Venus. The complex orbital perturbations in inclination have maximum amplitude $\sim 10^{-5}$, but can still produce significant obliquity perturbations as some terms have frequencies near the prograde FMN mode. Although such terms are formally included in modern theories of planetary quasi-secular perturbations, their amplitudes are significantly below usual cutoffs for published results. Fortunately, one can recalculate the dominant contribution with minimum effort. The method is described in appendix B. There are 8 primary modes affecting orbit eccentricity and inclination and when combined through the 2ω couple, These result in 288 distinct frequencies affecting the Venusian P variable.

The individual eigenmodes themselves decompose into several sidebands. Finally, the eigenfrequencies appear to wander by as much as $0.1'' \text{yr}^{-1}$ on time scales of order 10^8yr due to internal resonances which produce chaotic behavior. The amplitude, frequency and phase (epoch J2000) of the primary terms with amplitude greater than $\sim 1 \times 10^{-5}$ are listed in table 3, as are all terms with frequencies in range $44'' \text{yr}^{-1}$ to $47'' \text{yr}^{-1}$ and amplitude greater than 3×10^{-7} .

In order to analyze the nonlinear effect of these terms, we shall develop a slightly different formalism. Consider the secular part of the solar disturbing function R_{\odot} affecting obliquity.

$$R_{\odot} = \frac{1}{2} J_2 n^2 M R^2 (1 - e^2)^{-3/2} \left(\frac{3}{2} \cos^2 \bar{\epsilon} - \frac{1}{2} \right) \quad (73)$$

where the obliquity relative to the orbit $\bar{\epsilon}$ is related to the obliquity relative to the Laplacian plane ϵ and orbit inclination I by

$$\cos \bar{\epsilon} = \cos \epsilon \cos I + \sin \epsilon \sin I \cos(\Omega - \phi). \quad (74)$$

Replace $\sin I \cos \Omega$ and $\sin I \sin \Omega$ with the sum involving just the 2ω terms ($P(2\omega) = \sum I_j e^{-i\psi_j}$) and expand to first order in I_j . The resulting approximation is

$$R_{\odot} = -\frac{1}{2} \sigma_o \left(\cos^2 I \cos^2 \epsilon + \sin 2\epsilon \sum I_j \cos(\phi - \psi_j) - \frac{1}{3} \right) \quad (75)$$

Here, define σ_o as

$$\sigma_o = -\frac{3}{2} \frac{J_2 n^2 M R^2}{C\omega} (1 - e^2)^{-3/2}. \quad (76)$$

Consider the pair of canonical, action-angle variables $\{x, \phi\}$, where

$$x = C\omega(\cos \epsilon - 1). \quad (77)$$

The corresponding dynamical equations defining the motion are

$$\frac{d}{dt} \phi = -\frac{\partial}{\partial x} R_{\odot} = \frac{1}{C\omega \sin \epsilon} \frac{\partial}{\partial \epsilon} R_{\odot} \quad (78)$$

$$= \sigma_o \left(\cos^2 1 \cos \epsilon - \frac{\cos 2\epsilon}{\sin \epsilon} \sum I_j \cos(\phi - \psi_j) \right),$$

$$\begin{aligned} \frac{d}{dt}x &= \frac{\partial}{\partial \phi} R_{\odot} + \frac{d}{dt}x_s \\ &= \sigma_o \sin 2\epsilon \sum I_j \sin(\phi - \psi_j) + \frac{d}{dt}x_s \end{aligned} \quad (79)$$

and $\frac{d}{dt}x_s$ includes any secular torque due to tides or CMF. The equivalent equation for ϵ is

$$\frac{d}{dt}\epsilon = -\sigma_o \cos \epsilon \sum I_j \sin(\phi - \psi_j) + \frac{d}{dt}\epsilon_s \quad (80)$$

One reason for explicitly introducing the $\{x, \phi\}$ formalism is that determination of capture conditions is easily deduced from previous studies of orbit-orbit resonances in which a secular acceleration slowly drives the system toward exact commensurability. The primary deduction that can be applied is that capture mechanism relies substantially on the increase in x during the transition phase from circulation of the angle variable ϕ to libration of ϕ about a fixed point. Define ϵ_o as the mean *free* obliquity shortly before capture. Now the forced obliquity due to the retrograde terms in orbital P already considered might be larger than this value. However, these terms should not be a significant factor given the large difference in circulation frequencies associated with this forced part and the prograde FMN mode.

In order to make a more direct connection with orbit-orbit resonance studies, consider the following set of transformations which result in a dimensionless Hamiltonian. Assume that only a single term with driving frequency $\frac{d}{dt}\psi_k$ in the expansion of the orbit variable P affects Venus' figure. First, define \tilde{t} , $\tilde{\phi}$, \tilde{x} and $\tilde{\epsilon}$ as

$$\tilde{t} = t\sigma_o^{-1} \quad (81)$$

$$\tilde{\phi} = \phi - \psi_k, \quad (82)$$

$$1 - \tilde{x} = \frac{x}{C\omega(\cos \epsilon_o - 1)} \simeq \frac{-2x}{C\omega\epsilon_o^2} \simeq \frac{\sin^2 \epsilon}{\sin^2 \epsilon_o}, \quad (83)$$

$$\tilde{c} = 1 - \sigma_o^{-1} \frac{d}{dt} \psi_k. \quad (84)$$

The Hamiltonian H and dynamical equations are

$$H = \frac{1}{2} \left(\tilde{x} + c(t) \right)^2 - 4I_k \epsilon_o^{-3} \sqrt{1 - \tilde{x}} \cos \tilde{\phi}, \quad (85)$$

$$\frac{d}{dt} \tilde{\phi} = - \frac{\partial}{\partial \tilde{x}} H, \quad (86)$$

$$\frac{d}{dt} \tilde{x} = \frac{\partial}{\partial \tilde{\phi}} H. \quad (87)$$

This form is identical to that derived by Yoder(1974) (also see Peale, 1976 and Yoder and Peale, 1981). I find that unit capture probability ($P_c = 1$) occurs if the coefficient $4I_k \epsilon_o^{-3} = 2/\sqrt{54}$. Define a critical ϵ_c ,

$$\epsilon_c = \sqrt{6} |I_k|^{1/3}, \quad (88)$$

Then one finds that $P_c = 1$ for $\epsilon_o < \epsilon_c$ and $P_c < 1$ for $\epsilon_o > \epsilon_c$. Capture probability falls off rapidly for ϵ_o near ϵ_c . For example, $P_c \simeq 0.25$ for $\epsilon_o = 1.4 \epsilon_c$. For $\epsilon_o \gg \epsilon_c$,

$$P_c \simeq \frac{2}{\pi} \sqrt{\frac{4I_k}{\epsilon_o^3}} = 0.33 \left(\frac{\epsilon_c}{\epsilon_o} \right)^{3/2} \quad (89)$$

Only four terms within the expected frequency band have ϵ_c comparable or larger than ϵ_o (see table 3). The numerous driving terms which have $I_k \leq 1 \times 10^{-6}$ can be expected to have almost no influence on Venus' obliquity.

Next construct the approximate second order equation obtained by taking the time derivative of the $\frac{d}{dt} \phi$ equation and retaining only the major second order terms in I_j .

$$\begin{aligned} \frac{d^2}{dt^2} \phi + \sigma_o^2 \sin \varepsilon B(\tilde{\phi}) \sum I_j \sin(\phi - \psi_j) \\ = \cos \varepsilon \frac{d}{dt} \sigma_o + \omega \sin \varepsilon \frac{d}{dt} \varepsilon_s. \end{aligned} \quad (90)$$

with

$$B(\tilde{\phi}) = \left[1 + \frac{1}{\sin^3 \varepsilon} \sum I_j \cos(\phi - \psi_j) \right] \quad (91)$$

The term proportional to $\frac{d}{dt} \sigma_o$ includes changes in spin, J_2 or orbital eccentricity of whatever origin"

Again, consider the case where a single driving frequency- ω dominates and $\frac{d}{dt} \phi \simeq \frac{d}{dt} \psi_k$. If the lock is established, the libration amplitude is small, and the secular torques are relatively small, then the angle $\tilde{\phi}$ oscillates about 0 with libration frequency f_k ,

$$f_k = \sigma_o \sqrt{B(0) \sin \varepsilon I_k}. \quad (92)$$

Using $I_k = 3.0 \times 10^{-5}$, $\varepsilon = 2.1^\circ$ and $\sigma_o = 44.22'' \text{ yr}^{-1}$, then $B(0) = 1.6$. The libration frequency $f_k = 1.3 \times 10^{-4} \sigma_o = 0.058'' \text{ yr}^{-1}$, corresponding to a libration period of $22 \times 10^6 \text{ yr}$.

Next, consider the stability of the potential lock against, secular torques. Clearly,

$$\sigma_o^2 \sin \varepsilon I_j \geq \cos \varepsilon \frac{d}{dt} \sigma_o - \omega \sin \varepsilon \frac{d}{dt} \varepsilon_s \quad (93)$$

to prevent the secular terms from sweeping the figure node angle right through a given resonance.

The individual constraints in terms of relative importance for the 4)Z4S111 argument are

$$\begin{aligned} \left| \frac{d}{dt} J_2 \right| &\leq 1 \times 10^{-15} \text{ yr}^{-1}, \\ \left| \frac{1}{\sin \varepsilon} \frac{d}{dt} \varepsilon_s \right| &\leq 2 \times 10^{-7} \text{ yr}^{-1}, \\ \left| \frac{1}{\sigma_o} \frac{d}{dt} \sigma_o \right| &\leq 2.4 \times 10^{-10} \text{ yr}^{-1}, \\ \left| \frac{1}{\omega} \frac{d}{dt} \omega \right| &\leq 2.4 \times 10^{-10} \text{ yr}^{-1}. \end{aligned} \quad (94)$$

The constraint on spin rate might be exceeded if atmospheric and tidal torques are not in balance. The solid tide rate is $1.1 \times 10^{-8}/Q \text{ yr}^{-1}$ and exceeds the above bound if $Q \leq 80$ if we ignore contributions from the atmosphere. Clearly, because of this constraint and the small

magnitude of ε_0 for unit capture, these 2ω interactions will not have a significant effect until Venus is nearly damped to its equilibrium state in both spin and obliquity.

The constraint on obliquity rate comes into play only if CMB is dominant and $e_c \leq 17e_0$. Note that this bound is a factor of 1.7 smaller than the estimate based on the balance argument. For the resonant excitation to play any role, then $e_c > 17e_0$ and we are forced again to accept a large CMB ellipticity.

The constraint on σ_0 limits the amount that the precession rate could change without dominating over the largest 2ω interaction to about $\pm 1'' \text{yr}^{-1}$ over $1 \times 10^8 \text{yr}$ time scale. Thus, only nearby sidebands might have excited a significant obliquity.

The constraint on the J_2 rate is the most serious and implies that a lock is possible only if Venus is now tectonically quiescent. For example, if tectonic activity on Venus is episodic on time scales of $3 - 5 \times 10^8 \text{yr}$, then one might expect that J_2 varies by a factor of 2 (larger or smaller) over the same time period. Thus we might expect that the present rate is of order $5 - 15 \times 10^{-14} \text{yr}^{-1}$ in amplitude or a factor of 5 -- 15 larger than the above bound. Since the obliquity damping time scale $\leq 30 \times 10^6 \text{yr}$ due to CMB, Venus obliquity can retain a significant remnant from a temporary lock only for those terms within $\pm 1'' \text{yr}^{-1}$ of the present value for σ_0 . The frequencies which might have been encountered since the last resurfacing event must be considered are extended to $43'' \text{yr}^{-1} \leq f_k \leq 47'' \text{yr}^{-1}$. Figure 6 shows the amplitude of terms within this range, and we can see that the number of significant resonance lines are relatively sparse.

Consider the case where $\frac{d^2}{dt^2}\phi$, on average, vanishes. The secular equation for the obliquity is

$$\frac{d}{dt}\epsilon = \frac{1}{\sigma_0} \cot \epsilon \frac{d}{dt}\sigma_0 \quad (95)$$

and obliquity increases if J_2 increases or spin decreases in magnitude. If Venus is presently locked with the ψ_{243111} argument (no. 29), then an increase of only $0.03'' \text{yr}^{-1}$ in σ_0 could account for the observed obliquity. If $dJ_2/dt \simeq 2 \times 10^{-16} \text{yr}^{-1}$, and this is the only mechanism for secular change then the lock would be only $15 \times 10^6 \text{yr}$ old. Another possibility is the chaotic wander of

the $\frac{d}{dt}\psi_{243111}$ frequency could itself excite the observed obliquity.

9. Numerical integrations

Numerical integration of the dynamical equations has been performed, covering a wide range of initial conditions, tidal torques and changing J_2 . The purpose of this exercise is to show explicitly when the prograde rate terms are important and show what kind of conditions could account for the observed obliquity. There are two interesting limits: 1) The maximum CMF torque which can compete with resonance without totally overwhelming it. 2) The conditions for excitation for the case where the iron core is completely solid and the combined solid and atmospheric K_{ta} is negative. In order to compare numerical integrations with the present-day phase and amplitude of the free obliquity, the equations are integrated in the rotating frame of the near resonant driving frequency, $d\psi_j/dt$. Resonance passage occurs where $d\phi/dt - d\psi_j/dt$ reverses sign and can change the amplitude and phase of the free obliquity which is fixed relative to this frame. The p_x and p_y variables in this frame are

$$\begin{aligned} p_x &= \sin \epsilon \sin(\phi - \frac{d\psi_j}{dt}t), \\ p_y &= \sin \epsilon \cos(\phi - \frac{d\psi_j}{dt}t). \end{aligned} \quad (96)$$

The only limitation is that non-resonant terms will generate small oscillations whose phases do not match those of the present day, but one can visually adjust for their contribution. The following pair of equations omit the FCN mode as it damps so rapidly and are accurate for small obliquity variations.

$$\begin{aligned} \frac{d}{dt}p_x &= - \left(\sigma_o \cos \epsilon - \frac{d}{dt}\psi_j \right) p_y + K_{ta} \left(1 - \frac{\sin \epsilon}{\sin \epsilon_o} \right) p_x \\ &\quad - \sigma_o \sum_j I_j \sin \left(\frac{d}{dt}\psi_j t - \psi_j \right), \end{aligned} \quad (97)$$

$$\begin{aligned} \frac{d}{dt}p_y &= \left(\sigma_o \cos \epsilon - \frac{d}{dt}\psi_j \right) p_x + K_{ta} \left(1 - \frac{\sin \epsilon}{\sin \epsilon_o} \right) p_y \\ &\quad - \sigma_o \sum_j I_j \cos \left(\frac{d}{dt}\psi_j t - \psi_j \right). \end{aligned} \quad (98)$$

Only the near resonant terms shall be included in the sum over I_j terms: ($8 \leq j \leq 59$ in table 3), although their inclusion does not significantly change any result. Coupling to the retrograde

orbit terms and the eccentricity variations shall also be ignored. First, the effect of the retrograde P terms (see table 2) is only 0.0063 in a time average sense and should have a small effect on the prograde terms. Second, a factor of $(1 + 3/2e^2 - \sin^2 I)$ which should multiply σ_o has been omitted. The time average of this factor is $(1 + (12.7) \times 10^{-4})$ and changes σ_o by only $0.02'' \text{ yr}^{-1}$. Periodic variations in this factor are also relatively insignificant, even though they could couple to near resonant prograde terms.

First consider the case where the core friction equilibrium obliquity is progressively decreased. Figure 15 shows a numerical integration covering 750myr with $\sin \epsilon_o = 0.024$ or $2/3$ of the observed free obliquity. The system evolves from $\sigma_o = 43.8'' \text{ yr}^{-1}$ to $45.4'' \text{ yr}^{-1}$ after 750myr by introducing the constant rate $d \ln J_2 / dt = 5 \times 10^{-11} \text{ yr}^{-1}$. Panels 15b, c and d show $\{p_x(\psi_{\tilde{j}}), p_y(\psi_{\tilde{j}})\}$ histories during passage for the term no. $\tilde{j} = 29, 42$ and 48 , respectively. In panel 15b, the curve happens to cross the observed pole location (diamond) at $t = 176 \text{ myr}$ before passage and after passage at $t = 306 \text{ myr}$. Panel 15c, corresponding to $\psi_{243114} = 44.502'' \text{ yr}^{-1}$, passes near the pole for a few oscillations after passage, before decaying away for $t > 400 \text{ myr}$. Panel 15d displays that a pole crossing can occur just before passage and after passage, and perhaps for one oscillation thereafter.

Next decrease ϵ_o to $\sin \epsilon_o = 0.012$. Passage through ψ_{243111} (see panel 16b) does excite a large amplitude obliquity of 0.06 rad , but it decays so rapidly that the curve fails to pass through the pole location. Panel 16c shows that the evolution due to no. 42. does almost cover the pole location, partly due to the favorable phase of term no. 42 and non-resonant oscillations. Figure 17 displays an integration with $\sin \epsilon_o = 0.008$. We can safely conclude that resonant excitation can relax the constraint on core friction such that the equilibrium ϵ_o is reduced by *no more* than a factor of 2-3. This, in turn, reduces the required core ellipticity by a factor of only 1.25 to 1.5 since from eq.[55] the factor $\sin \epsilon_o (\epsilon_o / \epsilon_c)^3$ is fixed. See Fig. 18 for results with negative dJ_2 / dt .

The positive rate chosen for J_2 allows for only a small fractional change of 0.03 in J_2 over the 750myr integration, which is longer than the 300-500myr estimate of the last resurfacing event. A significantly larger J_2 rate might push evolution so fast that the resonances have substantially

less effect. Figures 19 and 20 display histories in which $\sin \epsilon_0 = 0.024$ and $d \ln J_2/dt$ is 4×10^{-10} and $-4 \times 10^{-10} \text{ yr}^{-1}$, respectively. The largest resonance term dominates and helps to wash out the effect of nearby terms. The large, positive J_2 rate also helps to retain memory of the ψ_{243111} excitation to larger σ_0 , which is within the model bound. This, in turn, suggests that ϵ_0 might be reduced by a factor of 2 or less for some narrow range of σ_0 within the bound. The history with negative J_2 rate produces a weaker response, partly because capture into permanent resonance is physically impossible.

So far, we have ignored the fact that the driving frequencies and amplitudes vary slightly over time. Fig. 21 shows the histories of 4 combinations of the primary frequencies, based on Laskar's [1990] FFT analysis covering a 200myr integration into the past. Unfortunately, equivalent histories of the amplitudes (and phases) are not displayed by Laskar, and so the following integrations are somewhat qualitative. Furthermore, I have assumed that the curves are flat over the past 15myr, partly due to uncertainty of the time interval of averaging and partly to allow some leeway in attempting to match the excitation with the present day pole location. The adjustable parameter for this suite of integrations is the present day value (here $t=0$) for σ_0 , and we shall search for histories which cover the pole at some time during the last 15myr.

I adopt here a negative $K_{ta} = -1 \times 10^{-8} \text{ yr}^{-1}$ which might be justified by assuming that the core is a Maxwell solid with large core viscosity $\sim \mu_c / \rho_c \omega \sim 2 \times 10^{18} \text{ cm}^2 \text{ S}^{-1}$ such that core tidal flexing is the primary source of 'solid friction' (see figure 10). The exact value is chosen such that solid friction has a strong inverse frequency dependence in the tidal band to counterbalance a similar, but necessarily weaker dependence in the atmosphere. The point is that a large positive value $\sim 1 \times 10^{-8} \text{ yr}^{-1}$ should have increased obliquity to even larger values than observed and hence is not acceptable (see figure 26 b). Another and perhaps more plausible alternative is that the core viscosity is near $10^6 \text{ cm}^2 \text{ s}^{-1}$ such that toroidal shear is the dominant damping mechanism (again, see figure 10). This requires that the core is only in the initial stages of solidification and is at this point in time a thick slurry. However, I shall set the toroidal coupling parameter $K_c = 0$

since for core viscosities $\geq 1 \text{ cm}^2\text{S}^{-1}$ this parameter is nearly independent of obliquity, much like K_{ta} . Finally I adopt a small $d \ln J_2 / dt = 1 \times 10^{-12} \text{ yr}^{-1}$. A rate $|d \ln J_2 / dt| \geq 2 \times 10^{-11} \text{ yr}^{-1}$ will dominate the chaotic variations.

Figures 22 and 23 display excitations for two of the more isolated lines with arguments ψ_{233151} and ψ_{234131} , respectively. The three panels in each case bracket the maximum excitation resulting from adjusting the end value for $\sigma_o(0)$. The middle panel shows a case which happens to cover the observed pole during the end stages of the integration (That is, the last 15myr). The width (represented by the outer panels) tends to scale with the square root of the driving amplitude. Also, there are only 1 or 2 values for $\sigma_o(0)$ which result in pole crossings in the last 15 myr of the integration.

Obviously, the largest term with frequency $44.223'' \text{ yr}^{-1}$ must be able to excite a large obliquity, and the model excitation is much more sensitive to initial conditions than the other terms considered. Figure 24 plots the history for $\sigma_o(0) = 44.3555'' \text{ yr}^{-1}$ where the curve passes close to the pole several times (panel a) during the last 50myr, and panel 23b with $\sigma_o(0) = 44.3600'' \text{ yr}^{-1}$ where no crossings occur. Increasing or decreasing $\sigma_o(0)$ by as little as $0.005'' \text{ yr}^{-1}$ results in a substantially smaller or larger excitation at the end, respectively.

Of the three lines well inside the predicted band for $\sigma_o(0)$, the excitation resulting from the ψ_{243141} argument with present day frequency $44.502'' \text{ yr}^{-1}$ is the broadest. In fact, there are several values for $\sigma_o(0)$ in the range $44.42'' \text{ yr}^{-1}$ to $44.56'' \text{ yr}^{-1}$ which result in pole crossings near the present. Panel 25a displays an excitation which almost matches the pole location at $t = -1 \text{ myr}$. Panel 25b graphs a case with slightly larger $\sigma_o(0)$ and only modest excitation.

I wish to emphasize that these model integrations are sensitive to several parameters, especially the adopted damping factor K_{ta} . Figure 26a shows an integration identical to 25a except that K_{ta} is changed from $-1 \times 10^{-8} \text{ yr}^{-1}$ to $-3 \times 10^{-8} \text{ yr}^{-1}$. This increase in magnitude is sufficient to completely damp the major excitation which occurs near $T \sim -11 \text{ Omyr}$ to an uninteresting obliquity amplitude at the present. This increase in K_{ta} narrows or eliminates significant excitations from

passage through **any of these** lines. If the model with high viscosity **toroidal** damping is the most plausible damping mechanism, then the allowed **range** for $\nu \sim 10^6 \text{ cm}^2 \text{ s}^{-1}$ is narrow.

Clearly, **the** chaotic orbital variations are enough to account for the observed obliquity, and it may not represent an equilibrium state. The primary limitation of this hypothesis is the very narrow range of $\sigma_o(0)$ where this mechanism can account for both amplitude and phase *and* the small $d \ln J_2 / dt$ rate.

Consider the range of $\sigma_o(0)$ for which **the** excited obliquity amplitude is equal to or larger than observed amplitude without regard to phase. The **range** of $\sigma_o(0)$ which satisfy this less restrictive constraint is

$$\begin{aligned}
 43.80 < \sigma_o(0) < 44.335'' \text{yr}^{-1} \\
 44.42 < \sigma_o(0) < 44.37 \\
 44.65 < \sigma_o(0) < 44.77 \\
 45.23 < \sigma_o(0) < 45.26
 \end{aligned}
 \tag{99}$$

Given that the plausible range for $\sigma_o(0)$ is: $44.2 < \sigma_o < 45.6'' \text{ yr}^{-1}$, (here, I have biased σ_o downward by $\sim 0.5\%$ to allow for a colder Venus) , a large excitation is observed over about 30% of this range. Thus, chaotic excitation is a plausible explanation, but still not quite as compelling as any involving core friction.

10. Summary

The principal result here is that we now have two plausible explanations for Venus' nonzero free obliquity $\simeq 2.1'$. The first **and** least constrained hypothesis predicts that Venus' obliquity (like its spin) has achieved steady state due to a large **CMB** oblateness $e_c \simeq 4 \times 10^{-4}$, which modulates the usually dominant **CMB** friction. The second option is that small, near resonant excitations maintain the free obliquity. The first mechanism is qualitatively rigorous despite possible shortcomings related to the estimate of the turbulent core friction coupling **constant**, uncertainties in atmospheric

thermal tide modeling and Venus core size, even resonant excitation, all of which might conspire to reduce the inferred CMB oblateness by at most $1/2$ to $1/3$. The inferred Venusian core oblateness is equal or greater than Earth's nonhydrostatic core oblateness, and is consistent with dynamic compensation within a D'' thermal boundary layer that is quite possibly much stiffer than earth's D'' . This result should provide an important constraint on Venus' mantle convection that must be accounted for in any detailed model,

If Arkani-Hamed and Toksöz' [1984] deductions concerning core solidification are valid, then obliquity excitation should be due to the chaotic variations in the orbital plane motion. The only limitation on this alternative hypothesis is the small range of present day values for σ_0 which produce the appropriate excitation compared to the uncertainty in this parameter.

Venus' core was certainly liquid before the last great resurfacing event and hence core friction should have had a major influence on Venus' tidal history. I find that core ellipticity dramatically shifts the timing of strong CMF friction to the end stages of tidal evolution. Finally, the atmospheric semiannual M_{ssa} constituent, if strong throughout history, can roll over Venus from prograde to retrograde rotation. One interesting avenue of future research is to examine the role of resonance passage in altering the range of tidal histories. Specifically, can resonance excitation help or hinder Venus' roll-over from prograde to retrograde orientation? Could retrograde rotation be almost inevitable?

One means of resolving which of the two hypotheses is correct is through measurement from orbiting spacecraft or landers such factors as 1) Love numbers k_2 and h_2 , 2) precession rate σ_0 (and hence moment of inertia) and 3) the 1mbar surface air pressure variations to better model the atmospheric thermal tide (and effectively determine the solid tidal Q). The predicted pole rate (for the p variable) is $1.1'' \text{yr}^{-1}$ or about 32m/yr drift for a lander at Venus' north pole. Of these three parameters, possibly the most valuable and assessable is k_2 . Earth's effective k_2 (including oceans) is presently known to about a part in 500. A 10% determination of Venusian k_2 should settle the issue concerning the core's fluidity given that $0.23 < k_2(\text{fluid core}) < 0.29$ while $k_2(\text{solid core}) \simeq 0.17$.

The Venusian tidal potential acting on a satellite is $k_2 GM_\odot R^5 (3/2 \hat{\mathbf{r}}_s \cdot \hat{\mathbf{r}}_\odot - 1/2) / (r_\odot r_s)^3$. Consider the largest Doppler velocity signal from a polar orbiting satellite near the planet and in a circular orbit. That part which is distinct from Venusian gravity perturbations can be derived using standard techniques [e.g. Plummer, 1960] and is

$$\begin{aligned} \delta v_s &= -\frac{3}{2} k_2 H_\odot v_s \left(\frac{R}{a_s} \right)^2 \sin 2\lambda_s \cos 2(\lambda_\odot - \Omega_s) \\ &\simeq -0.5 k_2 \sin 2\lambda_s \cos 2(\lambda_\odot - \Omega_s) \text{mm/s} \end{aligned} \quad (100)$$

The 0.1mm/s Doppler signal is largely radial and separable because of its dependence on solar longitude λ_\odot . Magellan X-band tracking accuracy for 60s compressed data is also 0.1mm/s [Konopliv *et al.*, 1993]. Geometrical effects and correlations may further reduce sensitivity to the tidal signal. Still, it may be possible to dig into the noise a factor of 2-10. Even if this experiment fails to produce a useful result, it does show that a future Venusian mission should and can attack this measurement with a high probability of success.

11. Appendix A: Venusian Structure Models

A suite of structural models for density ρ , rigidity μ and compressibility K have been constructed using Earth's known profile for each of these parameters as a basis. First, a simple earth model (PEM; Dziewonski *et al.*, 1975) has been converted from profiles in radius to profiles in terms of pressure. The basic idea is that Venusian structure will closely mimic Earth's if expressed in terms of pressure (except for shifts in phase boundaries such as the CMB), and that any differences in mantle parameters result from nearly uniform compositional differences or temperature offsets, to first order. A more primitive earth model has been chosen to sidestep second order issues related to complex boundary layers (e. g. D"), or the existence or absence of such features as a low velocity zone. The crustal - lithospheric components are simplified and include 1) a 20 km thick crust with density 2.85 g/cc and 2) a thermal transition zone which is matched with an earth-like profile at 30kbar pressure. Variations due to composition or temperature differences can then be estimated as scale changes to be applied to the PEM model. Variations in upper mantle composition [Basaltic Volcanism Study Project, 1981; Jeanloz and Thompson, 1983] shall be modeled using the molar fractions of forsterite Mg_2SiO_4 and fayalite Fe_2SiO_4 as the representative parameter.

The molar masses and volumes for the α , β , and γ crystalline phases of fayalite and forsterite are [Sumino, 1979; Jeanloz and Thompson, 1983]

$$\begin{aligned} M_{Fo} &= 140.69 \text{ g/mole}; M_{Fa} = 203.77 \text{ g/mole}; \\ (\alpha)V_{Fo} &= 43.67 \text{ cc/mole}; V_{Fa} = 46.27 \text{ cc/mole}; \\ (\beta)V_{Fo} &= 40.52 \text{ cc/mole}; V_{Fa} = 43.22 \text{ cc/mole}; \\ (\gamma)V_{Fo} &= 39.65 \text{ cc/mole}; V_{Fa} = 42.02 \text{ cc/mole}. \end{aligned} \tag{101}$$

Define f_{Fo} as the molar fraction of mantle which is Mg rich and adopt $f_{Fo} = 0.89$ as the nominal value for Earth. Therefore the fractional change in an earth-like mantle density ρ_m due to different

f_{Fo} is

$$F_{\rho_m}(f_{\text{Fo}}) = \frac{1 + 0.427(f_{\text{Fo}} - 0.89)}{\Gamma - y(f_{\text{Fo}} - 0.89)} \quad (102)$$

where $y = 0.059$, 0.066 and 0.059 for the α , β and γ phases, respectively. The uncertainty in the molar volume of the β phase is such that the y factor could be the same as the other two phases, and therefore I adopt $y = 0.059$ for each phase. Candidate Venusian mantles with different f_{Fo} are obtained by multiplying the nominal earth model without regard to temperature or pressure changes in molar volumes. One justification for this approximation is that the change in mantle compressibility is about $\pm 0.8\%$ for a change in f_{Fo} of $\pm 10\%$.

Changes in rigidity and compressibility due to composition are determined from compositional ratios $F_{\mu}(f_{\text{Fo}})$ and $F_K(f_{\text{Fo}})$, respectively. A first order estimate of the temperature and pressure dependence of forsterite [Kumazawa and Anderson, 1969]] and fayalite are included in this modelling and for the α phase are (units are Mbars)

$$\begin{aligned} \mu_{\text{Fo}} &= 0.881 - 0.130 \frac{T}{10^3 K} + 1.80 P_r \\ \mu_{\text{Fa}} &= 0.509 - 0.075 \frac{T}{10^3 K} + 0.70 P_r \\ K_{\text{Fo}} &= 1.286 - 0.150 \frac{T}{10^3 K} + 5.00 P_r \\ K_{\text{Fa}} &= 1.380 - 0.228 \frac{T}{10^3 K} + 5.00 P_r \end{aligned} \quad (103)$$

except that I adopt a value of 5 for the pressure derivative of the bulk modulus for both materials. From Jeanloz and Thompson's table 1, I adopt for the β phase a zero pressure bulk modulus of 1.67 Mbar, and for the γ phase: a zero pressure $K_{\text{Fo}} = 2.13$ Mbar and $K_{\text{Fa}} = 1.97$ Mbar. Otherwise the above expressions are assumed to hold for each phase.

Here, I adopt a very simple temperature profile for Venus to determine the thermal changes with depth for above parameters, namely that at 30 kbar pressure, the temperature is 1800° C and increases linearly with pressure, attaining 3000° C at 1 Mbar.

Finally, I use the arithmetic mean of the Hashini-Shtrikman bounds for a two component

mixture to estimate the variation due to changes in f_{Fo} . The explicit expressions for the rigidity are [Hashim, 1983]

$$\mu_1 = \mu_{\text{Fo}} + \frac{(1 - f_{\text{Fo}})V_{\text{Fa}}}{\frac{1}{(\mu_{\text{Fa}} - \mu_{\text{Fo}})} + \frac{\frac{2}{5}f_{\text{Fo}}V_{\text{Fo}}(K_{\text{Fo}} + \frac{6}{3}\mu_{\text{Fo}})}{\mu_{\text{Fo}}(K_{\text{Fo}} + \frac{4}{3}\mu_{\text{Fo}})}}, \quad (104)$$

$$\mu_2 = \mu_{\text{Fa}} + \frac{f_{\text{Fo}}V_{\text{Fo}}}{\frac{1}{(\mu_{\text{Fo}} - \mu_{\text{Fa}})} + \frac{\frac{2}{5}(1 - f_{\text{Fo}})V_{\text{Fa}}(K_{\text{Fa}} + \frac{6}{3}\mu_{\text{Fa}})}{\mu_{\text{Fa}}(K_{\text{Fa}} + \frac{4}{3}\mu_{\text{Fa}})}}, \quad (105)$$

$$\mu(f_{\text{Fo}}) = \frac{1}{2}(\mu_1 + \mu_2), \quad (106)$$

while the factor $F_{\mu}(f_{\text{Fo}}) = \mu(f_{\text{Fo}})/\mu(0.89)$. A change in f_{Fo} of 5% changes $F_{\rho_m}(f_{\text{Fo}})$ by $F_{\mu}(f_{\text{Fo}})$.

The lower mantle is modeled as a combination of the individual oxides, FeO, MgO [Jackson et al, 1978] and SiO₂ [Mizutani et al, 1977, 2].

$$\begin{aligned} K_{\text{FeO}} &= 1.82 \text{ Mbar} \\ \mu_{\text{FeO}} &= 0.59 \text{ Mbar} \\ K_{\text{MgO}} &= 1.63 \text{ Mbar} \\ \mu_{\text{MgO}} &= 1.31 \text{ Mbar} \\ K_{\text{SiO}_2} &= 3.46 \text{ Mbar} \\ \mu_{\text{SiO}_2} &= 1.30 \text{ Mbar} \end{aligned} \quad (107)$$

The effect of pressure on molar volume is obtained from the Birch-Murnaghan equation (with $dK/dP_r = 4$ for each oxide)

$$P_r = \frac{3}{2}K\left(\frac{V_0}{V(P_r, T)}\right)^{5/3} \left[\left(\frac{V_0}{V(P_r, T)}\right)^{2/3} - 1 \right]. \quad (108)$$

The density and elastic parameters of the equivalent compounds 2FeO+SiO₂ and 2MgO+SiO₂ are calculated using the Hashim-Shtrikman relations. These compounds are then combined again, using the molar fraction f_{Fo} to determine composition and material properties. The corresponding density factor is almost identical to the upper mantle expression.

A suite of candidate models has been constructed for different core radii in range 2700 km $\leq R_c \leq 3600$ km and molar fraction in range $0.79 \leq f_{\text{Fo}} \leq 0.99$. The variations of the scale factors F_μ , F_κ and F_ρ within the mantle are shown in Fig(27). Core density is adjusted by a constant value $\delta\rho_c$ to match the mean density, using

$$\rho_{\text{core}}(P_r) = \rho_{\oplus\text{core}}(P_r) + \delta\rho_c \quad (109)$$

Table 6 lists core radii and mean core density, $\delta\rho_c$, core and whole body moment of inertia and tidal Love numbers for a limited suite of models. The second degree elastic deformation of Venus due to tides is obtained for the same suite of models and is expressed in terms of Love Numbers, k_2 , h_2 and l_2 , where h_2 and l_2 are coefficients of the radial and lateral deformation, respectively [e.g. Saito, 1974].

To simplify the two point boundary problem, I first fit the core density to a quadratic, polynomial in radius $x = r/R_c$ and obtain an approximate solution for the core potential Φ and determine the ratio $x d\Phi/dx/\Phi$ at the CMB. Knowing this ratio enables a straightforward description of CMB boundary conditions in terms of *mantle* potential, stress and displacement.

Venera x-ray analysis of surface rocks indicate an earth-like basaltic composition, and therefore a plausible range for the molar fraction is $\pm 5\%$. Earth's solid core is only about 0.6g/cc more dense than the liquid phase and this increase ~~is~~ results from both freezing and partition of pure iron into the inner core. A larger fraction of alloying material such as sulfur or oxygen could decrease core density. Even if this process were sensitive to pressure, it is difficult to imagine that core density could be decreased by more than 5%. The bounded areas indicate the most plausible range for moment of inertia, and Love number k_2 based on the constraints,

$$\begin{aligned} 0.84 \leq f_{\text{Fo}} \leq 0.94; \\ |\delta\rho_c| \leq 0.6\text{g/cc}. \end{aligned} \quad (110)$$

These limits constrain the following parameters to the range

$$\begin{aligned}
0.331 &< \frac{C}{MR^2} < 0.341 \\
0.04 &\geq \frac{C}{MR^2} > 0.020 \\
0.290 &\geq k_2 \geq 0.230
\end{aligned}
\tag{111}$$

The range obtained for C obtained by the *Basaltic Volcanism Study Project* is quite close to the above bounds,

$$0.325 \leq \frac{C}{MR^2} \leq 0.340, \tag{112}$$

(from table 4.5.11 on p 684) and a value near 0.329 is preferred.

Within the context of this single parameter f_{Fo} , it is curious that k_2 happens to be a better proxy for core density rather than core moment of inertia or core radius. The ability to use this correlation to infer core density from a measurement of k_2 depends in part on our confidence that mantle rigidity profile closely mimics that of Earth.

If the iron core were completely solid, then we should expect a significant reduction in the tidal Love numbers, as indicated in table 6. In fact, k_2 is also an excellent test for distinguishing between a completely solid core and a core with, at least, a liquid outer layer.

12. Appendix B: **Prograde** Orbital Variations in Orientation Due to the 2ω Interaction

An alternative explanation for Venus' obliquity is that it may have recently passed through or is presently locked in a obliquity resonance arising from some very small orbital variations in inclination driven primarily by a fourth order ($\epsilon^2 I^2 \cos 2\omega$), interaction between Earth and Venus. These terms correspond to a sum of small terms which precess in a prograde sense and therefore can potentially resonate with Venus' free mantle nutation (FMN) or precession mode. The terms in the expansion of the Venus - Earth disturbing function which are important are

$$R(2\omega) = \frac{GM M_{\oplus} \alpha}{a_{\oplus}} \sin J_{\oplus}^2 \begin{bmatrix} e^2 C_{22} \cos 2\omega + \\ e_{\oplus}^2 C_{33} \cos 2\omega_{\oplus} + \\ 2ee_{\oplus} C_{23} \cos(\omega + \omega_{\oplus}) \end{bmatrix} \quad (113)$$

where $\alpha = a/a_{\oplus}$ and J_{\oplus} is the mutual inclination

$$\sin^2 J_{\oplus} \simeq \sin^2 I + \sin^2 I_{\oplus} - 2 \sin I \sin I_{\oplus} \cos(\Omega - \Omega_{\oplus}). \quad (114)$$

The Venusian argument of pericenter ω is measured from the ascending node on the elliptic. The C_{ij} coefficients are

$$\begin{aligned} C_{22} &= \frac{\alpha}{64} (11 + 7D_{\alpha} + D_{\alpha}^2) b_{\frac{3}{2}}^1(\alpha), \\ C_{33} &= \frac{\alpha}{64} (-1 - D_{\alpha} + D_{\alpha}^2) b_{\frac{3}{2}}^1(\alpha), \\ C_{23} &= \frac{\alpha}{64} (-1 + 3D_{\alpha} + D_{\alpha}^2) b_{\frac{3}{2}}^0(\alpha). \end{aligned} \quad (115)$$

The operator D_{α} is

$$D_{\alpha} = \alpha \frac{d}{d\alpha}, \quad (116)$$

and $b_s^j(\alpha)$ are Laplace coefficients, defined as

$$b_s^j(\alpha) = \frac{1}{\pi} \int_0^{2\pi} dx \frac{\cos jx}{(1 + \alpha^2 - 2\alpha \cos x)^s}. \quad (117)$$

For the Earth -Venus interaction, $\alpha = 0.72333$, and the values of the corresponding $b_s^j(\alpha)$ are

$$\begin{aligned} b_{\frac{3}{2}}^0 &= 9.992; \quad Db_{\frac{3}{2}}^0 = 46.354; \quad D^2b_{\frac{3}{2}}^0 = 403.354 \\ b_{\frac{3}{2}}^1 &= 8.872; \quad Db_{\frac{3}{2}}^1 = 46.341; \quad D^2b_{\frac{3}{2}}^1 = 401.594 \end{aligned} \quad (118)$$

The fact that the second derivatives for the Laplace coefficients are large For the Venus - Earth couple supports the expectation that the Venus - Earth interaction is dominant [see table 7]. However, both Mercury and Jupiter are important for certain frequency combinations.

The generalization of eq. (113) is

$$R_{ij}(2\omega) = \frac{GM_i M_j \alpha}{2a_j} \{ [C_{ii} Z_i^{*2} + C_{jj} Z_j^{*2} - 2C_{ij} Z_i^* Z_j^*] (P_i - P_j)^2 + \text{c.c.} \}, \quad (119)$$

where the variable $Z = e e^{-i\tilde{\omega}}$, the index $i < j$ refers to the inner planet of any pair and c.c. indicates complex conjugate. The periodic terms arising from these terms can be recovered from the suite of equations

$$\begin{aligned} \frac{d}{dt} P_j + i \sum_{k \neq j} B_{jl}^k P_l &= -\frac{2i}{n_j a_j^2} \frac{\partial}{\partial P_j^*} \sum_{k \neq j} R_j^k(2\omega) \\ &= -i F_{jkm0} e^{-i\psi_{mno}}, \end{aligned} \quad (120)$$

where $l = j$ or $l = k$. The components of the matrix B_{jl}^k are

$$B_{jl}^k = \frac{(1 - 2\delta_{jl})}{4} \frac{GM_k}{n_j a_j^2 a_k} b_{3/2}^1 \quad (121)$$

The coefficient F_{jkm0} and argument ψ_{mno} shall be defined momentarily. At this stage, slightly different formalisms shall be employed for left and right hand sides of this equation.

If the following variable \bar{P}_j is introduced,

$$\bar{P}_j = \sqrt{M_j n_j a_j^2} P_j, \quad (122)$$

then the left hand side of (120) is transformed to

$$\frac{d}{dt} \bar{P}_j + i A_{jl} \bar{P}_l, \quad (123)$$

where the symmetric matrix A is related to B by

$$A_{jl} = B_{jl}^k \sqrt{\frac{M_j n_j a_j^2}{M_l n_l a_l^2}}. \quad (124)$$

Next, define a unitary matrix U which diagonalizes the symmetric matrix A

$$s_k = U_{kl} A_{lm} U_{mk}^T, \quad (125)$$

such that s_k is the k 'th eigenfrequency and \tilde{u}_k is,

$$\tilde{u}_k(I) = U_{kj} \tilde{P}_j, \quad (126)$$

the corresponding eigenfunction (Here, the initial value of \tilde{u}_k is not unity). The perturbation of \tilde{u}_k is recovered from the diagonalized equation,

$$\frac{d}{dt} \tilde{u}_k(I) + i s_k \tilde{u}_k(I) = -i U_{kj} \sqrt{M_j n_j a_j^2} F_{j m n o} e^{i \psi_{m n o}}. \quad (127)$$

The solution for Venus is therefore

$$\delta P_2(n m o) = \sum_{j,k=1}^8 \sqrt{\frac{M_j n_j a_j^2 U_{k2} U_{kj} F_{j m n o} e^{-i \psi_{m n o}}}{M_2 n_2 a_2^2 \frac{d}{dt} \psi_{m n o} - s_k}} \quad (128)$$

Recall that

$$U^T U = 1, \quad (129)$$

or $U_{kl} U_{kj} = \delta_{lj}$. The unitary matrix plays the role of a weighting function for both contributions from other planets (excluding Pluto) and the 8 I-type eigenfrequencies. The function $F_{j m n o}$ is

$$F_{j m n o} = \frac{G}{n_j a_j^2} \sum_{\substack{k=1 \\ k \neq j}}^8 \frac{M_k}{\max(a_j, a_k)} (2 - \delta_{m,n}) \times \left\{ \begin{array}{l} C_{jj} S_{jm}(e) S_{jn}(e) \\ + C_{kk} S_{km}(e) S_{kn}(e) \\ - 2 C_{jk} S_{jm}(e) S_{kn}(e) \end{array} \right\} (S_{jo}(I) - S_{ko}(I)) \quad (130)$$

We shall adopt Laskar's [1990] formalism for expansion of the right hand side to find an explicit expression for $F_{j m n o}$. Laskar has obtained a solution for the normal modes using the eigenfunctions u_j (which have unit amplitude at time $t=0$) and eigenfrequencies s_j and which are related to P_l by

$$P_l = S_{lj}(I) u_j(I). \quad (131)$$

This matrices $S(1)$ and $S(e)$ for the 8 planets are given in table 2. Laskar defines $u_j(I) = e^{-i(s_j t + \theta_j^I)}$ and $u_j(e) = e^{-i(g_j t + \theta_j^e)}$, and therefore S_{lj} is the j 'th mode amplitude factor for the l 'th planet.

We can deduce that the argument ψ_{mno} is one of 288 distinct linear combinations of eigenfrequencies,

$$\psi_{mno} = (g_m + g_n - s_o)t + \theta_m^e + \theta_n^e - \theta_o^I, \quad (132)$$

with a range of frequencies from 1.3 to $\sim 80'' \text{ yr}^{-1}$.

There is a gap in potential excitations in the most plausible range for the FMN frequency deduced from structural models, if we consider only the first order solution for the eigenfunctions. The nearest frequency with amplitude $>10^{-6}$ lies just inside the predicted band with frequency $d\psi_{243}/dt = 44.223'' \text{ yr}^{-1}$ and amplitude 2.9×10^{-5} .

Laskar finds significant sidebands to each of the u_m eigenfunctions. His expansion takes the form

$$u_m = \sum_j u_{mj} e^{-i\phi_{mj}} \quad (133)$$

and typically includes 10 terms with the primary term corresponds to $j=1$.

Higher order, sideband contributions to the eigenmodes tend to fill this gap and can be recovered using

$$u_m(e)u_n(e)u_o^*(I) = \sum u_{mj}u_{nk}u_{ol}^* e^{-i(\phi_{mj} + \phi_{nk} - \phi_{ol})} \quad (134)$$

and expanded form for the general angle argument,

$$\psi_{mnojkl} = \phi_{mj} + \phi_{nk} - \phi_{ol}. \quad (135)$$

Table 3 contains the terms in δP_2 with prograde frequencies, amplitudes greater than 1×10^{-6} (no. 1-9, 11, 29, 60-65) and all terms with frequencies between $43'' \text{ yr}^{-1}$ and $47'' \text{ yr}^{-1}$. The remainder arise from sidebands to these primary frequencies. Laskar [1990] lists the first 10 terms for each u function in tables VI and VII. The next step is to substitute for these u functions, expand and collect terms with like frequencies. The final result is shown in table 3 and includes the identification numbers $\{mnojkl\}$ of the largest term in this collection and the total number (#) contributing to the total magnitude. One approximation to this process is the implicit use of the base frequency instead of the sideband frequency as required in (128).

There are three factors influencing the cutoff employed for the sidebands. First, the accelerations produced by this magnitude term or smaller cause *at maximum* a change in obliquity of only 0.4° over the tidal time scale of 10^8 yr . Second, the expansion by Laskar of $u_m(\epsilon)$ and $u_o(I)$ eigenfunctions for $m = 2, 3, 4$ and $s = 2, 3, 4$ have a cutoff that has relative magnitude of 0.01 to 0.06 of the main term. Finally, higher order terms which are $O(\epsilon^2)$ or $O(I^2)$ smaller contribute at this level [see Newcomb, [1895] for explicit expansions in Laplace coefficients].

13. **Appendix C: Solid Body Dynamics with Solar Torque and Tides**

The objective is to derive a linearized dynamical equation for non-axial motion which adequately describes the FMN and wobble modes. The introduction of fluid core coupling through Poincaré coupling via an ellipsoidal boundary is briefly discussed as is the lowest order effect of tides. The approach here is considerably different than that of either Peale [1969, 1973] or Ward [1975] in that I obtain dynamical equations relative to an inertial frame rather than a frame fixed in the orbit plane. Second, I use a Lagrangian [Smart, 1961] rather than a Hamiltonian formulation and finally I write down the equations directly in terms of order 2 gravity coefficients C_{2j} . The only limitation is that the equations are linearized, although it is not difficult to obtain the nonlinear contributions.

Start by writing down the kinetic energy of rotation T_r of a body with moment of inertia tensor

I_{ij} .

$$T_r = \frac{1}{2} \sum_{i,j=1}^3 I_{ij} \omega_i \omega_j, \quad (136)$$

with $i = 1, 2, 3$ corresponding to x, y and z axes, respectively. The rotation axis and z axis are assumed to be nearly aligned. Make the following identifications:

$$C_{20} = -\frac{3}{2}I_{33} + \frac{1}{2}(I_{11} + I_{22} + I_{33}) \quad (137)$$

$$C_{22} = \frac{1}{4}(I_{22} - I_{11}) - i\frac{1}{2}I_{23}$$

$$C_{21} = -I_{13} + iI_{23}$$

where the above is unusual only because I choose a complex representation for the coefficients. The non-principal axis contribution is retained in order to introduce dissipation. The transformed kinetic energy is

$$T_r = \frac{1}{2}MR^2 \left[\begin{array}{l} \tilde{C}\omega^2 - C_{20}(\omega_1^2 + \omega_2^2) \\ -C_{21}\omega_3(\omega_1 + i\omega_2) - C_{22}(\omega_1 + i\omega_2)^2 \\ -C_{21}^*\omega_3(\omega_1 - i\omega_2) - C_{22}^*(\omega_1 - i\omega_2)^2 \end{array} \right] \quad (138)$$

where $\omega^2 = \omega_1^2 + \omega_2^2 + \omega_3^2$ and \tilde{C} is a dimensionless polar moment factor ($\tilde{C} = C/MR^2$).

The spin components are related to the Euler angles $\{\phi, \epsilon, \theta\}$ (where θ is the rotation angle relative to the line of nodes with orientation ϕ) by

$$\begin{aligned} \omega_1 - i\omega_2 &= (Dp + 2 \sin^2 \frac{\epsilon}{2} D\epsilon) e^{-i\lambda_s} \\ \omega_3 &= D(\theta + \phi) - 2 \sin^2 \frac{\epsilon}{2} \cos \epsilon D\phi \\ &\quad \cdot D\lambda_s + \frac{1}{4}(pDq - qDp) \end{aligned} \quad (139)$$

with $\lambda_s = \theta + \phi$. Again, $D = \frac{d}{dt}$. Substitute the above into (138) and retain quadratic terms in p .

$$T_r = \frac{1}{2} M R^2 \left[\begin{aligned} & \tilde{C}((D\lambda_s)^2 + \frac{i}{2} D\lambda_s(pDq - qDp)) \\ & + (\tilde{C} + C_{20})DpDq \\ & - C_{21}\omega_3 e^{-i\lambda_s} Dq - C_{22}e^{-i2\lambda_s}(Dq)^2 \\ & - C_{21}^* \omega_3 e^{i\lambda_s} Dp - C_{22}^* e^{i2\lambda_s}(Dp)^2 \end{aligned} \right] \quad (140)$$

where $q = p^*$.

The solar disturbing function, [e.g. Borderies and Yoder, 1990] , when expressed in terms of these variables, is

$$R_\odot = \frac{3}{4} G \frac{GM_\odot R^2}{2r_\odot^3} \left[\begin{aligned} & C_{20} \left\{ \begin{aligned} & \frac{1}{2}(P - p)(Q - q) - \frac{1}{3} \\ & - \frac{1}{2}(P - p)^2 e^{iL_\odot} \end{aligned} \right\} \\ & + iC_{21} \left\{ (Q - q)e^{-i\lambda_s} - (P - p)e^{i(2L_\odot - i\lambda_s)} \right\} \\ & + C_{22} \left\{ \begin{aligned} & (2 + 2qP - pq - PQ)e^{2i(L_\odot - \lambda_s)} \\ & + (Q - q)^2 e^{-2i\lambda_s} \end{aligned} \right\} \\ & + O(p^3, P^3) + \text{c.c.} \end{aligned} \right], \quad (141)$$

and “c. c.” stands for complex conjugate of the previous terms. The angle L_\odot is true solar longitude. The next stage of expansion in terms of orbit eccentricity and mean longitude is straightforward [e.g. Plummer, 1960; Kaula, 1960; Jarnigan, 1965],

$$\left(\frac{a}{r} \right)^{n+1} e^{i(n-2p)L} = e^{i(n-2p)\lambda} \sum_{q=-\infty}^{\infty} G_{npq}(e) e^{iq\ell} \quad (142)$$

where ℓ is mean anomaly ($\ell = \lambda - \tilde{\omega}$), $G_{npq}(e)$ are Kaula's eccentricity functions: $G_{210} = (1 - e)^{-3/2}$; $G_{200} = 1 - 5/2e^2 + \dots$

In order to recover the appropriate latitude equation, one must be careful to decouple it from the axial dynamical equation. A decoupled form can be obtained from the following combination

of Lagrangians.

$$\begin{aligned} & \left(D \frac{\partial}{\partial D q} - \frac{\partial}{\partial q} - \frac{i}{2} p \left(D \frac{\partial}{\partial D \lambda_s} - \frac{\partial}{\partial \lambda_s} \right) \right) T_r \\ & = \left(\frac{\partial}{\partial x} - \frac{i}{2} p \frac{\partial}{\partial \lambda_s} \right) R_\odot \end{aligned} \quad (143)$$

The result is

$$\begin{aligned} & \frac{d}{dt} \left[(\tilde{C} - J_2) D p - \omega C_{12} e^{-i\lambda_s} - 2C_{22} D q e^{-i2\lambda_s} \right] + i\omega \tilde{C} D p \\ & = \frac{3}{2} n_\odot^2 \left[\begin{array}{c} (P - P)(J_2 + 2C_{22} e^{i2(L_\odot - \lambda_s)}) \\ - e^{-i2\lambda_s} (q - Q)(J_2 e^{-i2(L_\odot - \lambda_s)} + 2C_{22}^*) \\ - i e^{-i\lambda_s} (C_{12} + C_{12}^* e^{i2(L_\odot - \lambda_s)}) \end{array} \right] \quad (144) \end{aligned}$$

The rotation angle λ_s is replaced with ωt in section 5 to clarify how it affects the dynamics.

Tidal deformation of the moment tensor due the external mass \bar{M} at position \bar{r} is given by [Lambeck, 1980]

$$I_{ij}^t = -k_2 \frac{\bar{M} R^5}{\bar{r}^3} \left(\frac{\bar{r}_i \bar{r}_j}{\bar{r}^2} - \frac{1}{3} \delta_{ij} \right) \quad (145)$$

The latitude equation is affected by solid friction through the above contributions to C_{21} and C_{22} (see Eq. (167) in appendix D).

$$C_{21}^t \simeq \frac{i}{2} k_2 H_\odot \left[\begin{array}{c} (Q - q) e^{i(\lambda_s - 2L_\odot)} \\ -(P - p) e^{i\lambda_s} \end{array} \right] \quad (146)$$

$$C_{22}^t \simeq \frac{1}{4} k_2 H_\odot \left[e^{i(2\lambda_s - 2L_\odot)} \right], \quad (147)$$

with $H_\odot = M_\odot / M (R/a_\odot)^3$. Solid friction is introduced by subtracting a phase lag $\delta(s)$ from each of the three angle arguments with frequency s before substitution into (144).

The deformation caused by rotation is given by

$$I_{ij}^r = \frac{1}{3} k_2 \frac{R^5}{G} \left(\omega_i \omega_j - \frac{1}{3} \delta_{ij} \omega^2 \right) \quad (148)$$

but is usually important for only the wobble mode [Yoder and Ward, 1979]. The additional kinetic energy associated with the relative, nonaxial motion of a uniform fluid core in an oblate cavity is [e.g. Lamb, 1945]

$$T_f = \frac{I}{2} A_c [(m_c + Dp)(m_c^* - Dq) - DpDq] \quad (149)$$

if one drops terms of order ϵ_c^2 smaller. Recall that the *differential* core spin m_c is defined relative to the inertial frame and mantle spin $m = Dp$. If T_r is replaced with $T_r + T_f$ in (143), the core term seen in Eq. (36) is recovered.

Now, the core nutation is not force free because of the pressure exerted at the boundary proportional to ϵ_c , and the core motion is relative to the rotating frame of the mantle. The equivalent boundary torque is

$$IV_j = i\omega A_c \epsilon_c m_c, \quad (150)$$

while the effect of the rotating frame is to add an effective torque $i\omega A_c m$. The fluid core equation (36) is recovered from

$$2D \frac{\partial}{\partial m_c^*} T_f + i\omega A_c m = N_f \quad (151)$$

except for CMB friction.

An alternative is to treat the core as a plastic solid with free-slip at the CMB. The point is that this ‘fluid’ core has a definable surface to which one can attach a coordinate system and hence can define a core orientation variable p_c relative to inertial space. Consider a core equation like Eq. (144), except that we shall choose an axially symmetric core. The core equation is then

$$((1 - \epsilon_c)D^2 + i\omega D)p_c - \omega \tilde{C}_c^{-1} D(C_{21}^c e^{-i\omega t}) = \tilde{C}_c^{-1} N_f^\dagger \quad (152)$$

Since the CMB surface is fixed in the mantle, the above C_{21}^c factor is nonzero even for a rigid

boundary since the 'core' CMB surface moves relative to 'mantle' CMB.

$$\tilde{C}^{-1}C_{21}^c = e_c \omega^{-1} e^{i\omega t} (Dp_c - Dp) \quad (153)$$

The effect of this correction is to change the fluid core wobble period to *exactly* one sidereal day.

The core torque N_f^\dagger , acting on the core CMB depends 1) on the pressure torque arising from the differential orientation of core and mantle *and* 2) the angular acceleration of the mantle D^2p .

$$\tilde{C}_c^{-1}N_f^\dagger = ie_c \omega (D + i\omega)(p_c - p) - e_c D^2p. \quad (154)$$

Notice that if p_c precesses with the natural frequency $\sigma_c = -\omega e_c$, then the factor $(D + i\omega)p_c = \omega(1 - e_c)p_c$. The fluid core equation (36) is recovered from [152, 153, 154] if one identifies

$$m_c = (D + i\omega)(p_c - p) \quad (155)$$

The above core equation is effectively linearized. Busse [1968] finds that the dependence of the differential obliquity on the FCN mode is

$$\sigma_c = -e_c \omega_c \cos \Delta \epsilon \text{sign}(\cos \epsilon). \quad (156)$$

I have inserted the $\text{sign}(\cos \epsilon)$ factor since the core precession must have the same sign as the mantle FMN mode independent of the mantle obliquity if the core and mantle ellipticities and spins have the same sign.

14. Appendix D: Tidal Coefficients C_{nm}^t and Potential

A general expansion of the tidal potential is obtained here that includes the independent orientation of both the body and the orbit. The equivalent tidal perturbation of the unnormalized gravity coefficients is given by

$$C_{nm}^t = k_n \frac{M'}{M} \left(\frac{R}{r'} \right)^{n+1} (2 - \delta_{n,m}) \frac{(n-m)!}{(n+m)!} N_{nm} Y_{nm}^*(\Theta, \Phi), \quad (157)$$

$$N_{nm}^2 = \frac{4\pi (n+m)!}{2n+1 (n-m)!},$$

where $Y_{nm}(\Theta, \Phi)$ is a normalized spherical harmonic function and $\{\Theta, \Phi\}$ are the angular coordinates of the tide raising body with mass M' relative to the body-fixed frame of mass M .

Consider the rotational transformation of a spherical function [Rose, 1957; Levie, 1971]

$$Y_{nm}(\Theta, \Phi) = \sum_{j=-n}^n d_{jm}^n(\beta) e^{-i(j\alpha+m\gamma)} Y_{nj}(\bar{\Theta}, \bar{\Phi}) \quad (158)$$

where α is a counterclockwise rotation about the z-axis, β is a rotation about the new y-axis and finally γ is a rotation about the new z-axis. The function $d_{jm}^n(\beta)$ for $j \geq m$ is

$$d_{jm}^n(\beta) = (-1)^{j-m} \frac{(n+j)!(n-j)!}{[(n+m)! (n-m)!]}^{1/2} \quad (159)$$

$$\sum_s (-1)^s \begin{bmatrix} n+m \\ s \end{bmatrix} \begin{bmatrix} n-m \\ n-j-s \end{bmatrix} c_2^{2n-j+m-2s} s_2^{j-m+2s}$$

with $c_h = \cos \beta/h$ and $s_h = \sin \beta/h$. The sum over index s is limited to only terms for which the binomial coefficients are defined: $\max(0, n-j)$ to $\min(n+m, n-m)$. These functions satisfy the symmetry relations

$$d_{jm}^n(\beta) = (-1)^{j-m} d_{-j,-m}^n(\beta) = d_{mj}^n(-\beta) \quad (160)$$

and therefore, of the $(2n+1)^2$ components of $d_{jm}^n(\beta)$, only $(n+1)^2$ are unique. These are listed in Table 8 for $n=2$. Also

$$d_{jm}^n(0) = \delta_{jm}. \quad (161)$$

First, consider the sequence of rotations $\{\phi, \epsilon, \theta\}$ which rotate Y_{nm} from a body-fixed to a space-fixed coordinate frame. This corresponds to a rotation ϕ about the z-axis, a rotation ϵ about the new x axis and a rotation θ about the new z-axis. Identify $\alpha = \phi - \pi/2$, $\beta = \epsilon$ and $\gamma = \theta + \pi/2$. The new angles $\{\bar{\Theta}, \bar{\Phi}\}$ are the spherical coordinates of the tide raising body in the space-fixed frame.

Next, rotate the space-frame to an orbit frame in which the final x and z axes are parallel to the orbit radius vector and orbit normal, respectively. Define f, ω and Ω and I as the orbital true anomaly, argument of pericenter, node and inclination, respectively. Identify $\gamma = -\Omega + \pi/2$, $\beta = -I$ and $\alpha = -f - \pi/2$.

The final spherical coordinates $\{\bar{\bar{\Theta}}, \bar{\bar{\Phi}}\} = \{\frac{\pi}{2}, 0\}$. The $Y_{nk}(\bar{\bar{\Theta}}, \bar{\bar{\Phi}})$ function is [Abramowitz and Stegun, 1965]

$$Y_{nk}(\frac{\pi}{2}, 0) = \sqrt{\frac{2n+1}{4\pi}} \frac{\sqrt{(n-k)!(n+k)!}}{2^n (\frac{n-k}{2})! (\frac{n+k}{2})!} \cos(n-k)\frac{\pi}{2}, \quad (162)$$

and vanishes if $n-k$ is odd. Define $2p = n-k$ and let p range from 0 to n . The values for $n=2$ are:

$$\begin{aligned} Y_{20}(\frac{\pi}{2}, 0) &= -\frac{1}{2} \sqrt{\frac{5}{4\pi}} \\ Y_{21}(\frac{\pi}{2}, 0) &= 0 \\ Y_{22}(\frac{\pi}{2}, 0) &= \frac{6}{4} \sqrt{\frac{5}{4\pi}} \\ Y_{2-2}(\frac{\pi}{2}, 0) &= \frac{6}{4} \sqrt{\frac{5}{4\pi}}. \end{aligned} \quad (163)$$

The standard inclination function $F_{nmp}(I)$ is related to the above by

$$F_{njp}(I) = (-1)^p N_{nj} Y_{n, n-2p}(\frac{\pi}{2}, 0) d_{n-2p, j}^n(-I), \quad (164)$$

and is similar to the development of Allan[1967]. Note that

$$F_{n, -jp}(I) = (-1)^{n-j} \frac{(n-j)!}{(n+j)!} F_{njp}(I). \quad (165)$$

The expansion of the spherical function is therefore

$$Y_{nm}(\Theta, \Phi) = i^{n-m} \sum_{j=-n}^n N_{nj}^{-1} d_{jm}^n(\beta) F_{njp}(I) e^{i[(n-2p)(f+\omega) + j(\Omega-\phi) - m\theta]}. \quad (166)$$

If we include the expansion of the true anomaly in terms of the mean anomaly (142) and subtract a phase lag $\delta(\dot{\Psi})$, the final expansion for the gravity coefficients is

$$\begin{aligned} C_{nm}^t &= i^{m-n} k_n \frac{M'}{M} \left(\frac{R}{a'}\right)^3 \sum_{pq} \frac{N_{nm}}{N_{nj}} (2 - \delta_{m0}) \frac{(n-m)!}{(n+m)!} \times \\ &F_{njp}(I) d_{jm}^n(\epsilon) G_{npq}(\epsilon) e^{-i[\Psi_{nmpjq} - \delta_{nmpjq}(\dot{\Psi})]}, \end{aligned} \quad (167)$$

$$\Psi_{nmpjq} = (n - 2p)(\ell + \omega) + q\ell + j(\Omega - \phi) - m(\lambda_s - \phi).$$

The tidal disturbing function is obtained by substituting the above into the spin orbit function R after expanding the potential in the same manner. The expansion of the $\{nm\}$ components of the potential is

$$R_{nm}^t = \frac{GM'M'R^{2n}}{a^{n+1}} \mathcal{R} i^{n-m} C_{nm}^t N_{nm} Y_{nm}(\Theta, \Phi). \quad (168)$$

where \mathcal{R} = 'real part'. The final result is

$$\begin{aligned} R_{nm}^t = & \frac{GM'M'R^{2n+1}}{a^{n+1}} k_n \sum_{pjq} \sum_{\bar{p}\bar{q}} (2 - \delta_{m0}) \sqrt{\frac{\ell!}{(n-j)!(n+j)!}} \times \\ & d_{jm}^n(\bar{\epsilon}) d_{jm}^n(\epsilon) F_{n\bar{j}\bar{p}}^2(\bar{I}) F_{njp}^2(I) G_{n\bar{p},\bar{q}}(\bar{e}) G_{npq}(\epsilon) \times \\ & \cos[\Psi_{nmpjq} + \bar{\Psi}_{n\bar{m}\bar{p}\bar{q}} + \delta_{n\bar{m}\bar{p}\bar{q}}(\dot{\Psi})] \end{aligned} \quad (169)$$

where the overbar denotes the tide raising body. The tidal equations for obliquity and spin are obtained from partials of the unbarred variables

$$\begin{aligned} C \frac{d}{dt} \omega &= \frac{\partial}{\partial \theta} R_n^t, \\ C \omega \sin \epsilon \frac{d}{dt} \epsilon &= - \frac{\partial}{\partial \phi} R_n^t + \cos \epsilon \frac{\partial}{\partial \theta} R_n^t. \end{aligned} \quad (170)$$

If the tide raising body and the body affecting the disturbing body are the same, then the terms contributing to the secular rates have $p = \bar{p}$, $j = \bar{j}$ and $q = \bar{q}$. The $\{nmpjq\}$ term in the obliquity rate is

$$C \omega \sin \epsilon \frac{d}{dt} \epsilon_{nmpj0} = (m \cos \epsilon - j) T_{nmpjq} \sin \delta_{nmpjq}, \quad (171)$$

with

$$T_{nmpjq} = \frac{GM'^2 R^{2n+1} k_n}{a^{2n+2}} \frac{(n-j)!}{(n+j)!} (2 - \delta_{m0}) F_{njp}^2(I) d_{jm}^n(\epsilon)^2. \quad (172)$$

The special case where $\epsilon = I = 0$, have $71 - 2p = m$ and $g = 0$. The coefficients in eq.(67) can be derived from the above expression using table 8 and $F_{220} = 3$ and $F_{201} = 1/2$. The range over the indices is: $0 \leq m \leq n$ and $-n \leq j \leq n$.

The $\{nmpjq\}$ component of the tidal spin rate change is

$$C \frac{d}{dt} \omega_{nmpj0} = m T_{nmpjq} \sin \delta_{nmpjq} \quad (173)$$

For completeness, the tidal changes in the orbit $\{a, e, I\}$ are given by [Plummer, 1960]

$$\begin{aligned} \frac{na}{2} \frac{d}{dt} a_{nmpjq} &= -(n - 2p + q) T_{nmpjq} \sin \delta_{nmpjq}, \\ \frac{na^2 e}{1 - e^2} \frac{d}{dt} e_{nmpjq} &= -(n - 2p) \left(1 + \frac{1}{\sqrt{1 - e^2}} \right) + q \Big) T_{nmpjq} \sin \delta_{nmpjq}, \\ n a^2 \sin I \sqrt{1 - e^2} \frac{d}{dt} I_{nmpjq} &= -(\cos I (n - 2p) + j) T_{nmpjq} \sin \delta_{nmpjq}. \end{aligned} \quad (174)$$

Acknowledgments: This paper represents the results of one phase of research carried out at the Jet Propulsion Laboratory, California Institute of Technology, under NASA contract NAS 7-100, supported by the National Aeronautics and Space Administration. I wish to thank Tony Dobrovolskis and an anonymous reviewer for their careful and thoughtful reviews

REFERENCES

- Abramowitz, M. and I. I. Stegun 1965. *Handbook of Mathematical Tables*, Dover, New York.
- Akim, E. L., Z. P. Vlasova and I. V. Chuiko 1978, Determination of the dynamic compression of Venus from the measured trajectories of its first artificial satellites, Venera 9 and Venera 10, *Doklady akademii nauk SSSR*, 3, 556-559.
- Arkani-Hamed, J. and M. N. Toksöz 1984. Thermal evolution Of Venus, *Phys. Earth Planet. Inter.*, 34, 232-250.
- Arkani-Hamed 1993. On the tectonics of Venus, *J. Phys. Earth Planet. Inter.*, 76, 75-96.
- Allan, R. R. 1967. Resonance effects due to the longitude dependence of the gravitational field of a rotating primary, *Planet. Space Sci.*, 15, 53-76.
- Basaltic Volcanism Study Project 1981. *Basaltic Volcanism on the Terrestrial Planets*, Pergamon Press, New York, 1286pp.
- Hills, B. G., W. S. Kieffer, and R. L. J. Jones 1987. Venus gravity: a harmonic analysis, *Geophys. Res.*, 92, 10335-10351.
- Borderies, N. and C. F. Yoder 1990. Phobos' gravity field and its influence on its orbit and libations, *Astron. Astrophys.*, 233, 235-251.
- Busse, F. H. 1968. Steady fluid flow in a processing spherical shell, *J. Fluid Mech.*, 33, 739-751.
- Davies, M. E., T. R. Colvin, P. G. Rogers, P. W. Chodas, W. L. Sjorgren, E. L. Akim, V. A. Stepanyantz, Z. P. Vlasova and A. I. Zakharov, 1992. The rotation period, direction of the north pole, and geodetic control network, *J. Geophys. Res.*, 97, 13141-13152.
- Dickey, J. O., P. L. Bender, J. E. Faller, X. X. Newhall, R. L. Ricklets, J. G. Ries, P. J. Shelus, C. Veillet, A. L. Whipple, J. R. Wiens, J. G. Williams and C. F. Yoder 1994. Lunar laser ranging: a continuing legacy of the Apollo program, *Science*, 265, 482-490.
- Dobrovolskis, A. R. 1978. *The Rotation of Venus* (Phi) thesis, California Institute of Technology, Pasadena, 250pp).
- Dobrovolskis, A. R. and A. R. Ingersoll 1980. Atmospheric tides and the rotation of Venus I. tidal theory and the balance of torques, *Icarus*, 41, 1-17.
- Dobrovolskis, A. R. 1980. Atmospheric tides and the rotation of Venus II. spin evolution, *Icarus*, 41, 18-35.
- Dziwonski, A., A. L. Hales, and E. R. Lapwood 1975. Parametrically simple earth models consistent with geophysical data, *Phys. Earth Planet. Interiors*, 10, 12.

- Gans, R.F. 1972. Viscosity of the Earth's core, *J. Geophys. Res.*, 77, 360-366.
- Gold, T. and S. Soter 1969. Atmospheric tides and the resonant rotation of Venus, *Icarus*, **11**, 356-366.
- Goldreich, P. and S. J. Peale 1970, The obliquity of Venus, *Astron. J.* 75, 275-284.
- Goldstein, S. 1965. *Modern Developments in Fluid Mechanics*, Dover, New York.
- Goldreich, P. and S. J. Peale 1970. The obliquity of Venus, *Astron. J.*, 75, 273.
- Gwinn, C. R., T. A. Herring, and I. I. Shapiro 1986. Geodesy by radio interferometry: Studies of the forced nutations of the earth, 2. Interpretation, *J. Geophys. Res.*, **91**, 4755-4765.
- Hager, B. H., R. W. Clayton, M. A. Richards, R. P. Comer, and A. M. Dziewonski 1985. Lower mantle heterogeneity, dynamic topography and the geoid, *Nature*, **313**, 541-545.
- Hager, B. H., M. A. Richards 1989. Long-wavelength variations in Earth's geoid: physical models and dynamical implications, *Philos. Trans. Roy. Soc.*, A328, 309-327.
- Hashim, Z. 1983. Analysis of composite solids -a survey, *J. Applied Mech.*, 50, 481-505.
- Herrick, R. R. and R. J. Phillips 1992. Geologic correlations with the interior density structure of Venus, *J. Geophys. Res.*, 97, 16017-16034.
- Herring, T. A., C. R. Gwinn and I. I. Shapiro 1986. Geodesy by radio interferometry: Studies of the forced nutations of the Earth 1: Data analysis, *J. Geophys. Res.*, 91, 4755-4765.
- Hide, R., R. W. Clayton, B. H. Hager, M. A. Speith, and C. V. Voorhies 1992. Topographic core-mantle coupling and fluctuations in the earth's rotation, to appear in IUGG Jeffreys Symposium.
- Ingersoll, A. P. and A. R. Dobrovolskis 1978. Venus' rotation and atmospheric tides, *Nature*, 275, 37-38.
- Jackson, I., R. C. Liebermann and A. E. Ringwood 1978. The elastic properties of $(\text{Mg}_x\text{Fe}_{1-x})\text{O}$ solid solutions, *Phys. Chem. Minerals*, 3, 11-31.
- Jarnagan Jr., M. P. 1965. Expansions in elliptic motions, *Astron. papers, Am. Ephemeris & Naut. Almanac*, XVIII, 5.1-5.6.
- Jeanloz, R. and A. B. Thompson 1983. Phase transitions and mantle discontinuities, *Rev. of Geophys. Space Phys.*, **21**, 51-74.
- Kaula, W. M. 1960. *Theory of satellite geodesy*, Blaisdell, Waltham, 124pp.
- Kaula, W. M. 1964. Tidal dissipation by solid body friction and the resulting orbital evolution, *Rev. of Geophys.*, 2, 661-685.
- Kiefer, W. S., M. A. Richards, and B. H. Hager 1986. A dynamic model of Venus' gravity field, *Geophys. Res. Lett.*, **13**, 14-17.
- Konopliv, A. S., N. J. Borderies, P. W. Chodas, D. J. Christensen, W. L. Sjogren, B. G. Williams, G. Balmino, and B. G. Barriot 1993. Venus gravity and topography: 60th degree and order model, *Geophys. Res. Lett.*, 20, 2403-2406.
- Konopliv, A. S. and W. L. Sjogren, 1994. Venus Spherical harmonic gravity field to degree and order 60, *Icarus*, **112**, 42-54.
- Kumazawa, M. and O. I. Anderson 1969. Elastic moduli, pressure derivatives and temperature derivatives of single-crystal olivine and single-crystal forsterite, *J. Geophys. Res.*, 74, 5961.

- Lamb, H. 1945. *Hydrodynamics*, 6th ed., Dover, New York, 738pp.
- Lambeck, K. 1980. *The Earth's Variable Rotation*, Cambridge university press, Cambridge, 449pp.
- Laskar, J., 1988. Secular evolution of the solar system over 10 million years, *Astron. Astrophys.*, **198**, 341-362.
- Laskar, J. 1990. The chaotic history of the solar system: a numerical estimate of the size of chaotic zones, *Icarus*, **88**, 266-291.
- Laskar, J. and P. Robutel 1993. The chaotic obliquity of the planets, *Nature*, **361**, 608-612.
- Levie, S. L. 1971. Transformation of a potential function under coordinate rotations, *J. Astronaut. Sci.*, **18**, 217-235.
- McNamee, J. B., N. J. Borderies and W. I. Sjogren 1993. Venus: global gravity and topography, *J. Geophys. Res. Planets*, **98**, 9113-9128.
- Mizutani, H., Y. Hamano and S. Akimoto 1972. Elastic-wave velocities of polycrystalline Stishovite, *J. Geophys. Res.*, **77**, 3744-3749.
- Morgan, W. J. and R. J. Phillips 1983. Hot spot heat transfer: its application to Venus and implications for Venus and Earth, *J. Geophys. Res.*, **88**, 8305-8317.
- Morgan, W. J. and J. P. Morgan 1991. Two-deforming-plate model for Venus, *EOS(abstracts)*, **284**.
- Moroz, V. I., Results of Venera 13 and 14 1983. in *Venus* (Hunten, D. M., Colin, L. Donohue, I'. M. and Moroz, V. I. eds.), U. of Ariz. Press. 45-68.
- Mottinger, N. A., W. I. Sjogren, and B. G. Bills 1985. Venus gravity: a harmonic analysis and geophysical implications, *J. Geophys. Res.* **90**, 739-756.
- Newcomb, S. 1895. Development of the perturbative function in cosines of multiples of the mean anomalies and of angles between the perihelia and common node and in powers of the eccentricities and mutual inclination, *American Ephemeris and Nautical Almanac: Astron. Papers*, **5**, 1-48.
- Newsom, H. E. and S. R. Taylor 1989. Geochemical implications of the formation of the Moon by a single giant impact, *Nature*, **338**, 29-34.
- Neuberg, J., J. Hinderer, and W. Zürn 1987. Stacking gravity tide observations in central Europe for the retrieval of the complex eigenfrequency of the nearly diurnal free-wobble, *Geophys. J. R. Astr. Soc.*, **91**, 853-868.
- Peale, S. J. 1969. Generalized Cassini's Laws, *Astron. J.*, **74**, 266-291.
- Peale, S. J. 1973. Rotation of solid bodies in the solar system, *Rev. Geophys. Space Phys.*, **11**, 767-793).
- Peale, S. J. 1976. Orbital Resonances in the Solar System, *Annu. Rev. Astron. Astrophys.*, **14**, 215-246.
- Pechmann, J. B. and A. P. Ingersoll 1984. Thermal tides in the atmosphere of Venus: Comparison of model results with observations, *J. Atmos. Sci.*, **41**, 3290-3313.
- Plummer, H. C. 1960. *An Introductory Treatise on Dynamical Astronomy*, Dover, New York, 343pp.

- Poirier, J. P. 1988. Transport properties of liquid metals and the viscosity of the Earth's core, *Geophys. J.*, 92, 99-105.
- Richards, M.A. and B. H. Hager 1984. Geoid anomalies in a dynamic earth, *J. Geophys. Res.*, 89, 5987-6002.
- Ringwood, A. E. and D. L. Anderson 1977. Earth and Venus: a comparative study, *Icarus*, 30, 243-253.
- Roberts P. H. and K. Stewartson 1965, On the motion of a liquid in a spherical cavity of a processing rigid body. II, *Proc. Camb. Phil. Soc.*, 61, 279-288.
- Rose, M. E. 1957. *Elementary Theory of Angular Momenta*, John Wiley, New York, 48-64.
- Russell, C. T., P. J. Coleman Jr. and B. E. Goldstein 1981. Measurements of the lunar induced magnetic moment in the geomagnetic tail: evidence for a lunar core, *Proc. Lunar Planet. Sci.*, 12B, 831-836.
- Saito, M. 1974. Some problems of static deformation of the Earth, *J. Phys. Earth*, 22, 123-140.
- Sasao, T., I. Okamoto and S. Sakai 1977. Dissipative core-mantle coupling and notational motion of the earth, *Publ. Astron. Soc. Japan*, 29, 83-105.
- Sasao, T., S. Okubo and M. Saito 1980. Linear theory on the dynamical effects of a stratified core upon the notational motion of the earth, in *Nutation and the Earth's Rotation*, M. L. Smith and P. L. Bender eds., 165-183.
- Schaber, G. G. et al. 1992. Geology and distribution of impact craters on Venus: what are they telling us?, *J. Geophys. Res.*, 97, 13257-13301.
- Shapiro, I. I., J. F. Chandler, D. B. Campbell, A. A. Hines, M. A. Slade and R. F. Jurgens 1993. New radar value of the rotation vector of Venus, submitted to *Astron. J.*.
- Shen, M. and C. Z. Zhang 1989. Dynamical evolution of the rotation of Venus, *Earth, Moon & Planets*, 43, 275-287.
- Shen, M. and C. Z. Zhang 1990. A numerical solution for thermal tides in the atmosphere of Venus, *Icarus*, 85, 129-144.
- Smart, W. M. 1961. *Celestial Mechanics*, John Wiley, New York, 381pp.
- Stevenson, D. J., T. Spohn, . and G. Schubert 1983. Magnetism and thermal evolution of the terrestrial planets, *Icarus*, 54, 466-489.
- Sumino, Y. 1979. The elastic constants of Mn_2SiO_4 , Fe_2SiO_4 and Co_2SiO_4 and the elastic properties of olivine at high temperatures, *J. Phys. Earth*, 27, 209-238.
- Suppe, J. and C. Connors 1992. Tectonic settings of the mountain belts of Venus, in *Workshop on the mountain belts of Venus and Earth (abs.)* San Juan Capistrano Institute, 46-48.
- Turcotte, D. L., F. A. Cooke, and R. J. Williman 1979. Parametrized convection within the moon and the terrestrial planets, *Proc. Lunar Planet Sci. Conf. 10th*, 2378-2392.
- Turcotte, D. 1993. An episodic hypothesis for Venusian tectonics, *J. Geophys. Res. Planets*, 98, 17061-17069.
- Usselman, T. M. 1975. Experimental approach to the state of the core: part 1. the liquidus relations of the Fe-rich portion of the Fe-Ni-S system from 30 to 100kb, *Am. J. Sci.*, 275, 278-290.

- Vanyo, J. P. 1973. An energy assessment for liquids in filled processing spherical cavities, *J. Applied. Mech.*, 40, 851-856.
- Vanyo, J. P. and G. W. Paltridge 1981. A model for energy dissipation at the core mantle boundary, *Geophys. J. R. astr. Soc.*, 66, 677-690.
- Vanyo, J. P. 1991. A geodynamo powered by luni-solar precession, *Geophys. Astrophys. Fluid Dynamics*, 59, 209-234.
- Ward, W. R. 1975. Tidal friction and generalized Cassini's laws in the solar system, *Astron. J.*, 80, 64-70.
- Ward, W. R. and M. J. Reid 1973. Solar tidal friction and satellite loss, *Mon. Not. R. astr. Soc.*, 164, 21-32.
- Ward, W. R., and W. M. DeCamp 1979. Comments on the Venus rotation pole, *Ap. J. (Letters)*, 230, 1, 17.
- Yoder, C. F. 1974. On the Establishment and Evolution of Orbit-orbit Resonances, PhD Thesis, University of California, Santa Barbara.
- Yoder, C. F. and W. R. Ward 1979. Does Venus wobble?, *Astrophys. J. (Letters)*, 233, L33-L37.
- Yoder, C. F. 1981. Free librations of a dissipative moon, *Phil. Trans. Roy. Soc. London*, A303, 327-246.
- Yoder, C. F. and S. J. Peale 1981. The Tides of 10. *Icarus*, 47, 1-35.
- Yoder, C. F. 1995. Astrometric and geodetic properties of earth and the solar system, in *Global Earth Physics: A Handbook of Geophysical Constants, A GURreference shelf*, 1-31.

Table 1: Venusian Rotation and Vector		
Source	Type	Parameter
Shapiro <i>et al.</i> , (1993)	radar	$P = 243.027 \pm 0.002$ $\alpha_0 = 272.74 \pm 0.02$ $\delta_0 = 67.17$; 0.02
Davies <i>et al.</i> (1992)	Magellan SAR	$P = 243.0185 \pm 0.0001$ $\alpha = 272.763 \pm 0.02$ $\delta_0 = 67.16 \pm 0.01$
Konopliv <i>et al.</i> , (1993)	gravity field	$P = 243.01813 \pm 0.0005$

Period (in days), declination δ_0 and right ascension α_0 (in degrees) of Venus.

Table 2: Venus' Orbital Variation			
j	$S_{2j}(I)/2$ $\times 10^8$	s_j "/yr ⁻¹	$\theta_j(I)$ deg.
1	671554	-5.61755	348.703
2	-404451	-7.07963	273.772
3	954443	-18.85115	60.426
4	575863	-17.74818	123.278
5	1377171	0.0	107.587
6	5577	-26.33073	127.291
7	99208	-3.00557	140.330
8	65885	-0.69189	23.961
j	$S_{2j}(e)$ $\times 10^8$	g_j "/yr ⁻¹	$\theta_j(e)$ deg.
1	666756	5.59644	110.346
2	-2073299	7.45592	20.243
3	1167087	17.36469	123.952
4	1346367	17.91550	335.249
5	1963619	4.24882	30.672
6	-40659	28.22069	128.112
7	54130	3.08552	121.363
8	1088	0.66708	73.977

Table 2: Venusian Orbital variations in both eccentricity ($Z = \sum S_{2j}(e) c^{-i(*g_j + \theta_j^e)}$) and inclination ($P = \sum S_{2j}(I) e^{-i(t s_j + \theta_j^I)}$) from Tables V-VIII of Laskar [1990].

Table 3: Prograde Frequency Terms in Venusian Obliquity

	m	n	o	j	k	l	frequency "yr ⁻¹	phase deg.	I_{mnojkl} $\times 10^{-8}$	#	ϵ_c deg.
1	1	5	1	1	1	1	15.463	332.315	2583	1	4.15
2	1	1	1	1	1	1	16.810	51.989	8122	1	6.08
3	1	5	2	1	1	1	16.925	47.246	2556	1	4.13
4	1	1	2	1	1	1	18.273	126.920	7596	1	5.94
5	1	2	1	1	1	1	18.671	321.886	3088	1	4.40
6	1	2	2	1	1	1	20.132	36.817	2678	1	4.20
7	1	1	3	1	1	1	30.044	160.266	1465	1	3.44
8	4	5	3	1	1	1	41.015	304.866	2256	48	3.97
9	1	4	3	1	1	1	42.363	31.518	1266	26	3.27
10	2	3	3	1	1	2	43.121	50.480	848	18	2.86
11	2	3	3	1	3	1	43.390	313.684	1387	18	3.37
12	2	4	4	1	6	1	43.400	144.957	288	7	2.00
13	2	4	3	6	1	1	43.591	118.077	328	13	2.09
14	2	3	3	1	1	1	43.672	262.425	250	17	1.91
15	2	4	3	3	1	1	43.702	84.268	576	20	2.52
16	2	4	3	4	1	1	43.822	279.957	381	15	2.19
17	2	4	3	1	2	1	43.938	338.505	869	8	2.89
18	2	3	3	1	8	1	43.943	173.989	404	5	2.24
19	2	4	3	2	5	1	44.003	200.580	35	2	0.99
20	2	3	3	1	6	3	44.016	30.362	21	8	0.84
21	2	4	3	1	7	1	44.030	188.277	330	1	2.09
22	2	4	3	1	1	7	44.069	304.015	84	4	1.32
23	2	4	3	4	1	4	44.102	19.437	56	3	1.16
24	2	4	3	2	1	1	44.108	122.856	437	8	2.30
25	2	4	3	1	5	1	44.118	198.381	437	1	2.30
26	3	4	2	5	1	2	44.129	200.564	445	4	2.31
27	2	4	3	1	1	8	44.151	324.396	113	17	1.46
28	2	4	3	2	8	1	44.208	192.253	23	1	0.87
29	2	4	3	1	1	1	44.223	114.539	2966	12	4.34
30	2	4	3	3	3	1	44.254	291.725	55	15	1.16
31	2	4	3	1	8	1	44.323	183.902	282	3	1.99
32	2	3	3	1	9	3	44.335	246.220	46	4	1.09
33	2	4	3	5	1	1	44.340	291.145	130	8	1.53
34	2	4	3	4	3	1	44.375	139.607	51	8	1.12
35	2	4	3	2	1	4	44.387	221.358	66	2	1.23
36	2	4	3	1	10	1	44.393	135.987	162	1	1.65
37	2	4	3	1	5	4	44.398	312.908	40	1	1.04
38	2	3	3	1	10	3	44.410	188.777	29	2	0.93
39	2	4	3	1	1	10	44.437	121.598	77	3	1.29

Table 3: Prograde Frequency Terms (cont.)												
m	n	o	j	k	l	frequency "yr ⁻¹	phase deg.	I_{mnojkl} × 10 ⁻⁸	#	ϵ_c deg.		
4	0	2	4	3	1	2	3	44.489	188.874	122	8	1.50
4	1	2	3	3	1	8	3	44.494	24.968	40	2	1.04
42	2	4	3	1	1	4		44.502	213.753	787	2	2.79
4	3	2	4	3	1	7	3	44.581	41.199	66	3	1.22
44	2	4	3	1	8	4		44.603	313.655	28	4	0.93
4	5	2	4	3	5	1	4	44.619	25.492	38	5	1.02
4	6	2	4	3	2	3	1	44.660	334.363	50	5	1.12
4	7	2	4	3	1	5	3	44.669	47.545	84	3	1.33
48	2	4	3	1	3	1		44.775	327.003	582	8	2.53
4	9	2	4	3	1	6	4	44.782	310.677	34	2	0.98
50	2	3	3	3	5	1		44.805	329.770	47	7	1.09
51	2	4	3	1	8	3		44.874	35.937	54	2	1.14
52	2	4	3	5	3	1		44.892	136.813	50	7	1.12
5	3	2	3	3	4	5	1	44.925	158.475	33	4	0.97
5	4	2	4	3	1	10	3	44.944	347.277	31	2	0.95
5	5	2	4	3	1	3	4	45.055	24.462	50	4	1.12
56	2	3	3	2	5	1		45.211	7.143	39	4	1.03
57	2	3	3	1	5	1		45.326	359.336	443	5	2.31
58	2	3	3	1	5	4		45.605	114.091	34	1	0.98
5	9	2	3	3	1	5	3	45.877	210.878	72	2	1.26
6	0	3	4	4	1	1	1	53.028	325.765	1081	84	3.10
6	1	3	4	3	1	1	2	53.580	182.894	1826	66	3.70
6	2	3	4	3	3	1	1	53.849	104.727	1028	54	3.05
6	3	3	4	3	1	1	1	54.131	41.941	2753	71	4.24
6	4	3	4	3	1	1	4	54.411	138.366	1023	25	3.05
6	5	4	4	3	1	1	1	54.682	247.735	1964	51	3.79

Table 3: Prograde frequency orbital variations (see Eq. (7) and appendix B). The identification number $\{mnojkl\}$ of the largest term of a total number # contributing to a given amplitude (eq. 133) is given. A critical excitation obliquity ϵ_c (eq. 88) for each term is indicated. Terms 29, 42, 48 and 57 have been identified with the following combinations of the eigenfrequencies

$$\begin{aligned}
\frac{d}{dt}\psi_{243111} &= g_2 + g_4 - s_3, \\
\frac{d}{dt}\psi_{234114} &= g_2 + g_4 - s_3 + \delta f_1, \\
\frac{d}{dt}\psi_{243131} &= g_2 + 2g_4 - g_3 - s_3, \\
\frac{d}{dt}\psi_{233151} &= g_2 + g_4 + s_4 - 2s_3.
\end{aligned}$$

Laskar [1990] found that he had to introduce new frequencies $\delta f_1 = 0.28'' \text{ yr}^{-1}$ and $\delta f_2 = 0.12'' \text{ yr}^{-1}$ to aid this identification. Also $2\delta f_1 = g_3 - g_4$.

Table 4: Atmospheric Pressure Amplitudes				
Source	$\delta P(2n - \omega)$	$\delta P(-\omega)$	$\delta P(2n - 2\omega)$	$\delta P(2n)$
D V	1.3	1.8	0.61	1.5
D VI	1.4	3.1	0.79	1.2
D VII	2.0	4.0	1.2	1.8
D VIII	3.9	12	2.2	5.5
PI 1			(1.30	
PI 2			1.6	
SZ			0.7	

Table 4: Pressure amplitudes (in mbar) for 4 thermal tide constituents derived from models constructed by Dobrovolskis [1978] (see DV-DVIII), Pechmann and Ingersoll [1984] (see PI1 and PI2), and Shen and Zhang [1989,1990] obtained estimates for the semi-diurnal tide. Only models in which bottom heating is significant are included here. The DVIII, PI2 and SZ models assume heating close the ground. Models D VII (and PI1), D VI and D V limit heating to a thermal skin depth of $\sim 1.1\text{km}$, $\sim 3.5\text{km}$ and $\sim 20\text{ km}$, respectively. The Dobrovolskis' models (values quoted are average of submodels C and D obtained using method 1 for the equivalent depth: See pages 68-71 of thesis) assume an integrated column heat flux of 100W m^{-2} . To achieve the appropriate scaling, the diurnal and zonal tidal amplitudes of Dobrovolskis models have been multiplied by 2/3 and 3/4, respectively.

Table .5: Nominal Venusian Structure Profile

Crust:	Thickness= 20km
ρ	2.25gcm^{-3}
K	0.564Mbar
μ	0.358Mbar
Upper mantle:	$P_r < 0.14\text{Mbar}$
P	$(3.2979 + 1.9247P, -- 0.79409P_r^2)F_\rho$
K	$(1.1694 + 3.8885 P, + 2.209P_r^2)F_K$
μ	$(0.55031 + 1.7642 P, + 1.0441P_r^2)F_\mu$
	$0.141\text{Mbar} < P, < 0.239\text{Mbar}$
P	$(3.2617 + 3.8224P, - 1.7296P_r^2)F_\rho$
K	$(1.6813 + 3.4164P_r - 0.31619P_r^2)F_K$
μ	$(0.6237 + 2.256971; + 1.0403 P_r^2)F_\mu$
Lower mantle:	$P_r > 0.239\text{Mbar}$
P	$(4.0370 + 1.4995P, - 0.3233P; + 0.0304P_r^3)F_\rho$
K	$(2.2571 + 3.2436P, + 0.2726P_r^2 - 0.2283 P_r^3)F_K$
μ	$(1.2793 + 1.6682P, - 0.4046P_r^2 + 0.0542 P_r^3)F_\mu$
Core	
P	$7.2952 + 2.4174P, - 0.4106P_r^2 + 0.0375P_r^3 + \delta\rho$
K	$2.6737 + 1.5670P, + 1.1227P_r^2 - 0.2020P_r^3$
μ	$0.4390 + 0.2186P, + 0.0318P_r^2$

This extrapolation from Earth's solid inner core is used to determine rigidity of hypothetical Venusian solid core. If Venus' mantle has the same composition as Earth's then the Venusian iron core must contribute about 4% less to the total mass as compared to Earth's core [Ring wood and Anderson, 1977].

Table 6: Venusian structure and Love numbers

$f_{\text{Fo}}(Mg)$	R_c	ρ_c	C/MR^2	C_c/MR^2	$\delta\rho_c$	h_2	l_2	k_2
%	(km)	g cm^{-3}			g cm^{-3}			
94	3000	11.806	0.33089	0.02657	1.065	0.4496	0.0750	0.2256
94	3100	11.201	0.33181	0.02968	0.561	0.4763	0.0766	0.2398
94	3200	10.665	0.33274	0.03309	0.120	0.5064	0.0784	0.2556
94	3300	10.189	0.33371	0.03684	-0.265	0.5390	0.0809	0.2729
94	3400	9.763	0.33471	0.04091	-0.605	0.5742	0.0839	0.2915
94	3500	9.380	0.33573	0.04544	-0.904	0.6115	0.0873	0.3116
89	2900	11.782	0.33499	0.02247	1.034	0.4393	0.0769	0.2216
89	3000	11.173	0.33577	0.02517	0.523	0.4649	0.0781	0.2353
†89	3100	10.636	0.33657	0.02821	0.078	0.4931	0.0796	0.2503
89	3200	10.161	0.33739	0.03155	-0.310	0.5239	0.0814	0.2667
89	3300	9.737	0.33825	0.03524	-0.650	0.5566	0.0839	0.2842
89	3400	9.358	0.33913	0.03925	-1.213	0.6301	0.0869	0.3034
84	2800	11.681	0.33927	0.01868	0.940	0.4310	0.0790	0.2184
84	2900	11.076	0.33992	0.02109	0.428	0.4555	0.0798	0.2320
84	3000	10.545	0.34060	0.02377	-0.016	0.4814	0.0811	0.2459
84	3100	10.076	0.34130	0.02674	-0.401	0.5103	0.0824	0.2614
84	3200	9.660	0.34203	0.03003	-0.738	0.5416	0.0847	0.2785
84	3300	9.289	0.34276	0.03365	-1.033	0.5745	0.0870	0.2963
89*	3000	11.173	0.33577	0.02517	0.523	0.3410	0.0818	0.1704
84''	2800	11.681	0.33927	0.01868	0.940	0.3300	0.0814	0.1674
84*	2900	11.076	0.33992	0.02109	0.428	0.3397	0.0796	0.1711

The (*) members have solid iron cores, but are otherwise identical to their fluid counterparts.†The equivalent Love numbers (see equation 42) due to core tidal potential ($\tilde{\gamma}$) and core rotational potential ($\tilde{\beta}$) for this model are: $\tilde{\gamma} = 0.502$ and $\tilde{\beta} = 0.117$.

Table 7: Coefficients C_{ij}

i	j	α	C_{ii}	C_{ij}	C_{jj}
1	2	0.535161	0.999175	0.181914	-0.848870
1	3	0.387098	0.257424	0.016035	-0.130126
1	4	0.254058	0.075304	-0.000401	-0.012402
1	5	0.074394	0.005041	-0.000246	0.004115
1	6	0.040589	0.001477	-0.000076	0.002452
2	3	0.723331	9.308230	3.914970	12.047100
2	4	0.474732	0.564162	0.071555	-0.400567
2	5	0.139012	0.018625	-0.000723	0.004964
2	6	0.075844	0.005244	-0.000255	0.004173
3	4	0.656314	3.746720	1.210460	-4.245600
3	5	0.192184	0.038306	-0.000995	0.001306
3	6	0.104854	0.010240	-0.000459	0.005017
4	5	0.292823	0.109762	0.001201	-0.029789
4	6	0.159762	0.025239	-0.000867	0.004162
5	6	0.545593	1.107610	0.213283	-0.967739

Table 8: Obliquity function d_{jm}^2 ($n = 2$)

j	m	d_{jm}^2
2	2	c_2^4
	1	$2c_2^3s_2$
	0	$-\sqrt{6}c_2^2s_2^2$
	-1	$-2c_2s_2^3$
	-2	s_2^4
1	1	$c_2^4 - 3c_2^2s_2^2$
	0	$\sqrt{6}c_1c_2s_2$
	-1	$s_2^4 - 3c_2^2s_2^2$
0	0	$1 - 6c_2^2s_2^2$

Figure Captions

1: Components of Venusian obliquity. The total obliquity (free plus forced) relative to the orbit is 2.6° .

2: Nominal profile of density ρ (g cm⁻³), compressibility K (Mbar) and rigidity μ (Mbar) as a function of pressure for an earth-like model.

3: Love number k_2 versus moment of inertia with lines joining models with common mantle molar fraction $f_{\text{Fo}} = (Mg/(Fe + Mg))$.

4: Love number k_2 versus core moment.

5: Love number k_2 versus core density difference $\delta\rho_c$. The apparent clustering of models with 100km difference in core radii is coincidental.

6: Spectral amplitudes of prograde frequency terms in orbit inclination for a limited frequency range: $41'' \text{ yr}^{-1}$ to $53'' \text{ yr}^{-1}$. Light grey band corresponds to predicted range in (6) while narrow dark bands indicate resonance widths of major lines within band.

7: Forced component of Venusian obliquity as a function of the precession frequency, σ derived from a linear response model. The free obliquity is the difference between the observed location and some point on the curve. Fig. 7a plots p_x versus p_y , with location of prominent resonances indicated, Origin is the invariable plane normal. Fig 7b plots amplitudes of both free obliquity and obliquity relative to invariable plane normal.

8: Mantle response ($p = p_r - ip_i$) as a function of core σ_c for unit forcing with frequency $s = -18.85'' \text{ yr}^{-1}$. Here $\alpha = 0.15$ and $\sigma_0 = 45.5'' \text{ yr}^{-1}$. Curves for $\hat{K}_c (= K_c(s - \sigma_0)/\alpha s^2)$ fixed at 1.5, 0.75, 0.5 and 0.25 are shown.

9: The forced obliquity as a function of CMB, retrograde FCN σ_c for a choice of parameters which result in the curve passing through the observed pole at $\sigma_c = -18.5'' \text{ yr}^{-1}$. Note that the moment of inertia ratio is large ($\alpha = 0.15$) and CMB friction parameter $K_c = 6 \times 10^{-7}$ is exceptionally small. The orbit normal and the predicted position of the forced obliquity for $CC = 29e_0$ (b) is also shown relative to the invariable plane normal at (0,0). Line c-b is the free component vector.

10. Venusian obliquity damping rate resulting from toroidal shear caused by either free precession or spheroidal tidal deformation of a uniformly viscous core. The dashed lines correspond to Vanyo's [1991: eq. (13) and figure 7] result for the onset of turbulence assuming $\epsilon = 2.1^\circ$, and are to be compared with the model calculation shown for two values of σ_0/σ_c . The Stokes limit applies when $\nu/\omega R_c^2 \gg 1$ and the equivalent core $K_c = 35\nu/R_c^2$.

11: Earth's obliquity decay (or growth) rate caused by a viscous fluid core.

12: Tidal histories of obliquity $\epsilon(t)$ as a function of both time T/T_0 (a) and spin $\omega(T)/\omega(\text{now})$ (b). The atmospheric, thermal, semi-annual tide dominates near 90° and allows evolution from prograde to retrograde orientation. The time scale $T_0 = 1/K_{ts}(\text{now}) \sim 5 \times 10^7 \text{ yr}$. The mantle nonhydrostatic e_o is set equal to $3e_o(\text{now})$ until $T = 70T_0$, after which $e_o = e_o\omega(T)/\omega(\text{now})$. This choice tends to speed up the onset of core friction. Here the separatrix starts at a prograde obliquity of $\simeq 45^\circ$ (retrograde obliquity of 135°) and $\omega(0)/\omega(\text{now}) = 30$.

13: Tidal history of the FMN frequency $\simeq \sigma_o \cos \epsilon$, for a few of the curves in Figure 8 which begin with prograde orientation.

14: Tidal histories of obliquity for the case where the semi-diurnal tides are omitted. The maximum starting obliquity at $T=0$ and $\omega(0)/\omega(\text{now}) = 30$ on the separatrix is $\sim 28^\circ$. Only the onset of core friction preserves a potential retrograde end state.

15: Temporal history of obliquity with linearly increasing $J_2(d \ln J_2/dt = 5 \times 10^{-11} \text{ yr}^{-1})$ and initial $p_x = 0.002$, $p_y = 0.000$ and $\sigma_o(J_2) = 43.8'' \text{ yr}^{-1}$. Tidal $K_{ts} = 2.4 \times 10^{-8} \text{ yr}^{-1}$, and from core friction, the equilibrium $\sin \epsilon_0 = 0.024$. Plots b, c and d show $\{p_x, p_y\}$ history during passage through resonances associated with arguments $\psi_{243111}(170 \text{ myr} \leq t \leq 310 \text{ myr})$, $\psi_{243114}(320 \text{ myr} \leq t \leq 400 \text{ myr})$, and $\psi_{243131}(420 \text{ myr} \leq t \leq 500 \text{ myr})$, respectively. For each case, p_x and p_y are shown relative to rotating frame of each argument such that phase relative to the present is preserved. Observed pole location pole (diamond) is indicated, and origin is predicted pole position (see eq. 9) due to non-resonant, retrograde terms.

16: Obliquity history with positive rate $d \ln J_2/dt = 5 \times 10^{-11} \text{ yr}^{-1}$ and $\sin \epsilon_0 = 0.012$. Panel b displays the $\{p_x, p_y\}$ history for $\psi_{243111}(171 \text{ myr} \leq t \leq 290 \text{ myr})$ while panel c shows $\psi_{243114}(325 \text{ myr} \leq t \leq 351 \text{ myr})$. These $\{p_x, p_y\}$ panels in this and other figures cover only the interesting time interval of the pertinent variable.

17: Obliquity history with positive rate $d \ln J_2/dt = 5 \times 10^{-11} \text{ yr}^{-1}$ and $\sin \epsilon_0 = 0.08$. Panel b shows the $\{p_x, p_y\}$ history covering $140 \text{ myr} \leq t \leq 240 \text{ myr}$ in the rotating frame of the ψ_{243111} angle variable.

18: Obliquity history with negative $d \ln J_2/dt = -5 \times 10^{-11} \text{ yr}^{-1}$, $\sin \epsilon_0 = 0.024$ and $p_x = 0.002$, $p_y(0) = 0.000$. Venus first encounters the argument ψ_{243131} (panel d).

19: Obliquity history with $d \ln J_2/dt = 4 \times 10^{-10} \text{ yr}^{-1}$ and $\sin \epsilon_0 = 0.024$ and initial $\sigma_o(J_2) = 43.5'' \text{ yr}^{-1}$.

20: Obliquity history with $d \ln J_2/dt = -4 \times 10^{-10} \text{ yr}^{-1}$, $\sin \epsilon_0 = 0.024$, initial $\sigma_o(J_2) = 47.8'' \text{ yr}^{-1}$ and $p_x(0) = 0.024$.

21: Frequency histories of four arguments $\{\psi_{243111}, \psi_{234114}, \psi_{243131}, \psi_{233151}\}$ which cover the past 150 myr (from figures 8 and 9 in [Askar, 1990]).

22. Obliquity history from -150myr to present due to temporal change in ψ_{234151} , with a) final $\sigma_o(t=0) = 45.23'' \text{ yr}^{-1}$, b) $\sigma_o(t=0) = 45.25'' \text{ yr}^{-1}$ and c) $\sigma_o(t=0) = 45.27'' \text{ yr}^{-1}$. Tidal $K_{ta} = -1 \times 10^8 \text{ yr}^{-1}$, the rate $d \ln J_2 / dt = 1 \times 10^{-12} \text{ yr}^{-1}$. Only the end stage of the $\{p_x, p_y\}$ history is shown, and again the $\{p_x, p_y\}$ panels are in the rotating frame of ψ_{234151} angle so that phase of excitation relative to observed pole position at present time can be compared with the numerical integration.

23. Obliquity history due to ψ_{234131} with fins] a) $\sigma_o(t=0) = 44.720'' \text{ yr}^{-1}$, $\sigma_o(t=0) = 44.728'' \text{ yr}^{-1}$ and $\sigma_o(t=0) = 44.732'' \text{ yr}^{-1}$.

24. History for the ψ_{234111} argument with a) final $\sigma_o(t=0) = 44.3555'' \text{ yr}^{-1}$ and b) $\sigma_o(t=0) = 44.3600'' \text{ yr}^{-1}$.

25: Obliquity history from -150myr to present due to temporal change in ψ_{234114} . Two values for the final $\sigma_o(t=0)$ are shown which delineate the upper bound on $\sigma_o(0)$: a) $\sigma_o(0) = 44.555''$ and b) $\sigma_o(0) = 44.580'' \text{ yr}^{-1}$.

26: Obliquity history from -150myr to present due to temporal change in ψ_{234114} . This integration is identical to figure 25 except that the K_{ta} damping rate is changed in each panel.

27. Profiles of the scaling factors F_ρ , F_K and F_μ for $f_{Fo} = 0.94$ and 0.84 .

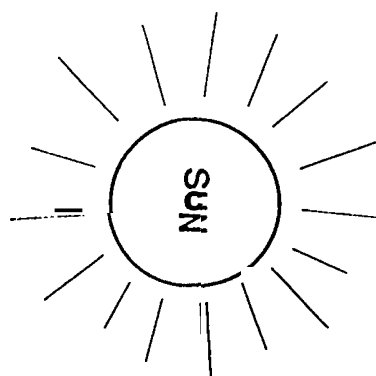
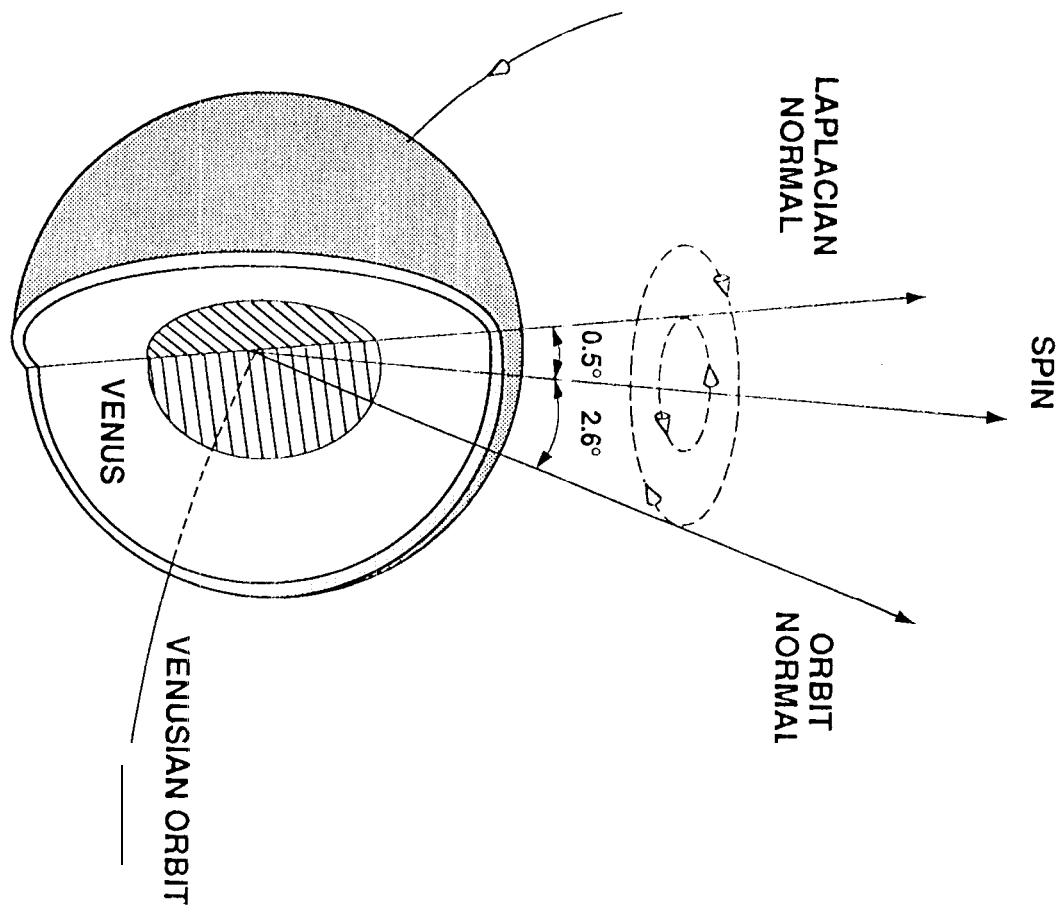
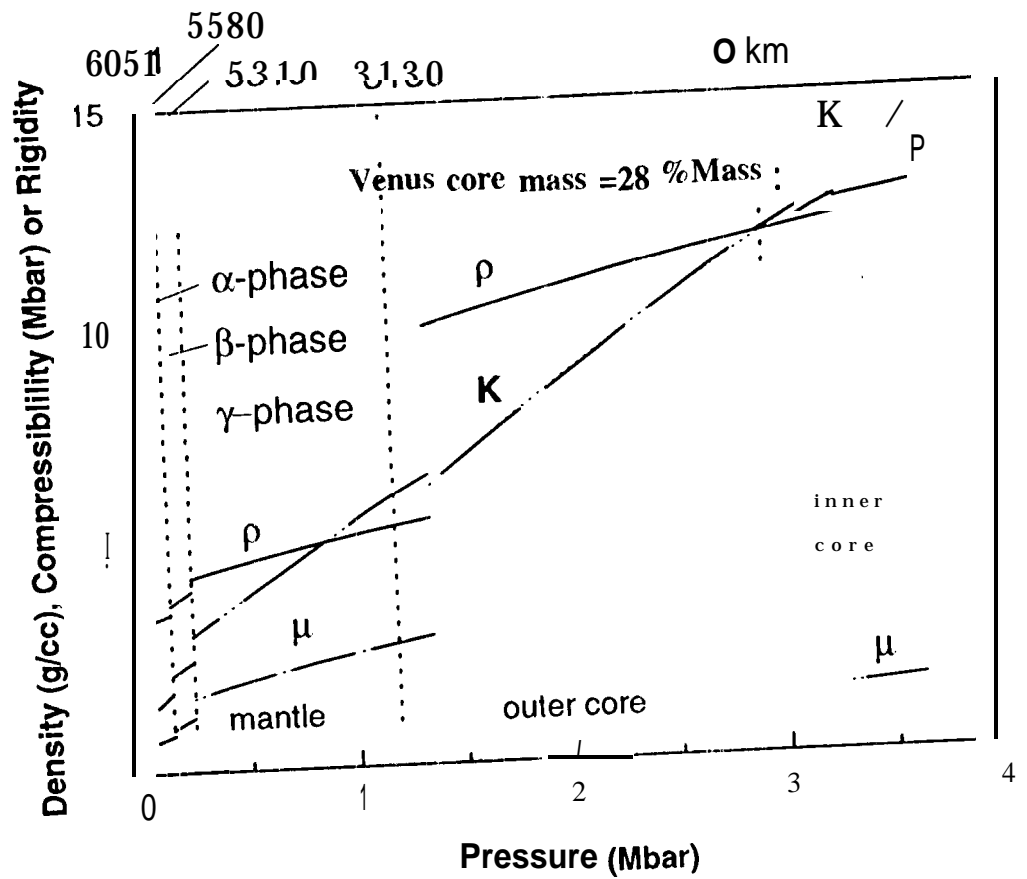
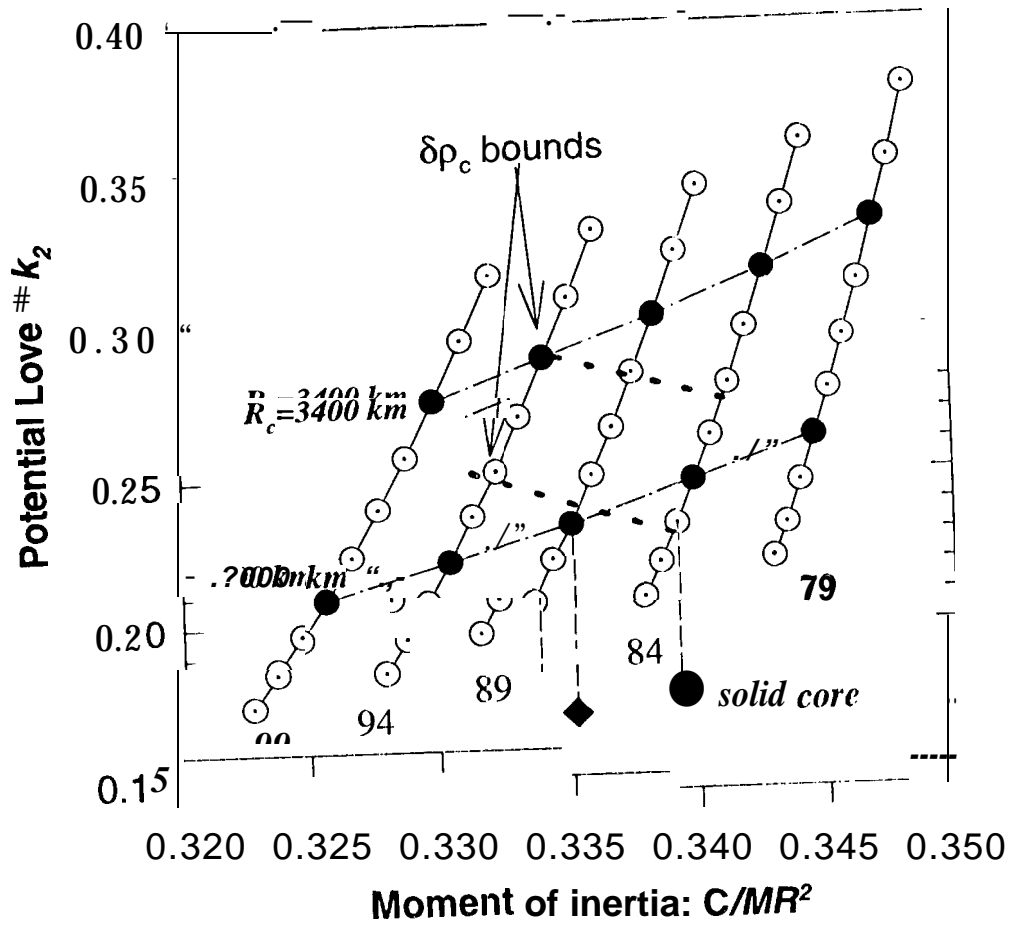


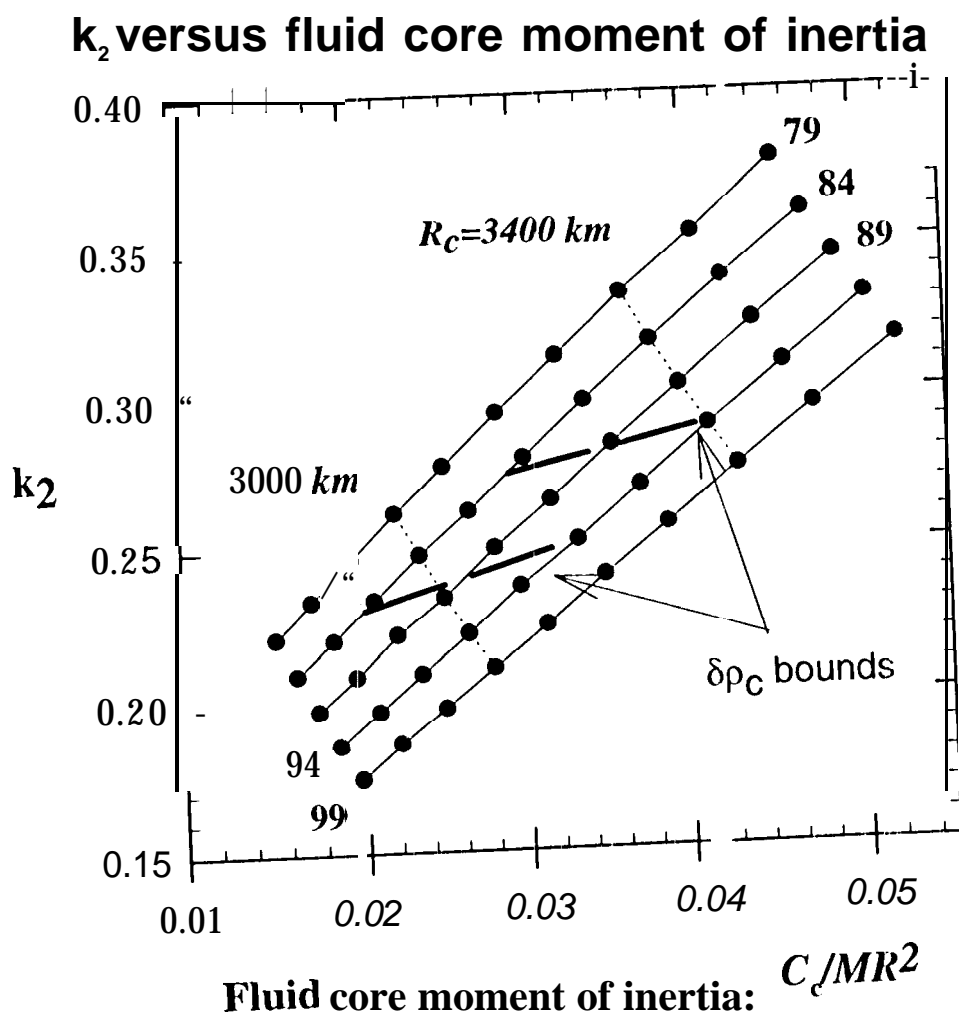
Fig 1 p 77

Earth-like Venus Model

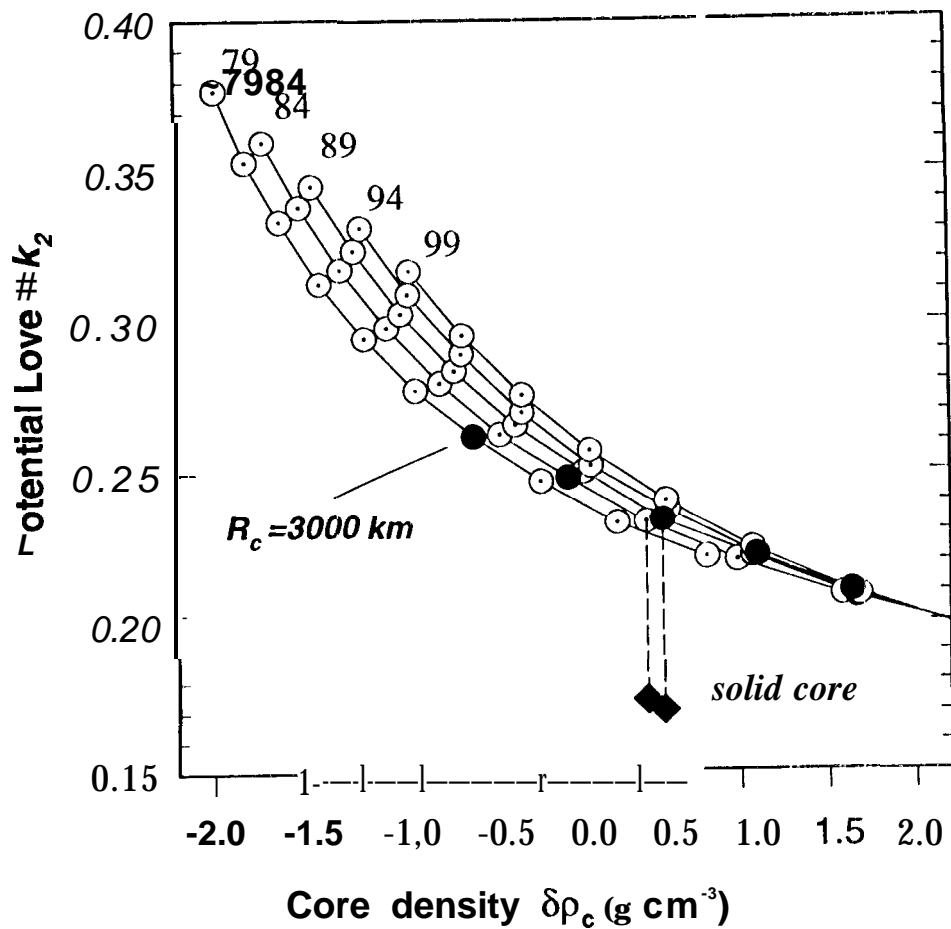


Venusian Structure from C and k_2

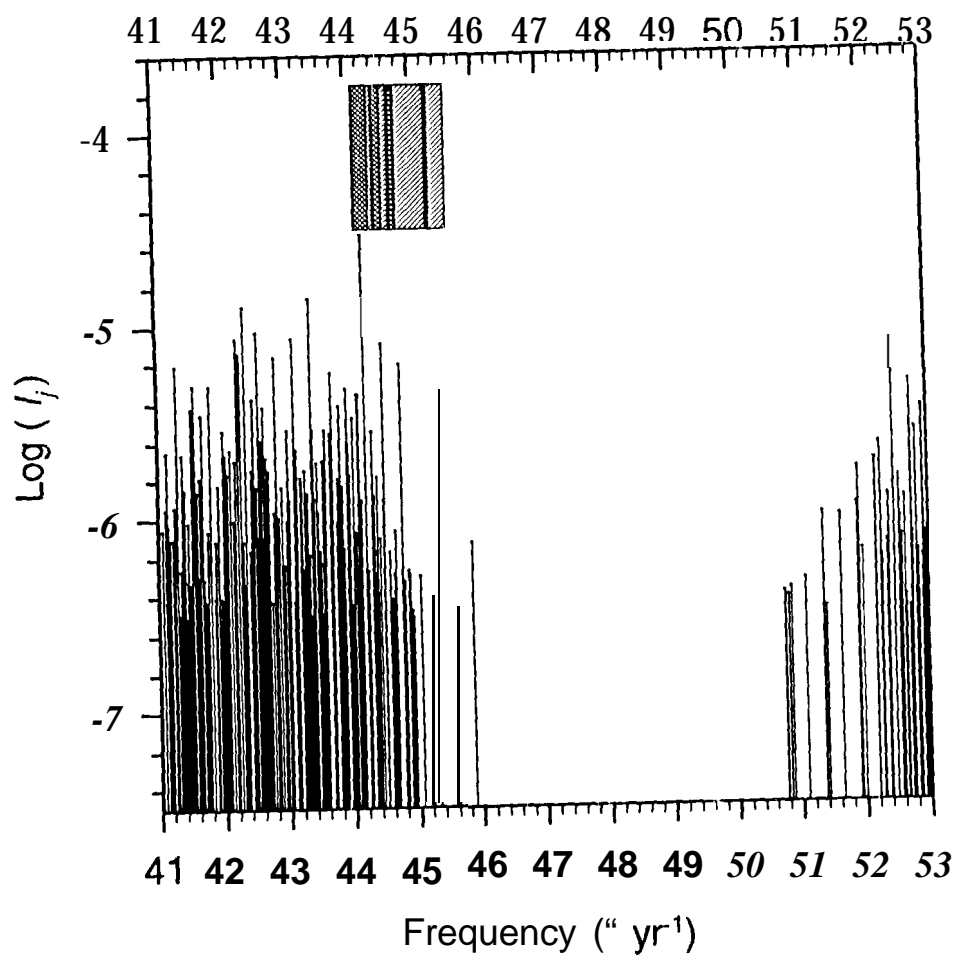




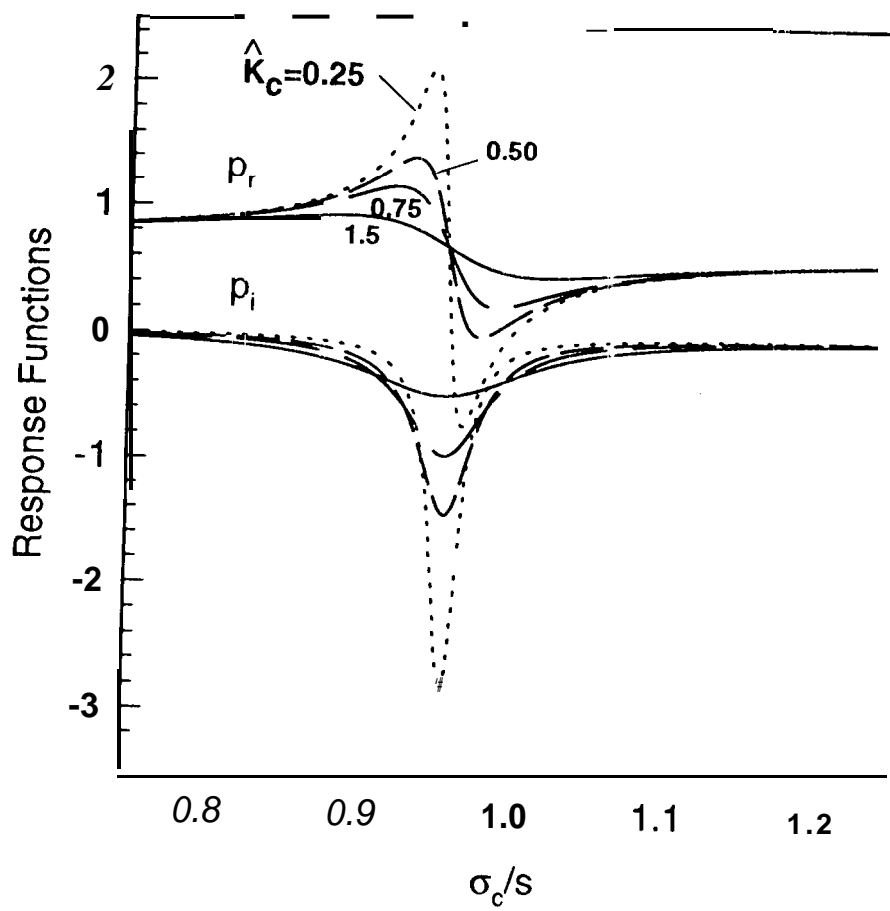
Venusian k_2 versus core density difference



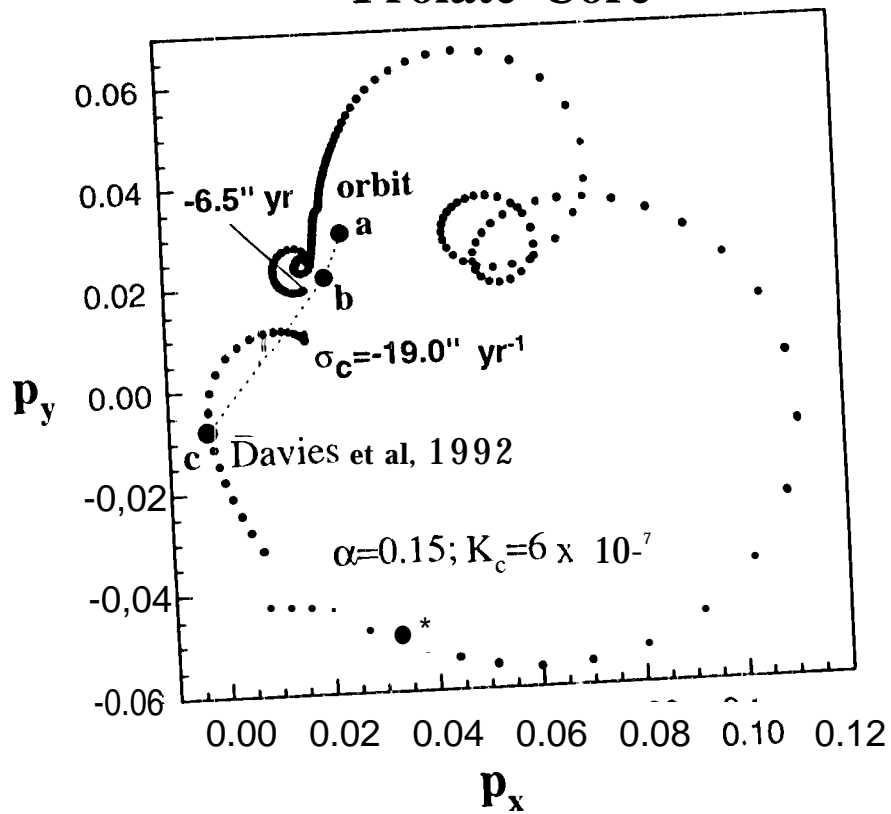
Spectral Amplitudes



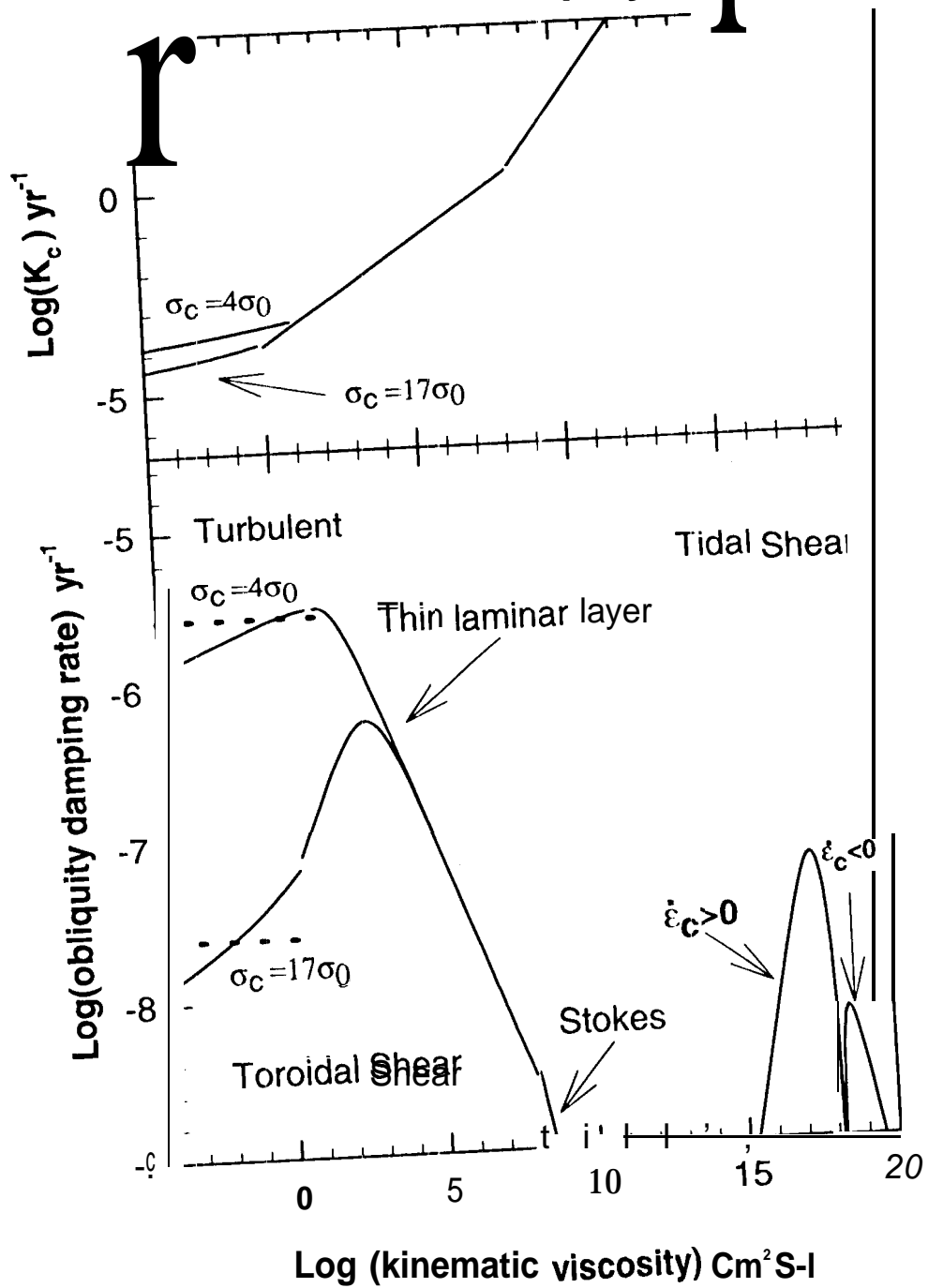
Mantle Response to Core Resonance



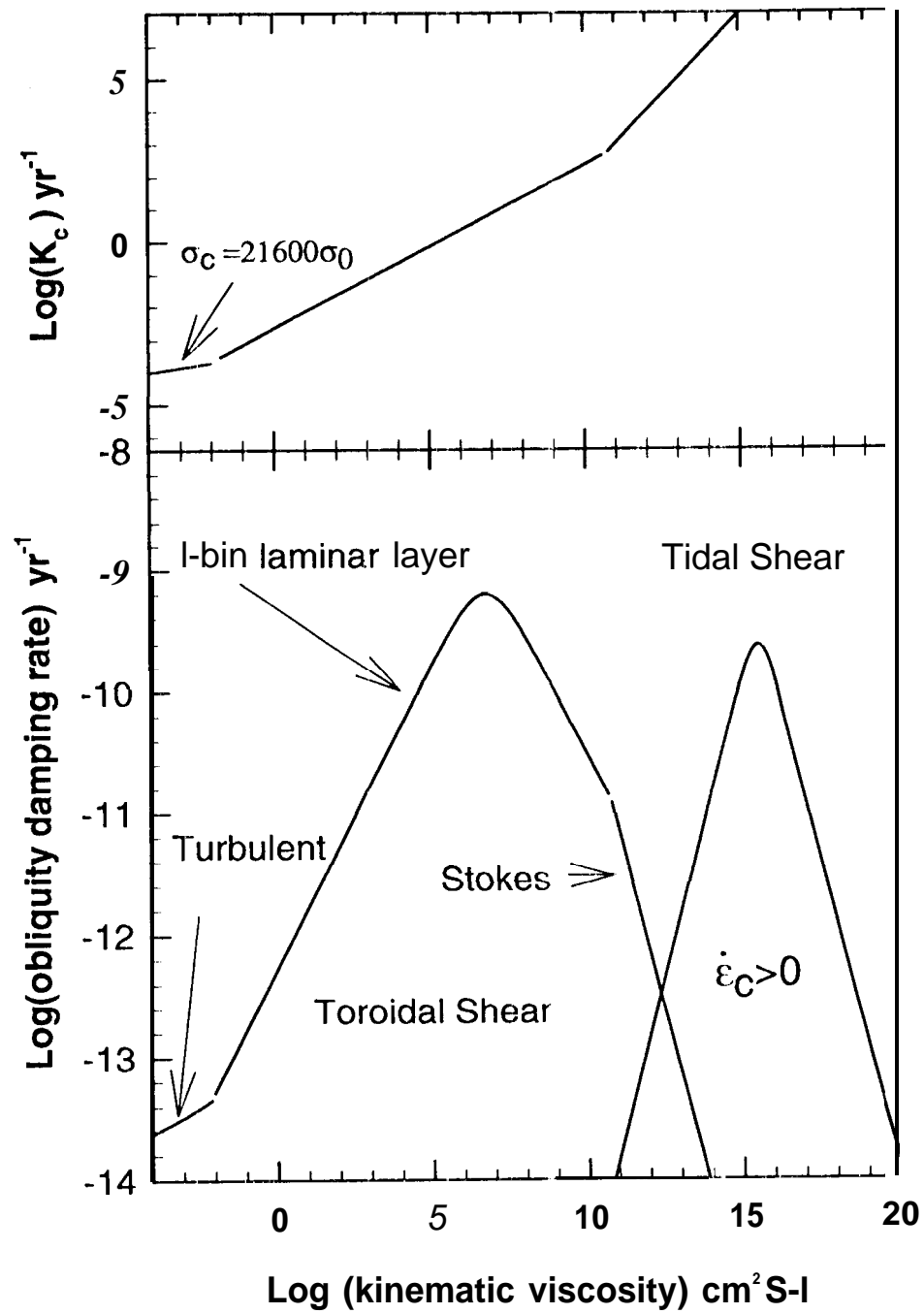
Model Pole position for Prolate Core



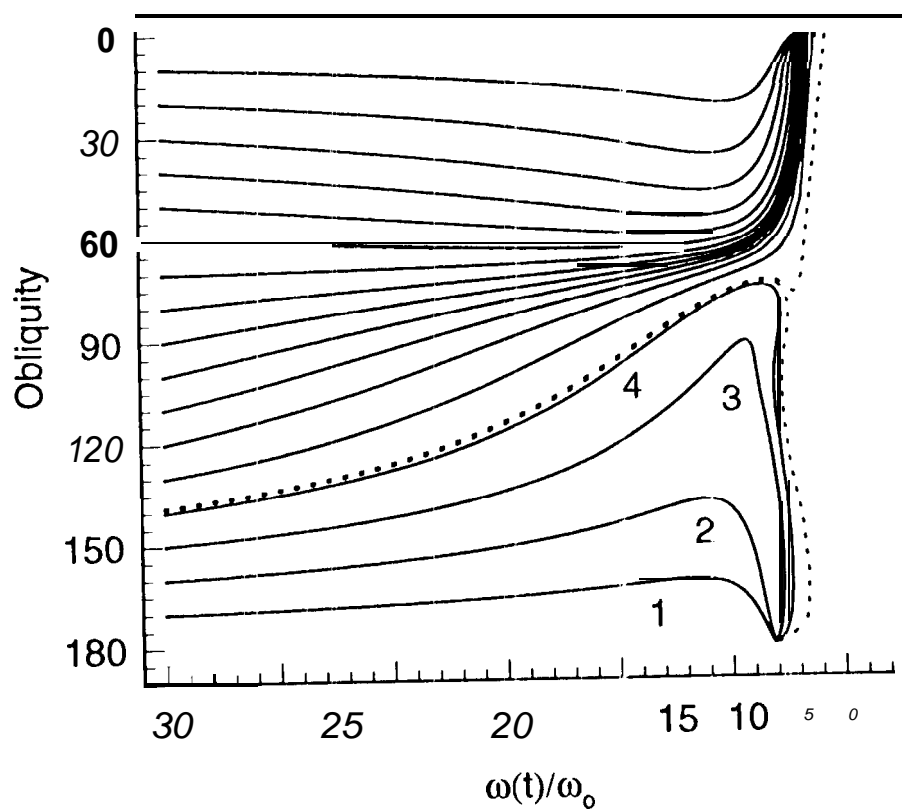
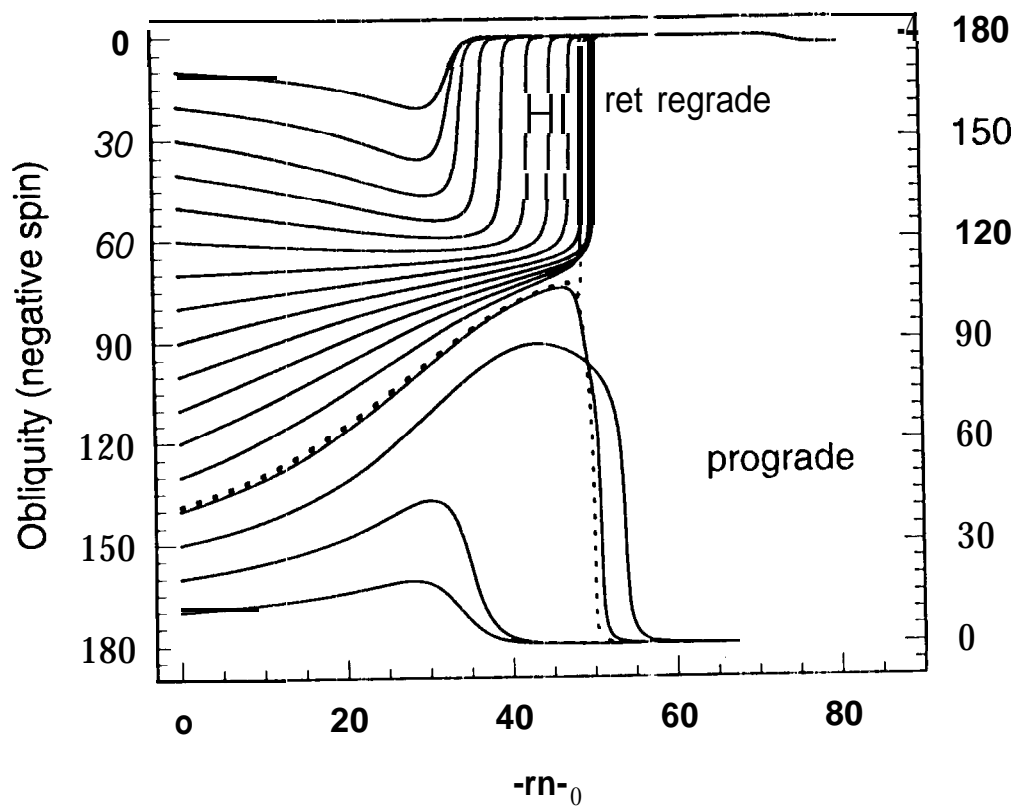
Venusian Viscous Core's Contribution to Obliquity Damping



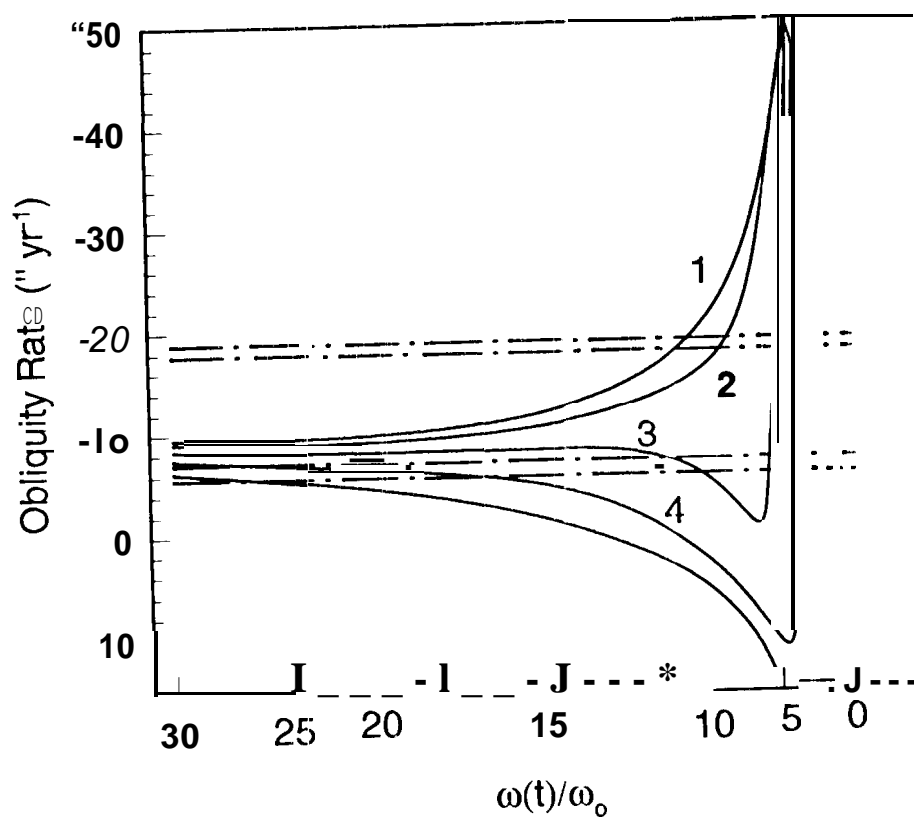
Earth-1ike Viscous Core's Contribution to Obliquity Damping



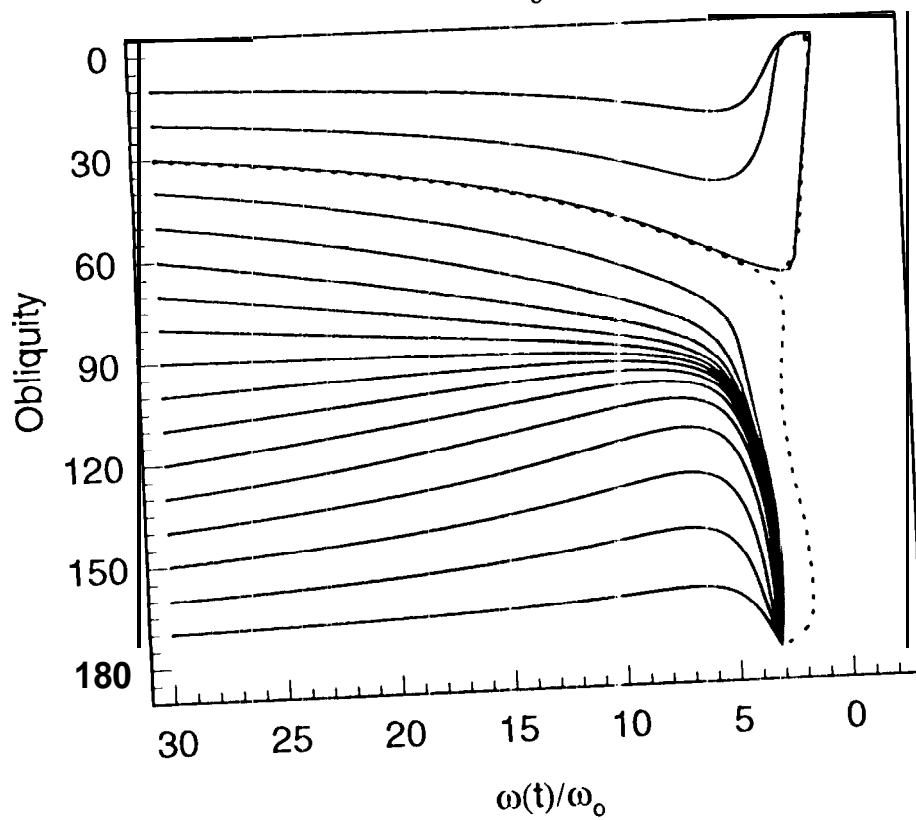
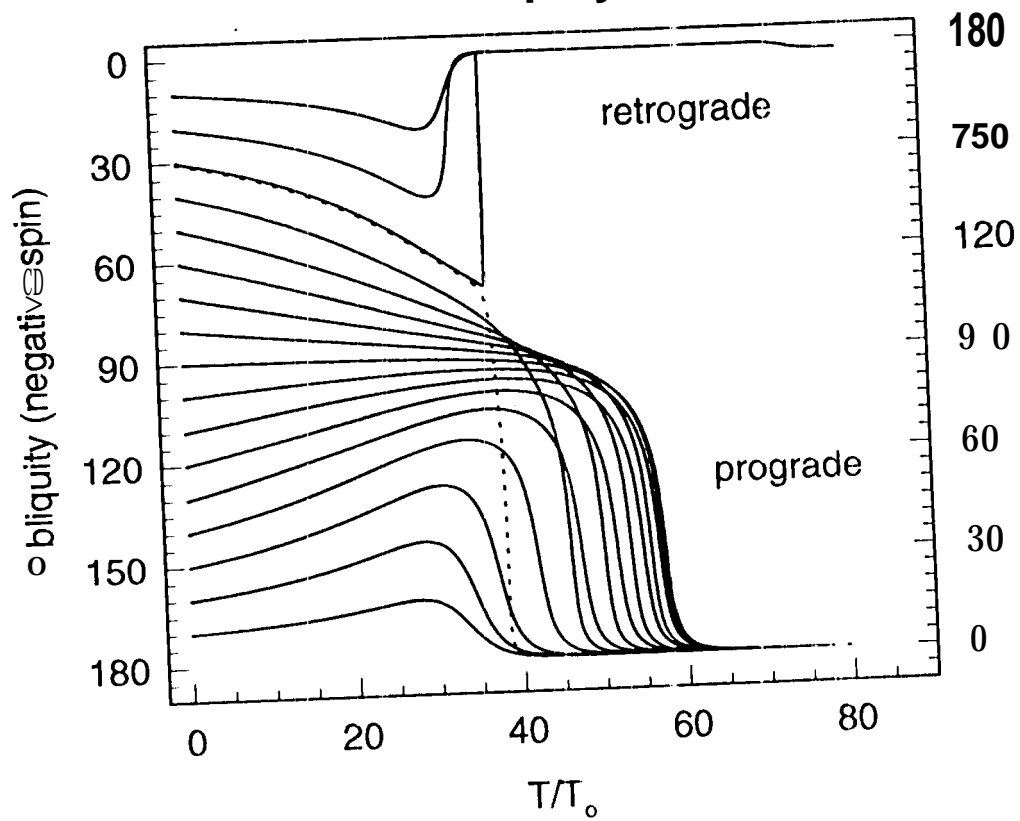
Venusian Obliquity Histories



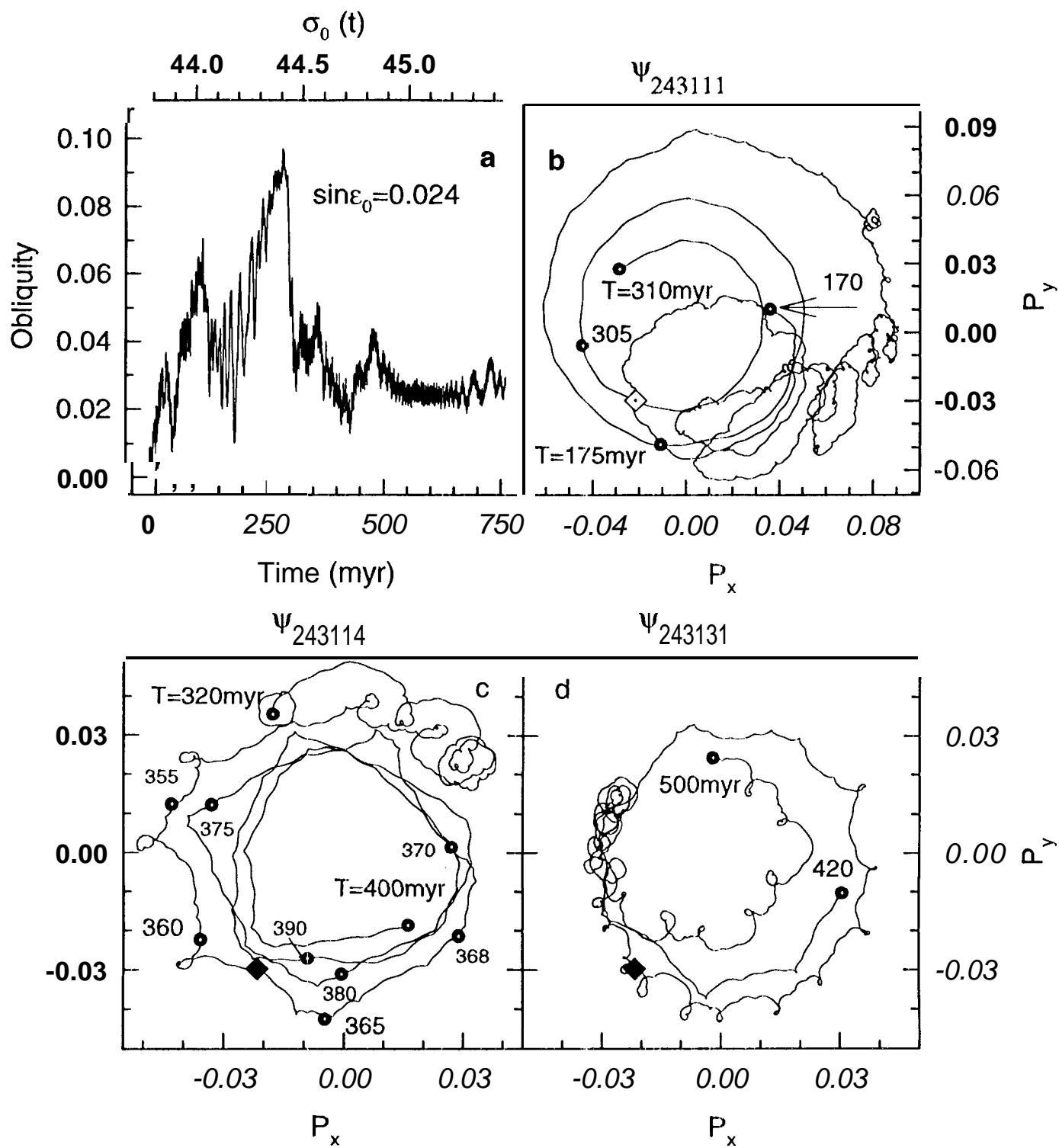
Obliquity Rate History



Venusian Obliquity Histories



$$f \sim 1/t^4$$



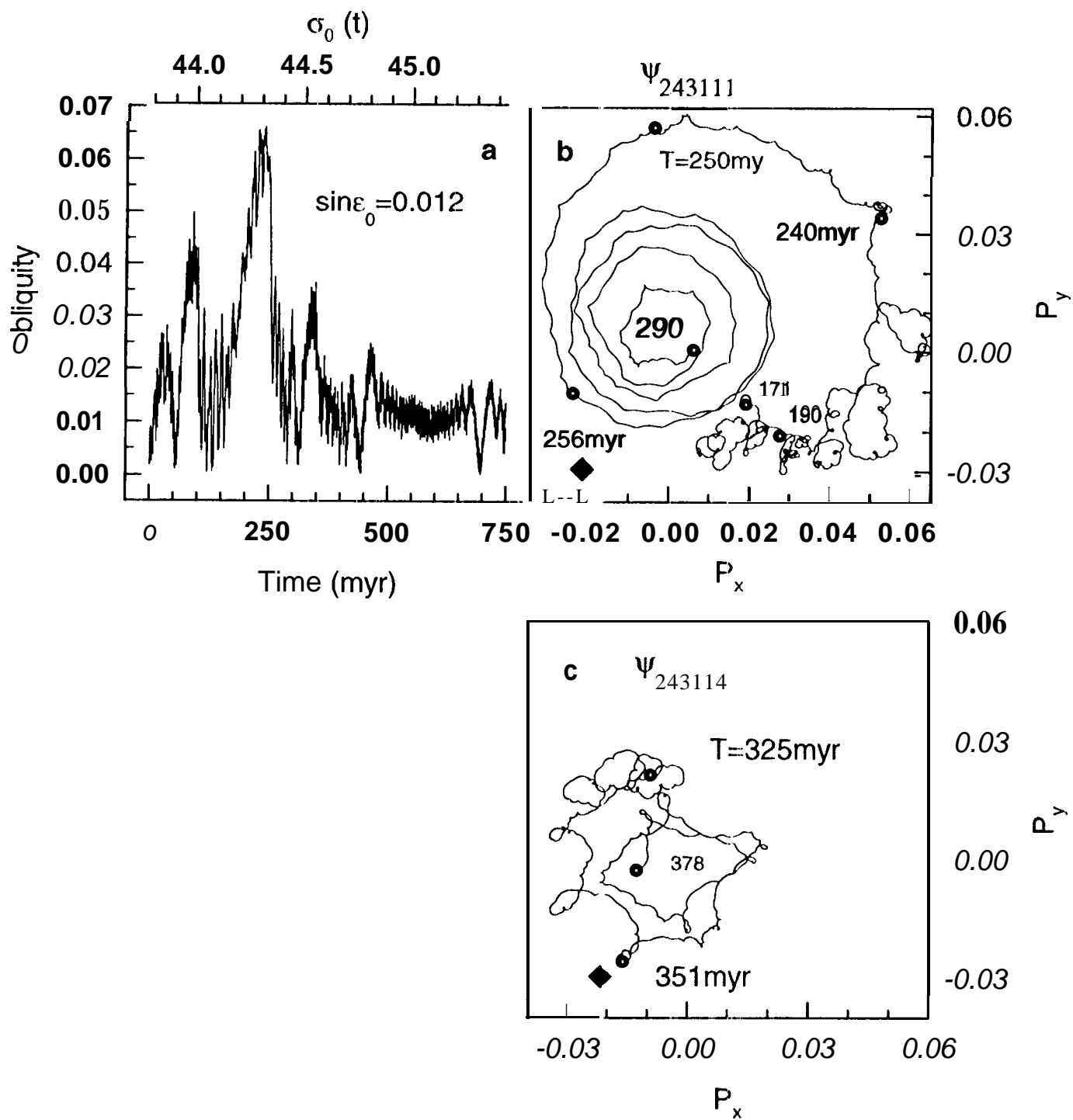
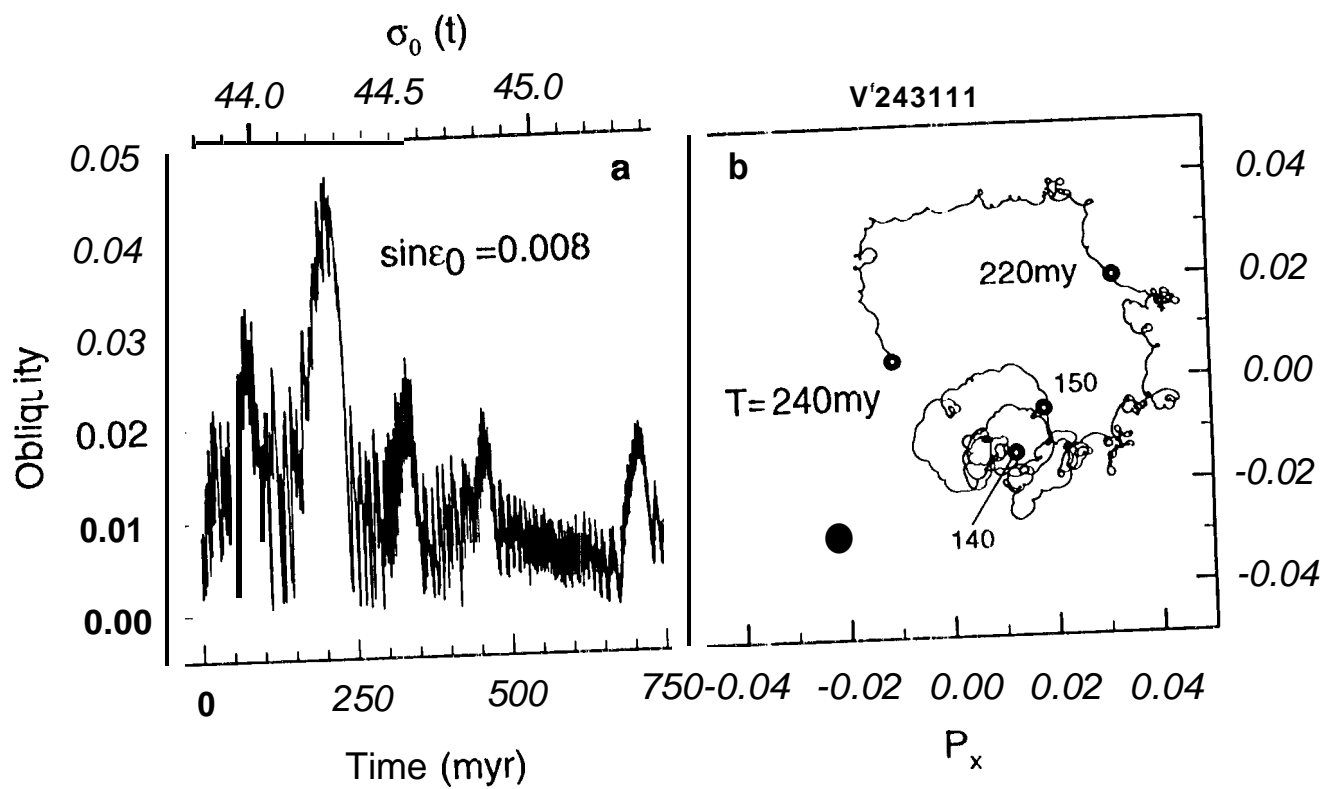
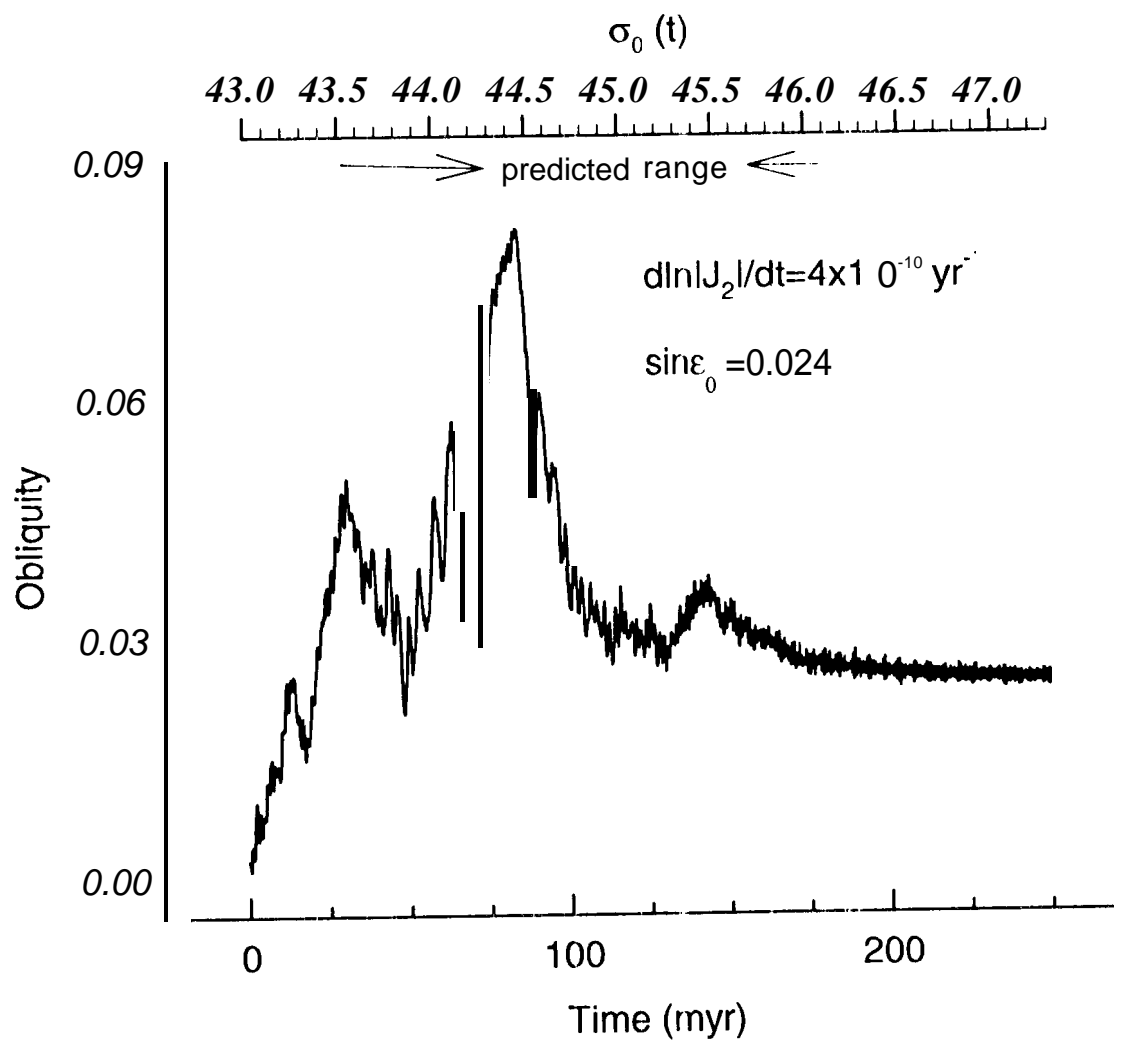
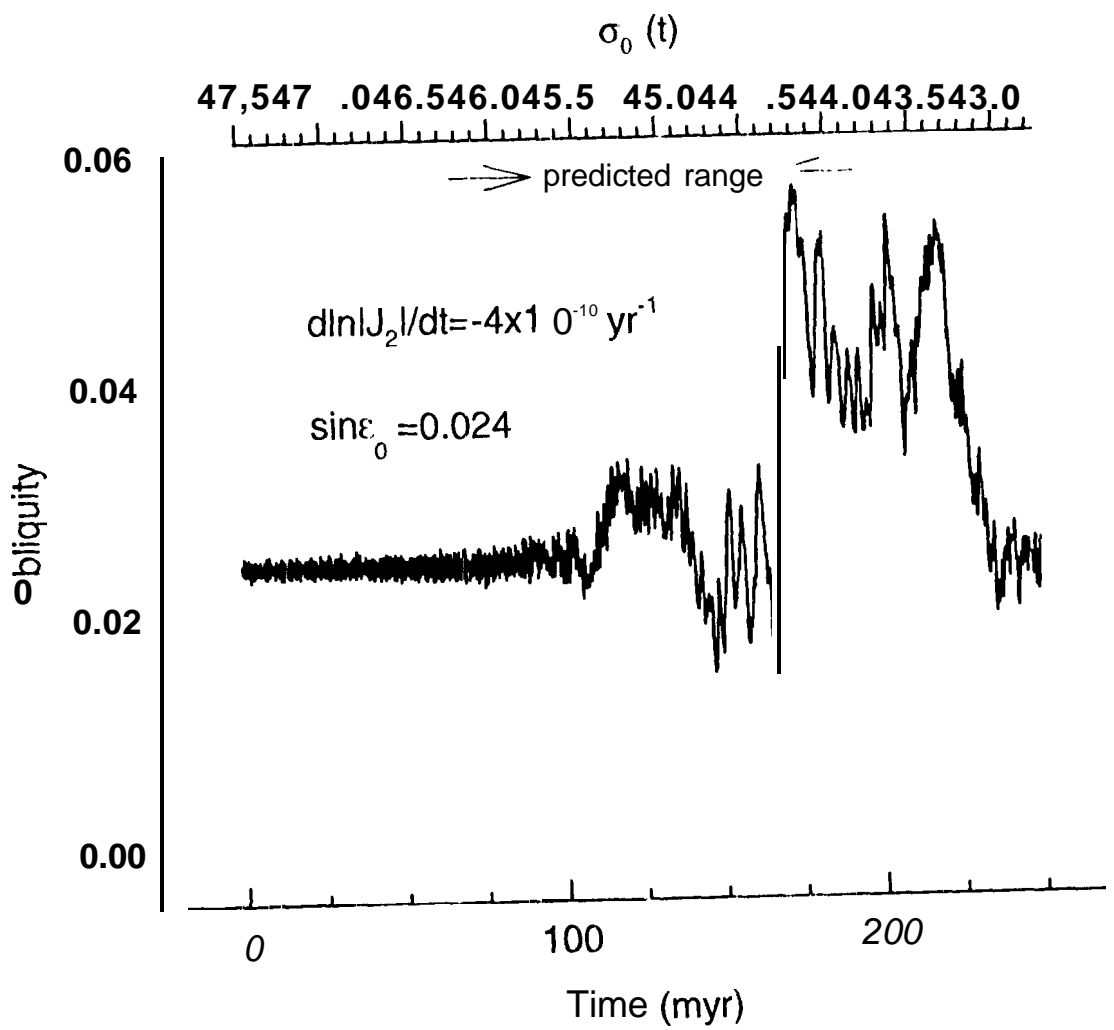
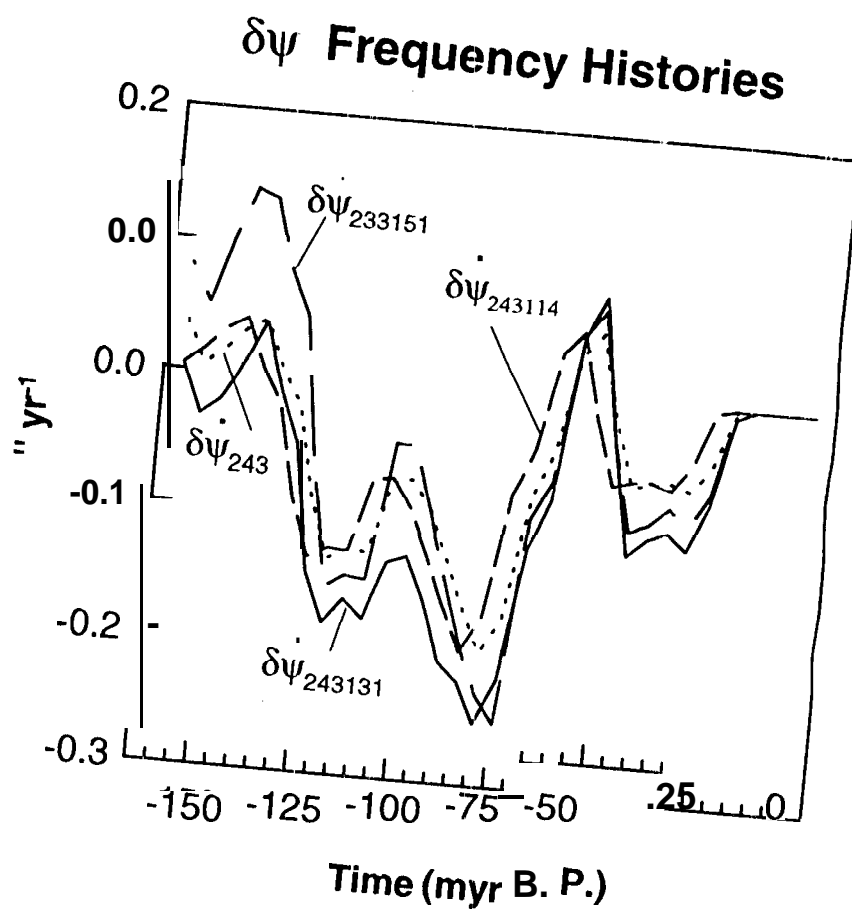


Fig 16

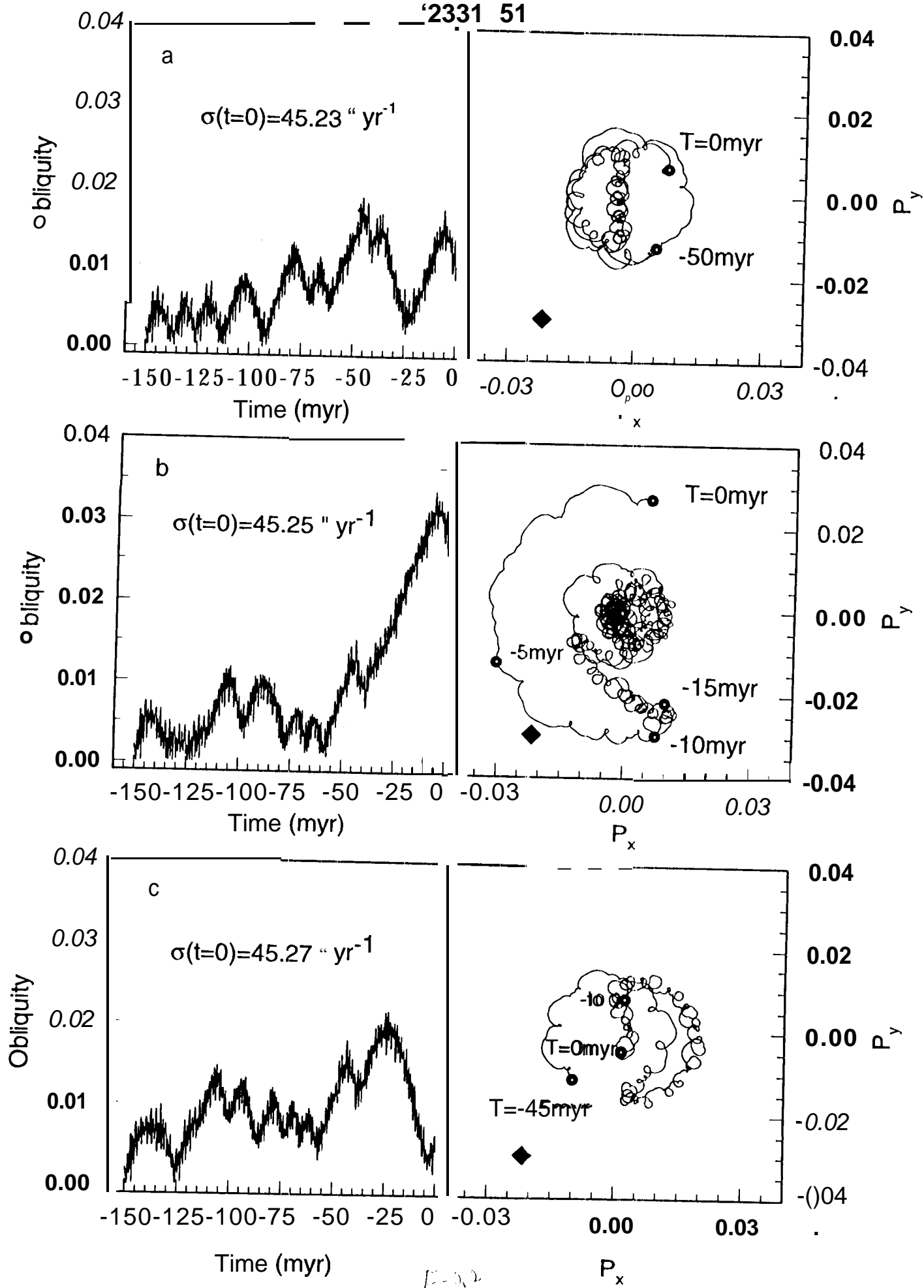




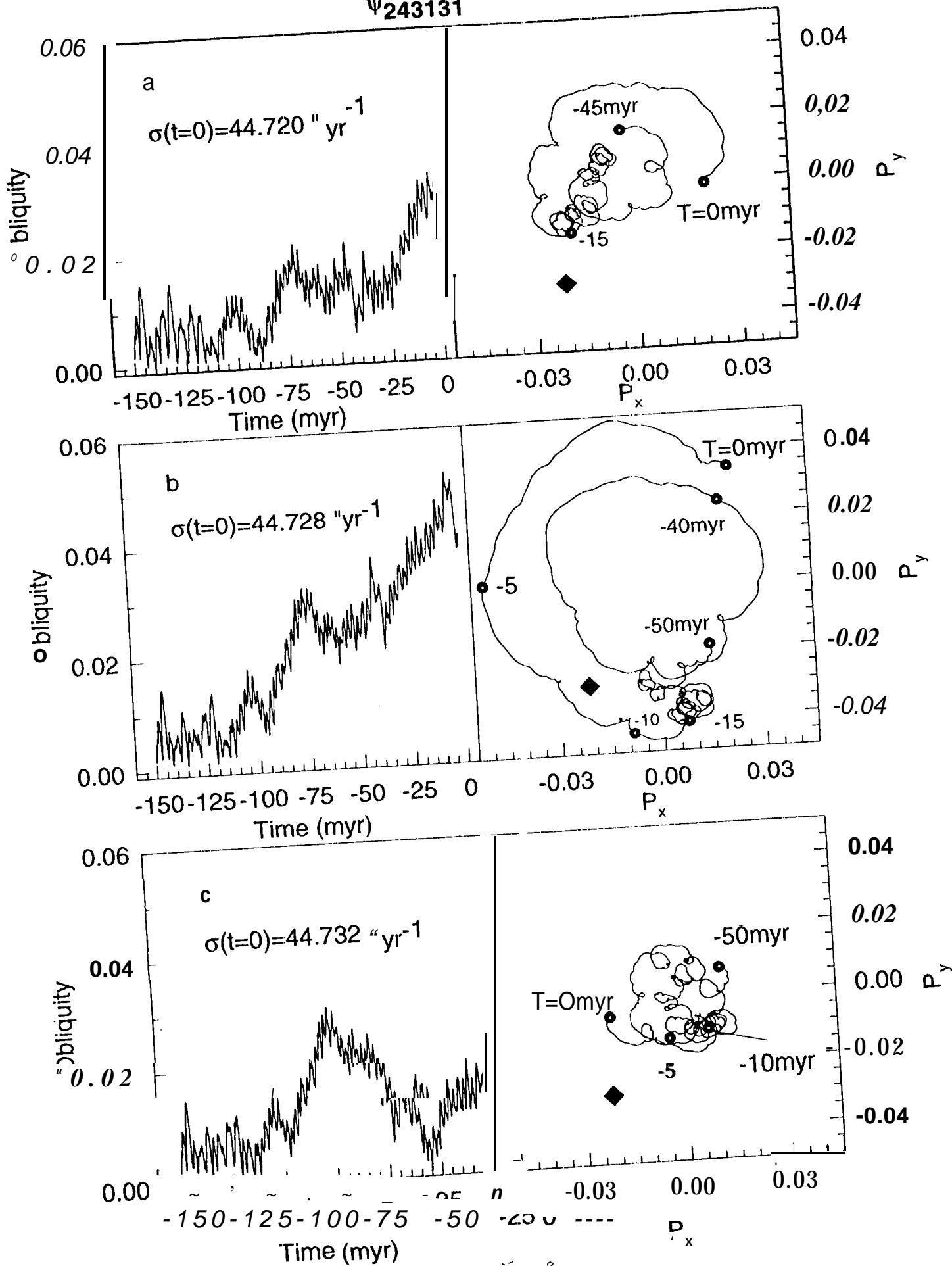




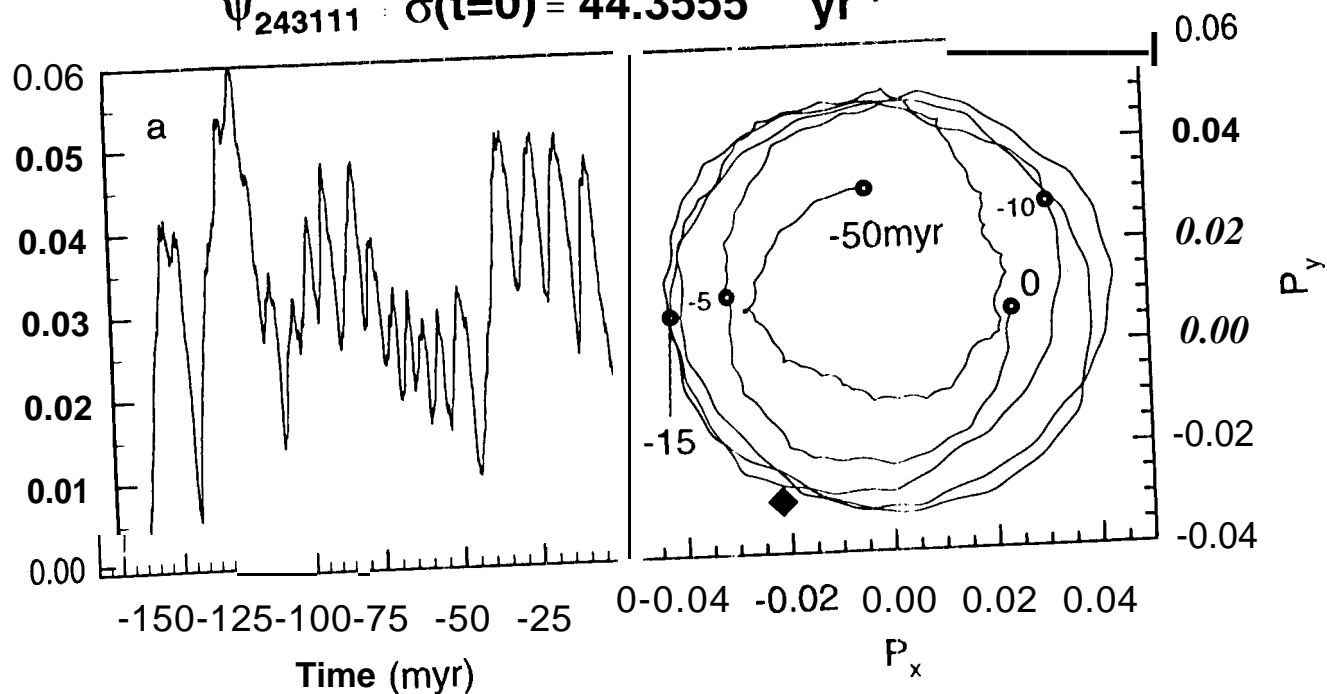
'2331 51



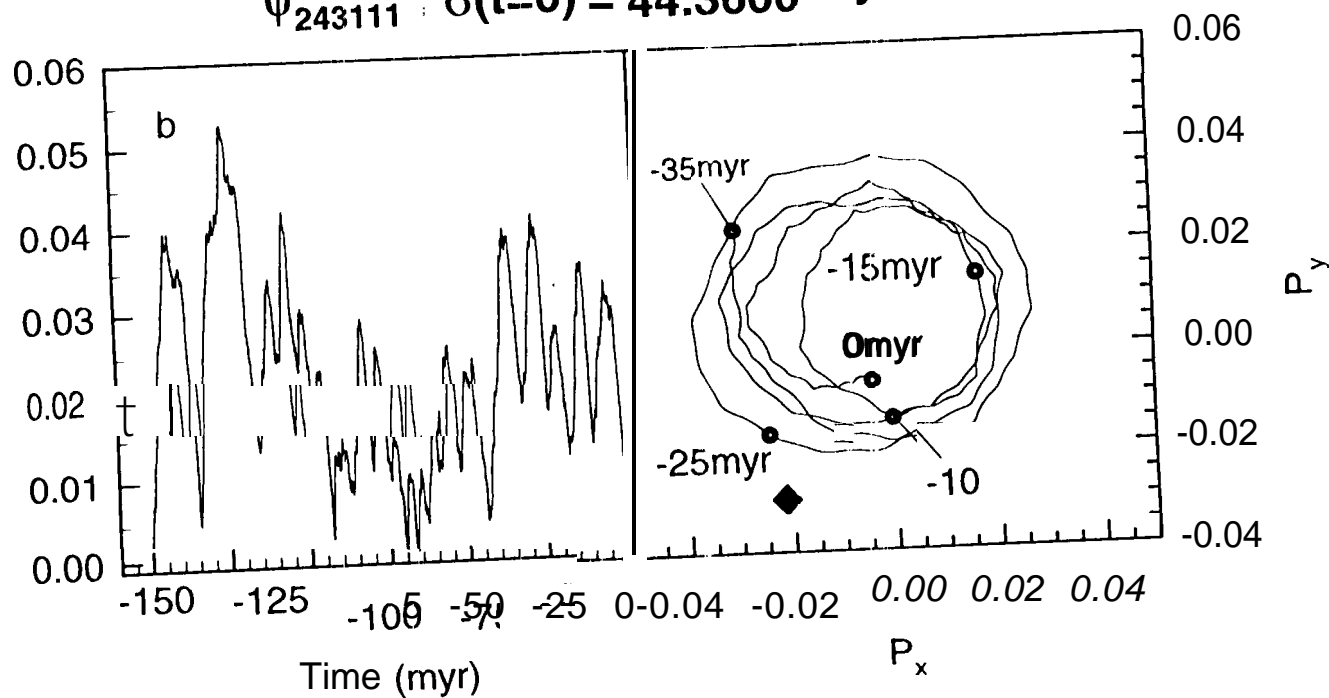
Ψ_{243131}



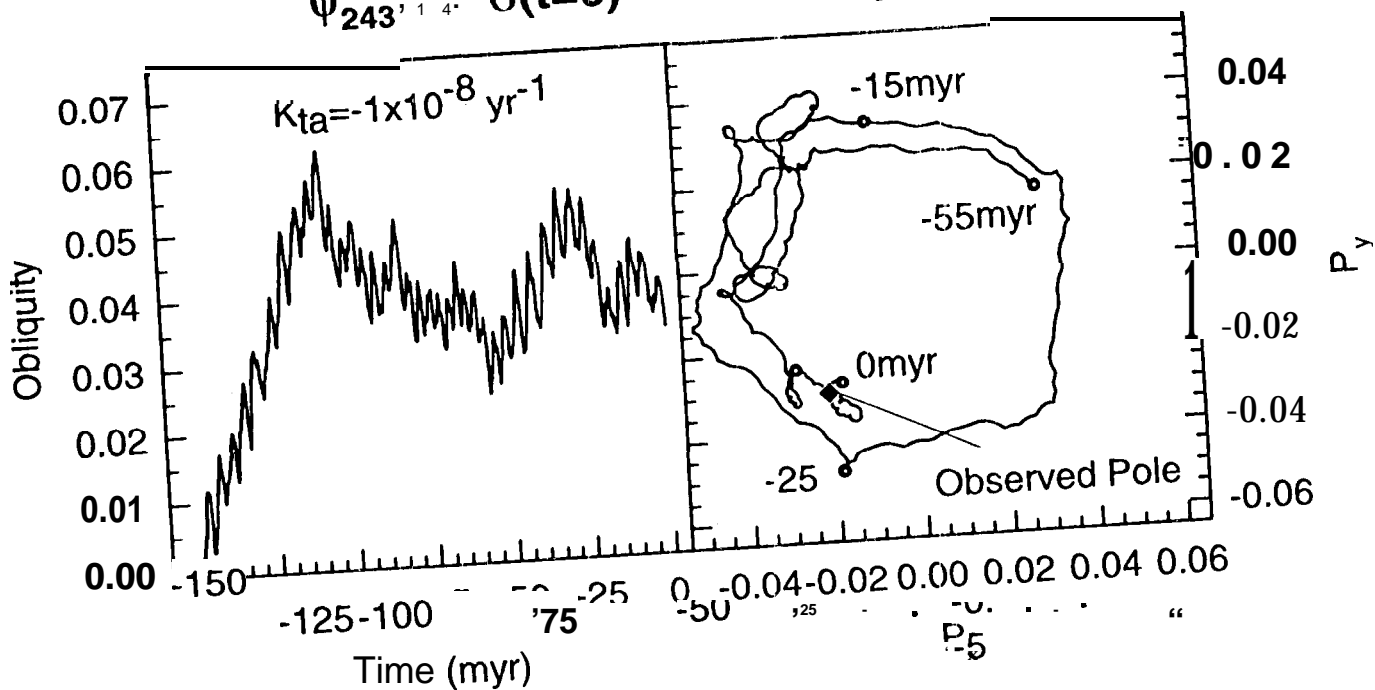
$$\psi_{243111} : \sigma(t=0) = 44.3555 \text{ " yr}^{-1}$$



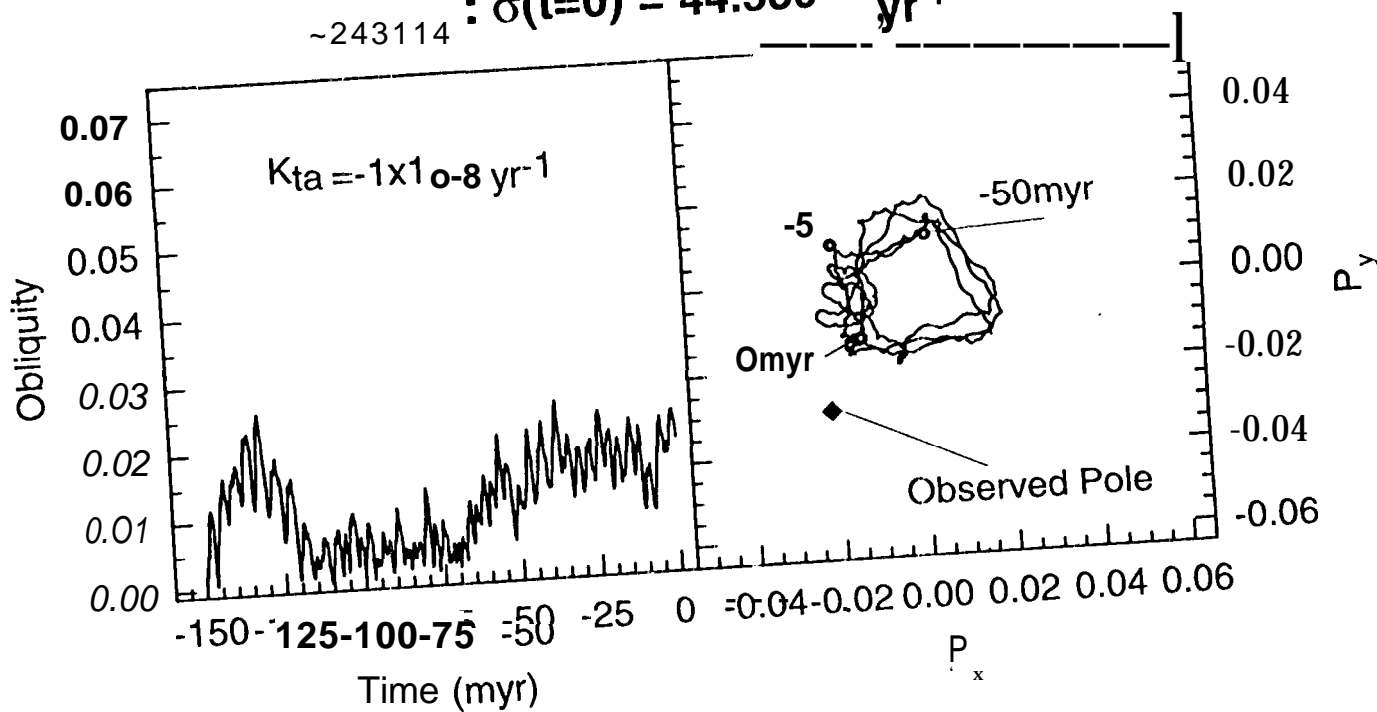
$$\psi_{243111} : \sigma(t=0) = 44.3600 \text{ " yr}^{-1}$$



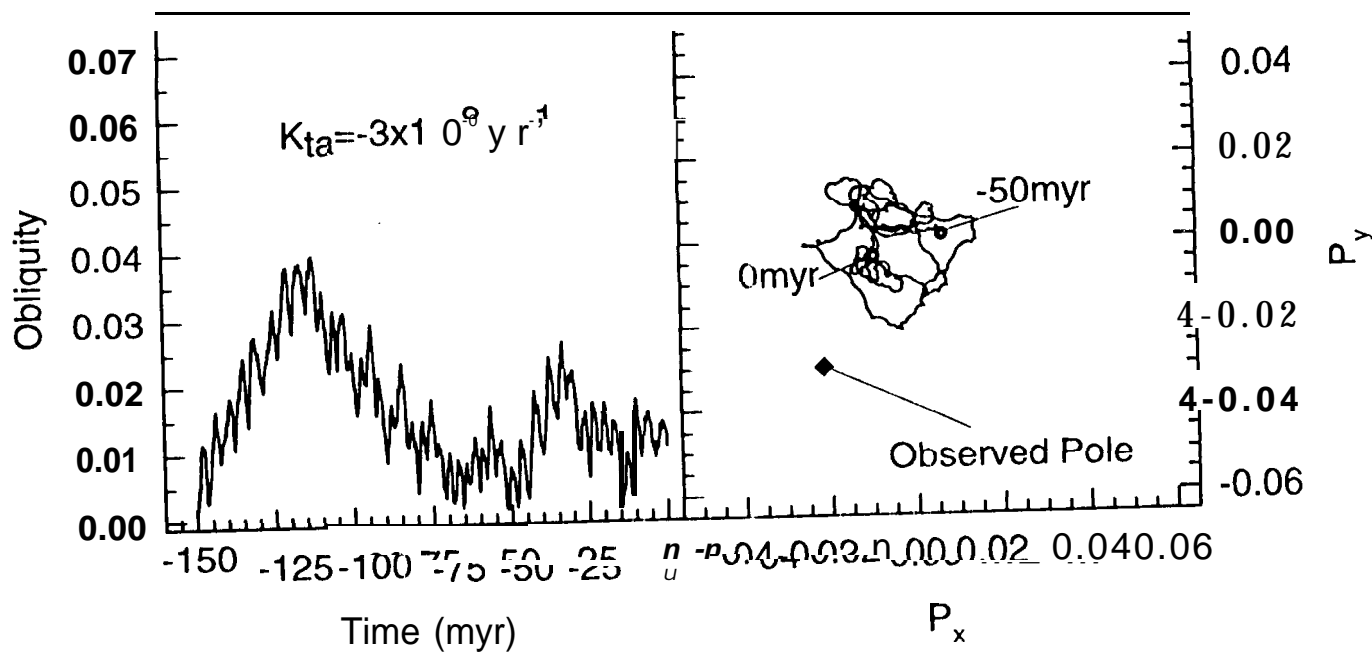
$$\psi_{243,14} : \sigma(t=0) = 44.555'' \text{ yr}^{-1}$$



$$\sim 243114 : \sigma(t=0) = 44.580'' \text{ yr}^{-1}$$



$$\Psi_{243114} : \sigma(t=0) = 44.555 \text{ " yr}^{-1}$$



$$\Psi_{243114} : \sigma(t=0) = 44.580 \text{ " yr}^{-1}$$

